DISSERTATION

CHARACTERIZATION AND MODIFICATION OF CARBON COMPOSITE ELECTRODES TOWARDS MORE AFFORDABLE BIOSENSING APPLICATIONS AND INTEGRATION INTO FLUIDIC DEVICES

Submitted by

Kaylee M. Clark

Department of Chemistry

In partial fulfilment of the requirements

For the Degree of Doctor of Philosophy

Colorado State University

Fort Collins, Colorado

Summer 2022

Doctoral Committee:

Advisor: Charles S. Henry

Alan Van Orden
Amy L. Prieto
John Volckens

Copyright by Kaylee M. Clark 2022

All Rights Reserved

ABSTRACT

CHARACTERIZATION AND MODIFICATION OF CARBON COMPOSITE ELECTRODES TOWARDS MORE AFFORDABLE BIOSENSING APPLICATIONS AND INTEGRATION INTO FLUIDIC DEVICES

Fast, accurate, and low-cost medical tests and platforms for biomolecule monitoring are essential to the diagnosis, management, and treatment of many diseases. Electrochemical detection allows for highly sensitive measurements with fast response times. Carbon composite electrodes are an attractive option for electrochemical detection due to their low cost, resistance to biological fouling, large electrochemical solvent windows, and ability to be patterned. However, they often suffer from poor electrocatalytic activity, inability to be molded, and need for complex modifications to effectively detect certain analytes. Combining electrochemistry with fluidics is attractive for a wide array of applications including multiplexing, automation, and high-throughput screening. However, fabrication of electrochemical fluidic devices with integrated carbon electrodes remains a challenge. Thermoplastic electrodes (TPEs) are a new class of composite electrodes discussed in this dissertation that exhibit superior electrochemical properties to typical carbon composite electrodes and can be easily molded into intricate structures. Overall, this dissertation aims to improve carbon composite materials for biosensing applications and integration of electrochemical sensors into fluidic devices.

Chapter 2 introduces polycaprolactone (PCL) as a new binder material for TPEs and focuses on the electrochemical characterization of the new material. The PCL-based TPEs have excellent electrochemical activity towards a wide range of analytes as well as high electrical conductivity. Chapter 2 also introduces a simple technique for integrating PCL and carbon composite electrodes into microfluidics. The presented electrode-integrated microfluidic devices

are quickly fabricated with a laser cutter using PCL as a bonding layer. As a proof-of-concept application, water-in-oil droplets are electrochemically analyzed.

Chapter 3 focuses on use of PCL-based TPEs for enzymatic sensors. The simple fabrication of TPEs also allows catalysts and enzymes to be mixed directly into the material to enhance detection. In Chapter 3, the TPE material is bulk-modified with cobalt phthalocyanine, an electrocatalyst, and glucose oxidase, resulting in a robust glucose sensor that demonstrates long-term current response stability. These sensors can be molded into intricate shapes and sanded for surface renewal (without requiring additional steps to maintain the modification), allowing the sensors to be continuously reused even if damaged or fouled.

Chapter 4 investigates the properties of TPEs using two different binders – polycaprolactone (PCL) and polystyrene (PS) – with sanded and heat-pressed surface treatment. XPS and SEM analysis suggested that sanded TPEs have a higher density of graphitic edge planes and improved electrochemistry as a result. Electrochemical detection of O_2 and H_2O_2, which are typically difficult to detect on carbon composites without complex modification, was demonstrated on sanded PS-based TPEs. Additionally, Chapter 4 introduces a new 3D-printed TPE sensor module that is reversibly sealed with magnets. A proof-of-concept sensor for detecting H_2O_2 in flow with the sensor module is presented.

Chapter 5 presents a low-cost flow device, made of inexpensive polyethylene terephthalate (PET) and adhesive films, developed to detect SARS-CoV-2 nucleocapsid (N) protein. Upon addition of a sample in the device, reagents and washes are sequentially delivered to an integrated screen-printed carbon electrode for detection thus automating a full sandwich immunoassay with a single end-user step. The modified electrodes are sensitive and selective for COVID-19 N protein

and stable for over seven weeks. The flow device was also successfully applied to detect nine different SARS-CoV-2 variants, including Omicron.

In summary, this dissertation presents work to improve carbon composite electrodes, their modification, and integration into fluidic devices for applications as biosensors and beyond. The TPEs presented show improved electrochemical and physical properties, that allow for simple modifications. This work also demonstrates simple electrode integration strategies in several types of fluidic devices for easier and more sensitive detection of biologically relevant analytes. Moreover, the platforms established in this dissertation can be easily adapted for a wide variety of analytes and applications. This work provides materials, methods, and platforms to create more affordable biosensors for medical and other biological sensing.

ACKNOWLEDGEMENTS

First and foremost, I would like to thank my advisor, Dr. Chuck Henry. Throughout my time under his guidance, I have grown immensely as a researcher and person thanks to his knowledge, challenging research-related counterarguments, and patience. Throughout my time in his group, he has been an excellent example on how to be hardworking, accomplished, kind, and understanding all at once. His optimism, while also a source of frustration at times, is truly the reason I have made it through this program.

I would also like to thank my thesis committee for contributing excellent ideas for my work and stepping in for advice when needed. Dr. Amy Prieto has inspired me as a scientist and a woman, and Dr. Alan Van Orden has provided lightheartedness that has helped my journey through graduate school. In addition to help on a project not discussed in this dissertation, Dr. John Volckens stepped in at the last minute to fill a vacancy on my committee. I would like to thank Dr. Carlos Garcia, who mentored me and introduced me to chemistry research as an undergraduate at Clemson University. He inspired me to love research when I was determined to not attend graduate school, and I would not be here without his mentorship and encouragement. I would like to thank Rebecca Miller for training me on several instruments and patiently answering my never ceasing questions.

I would like to thank my fellow Henry Group members for their help and support throughout my PhD. The collaboration and friendship in the Henry Group have made my work and life so much more meaningful. I will always remember their help as we celebrated success and bemoaned failures together over lunch breaks. In particular, I would like to thank Dr. Isabelle Samper for her friendship and arriving at the perfect time to pull me through one of the most overwhelming parts of my PhD. I am extremely grateful for her continued help and check-ins,

even after finishing her post doc with the Henry Group. I would also like to thank my undergraduate researcher Josi Beck. While the project she worked on was not included in this dissertation, her contributions to that project allowed me to free up the time needed to complete the work presented here.

Most importantly, I would like to thank to thank my friends and family for their support through my life and my PhD journey. My friends, both in Colorado and across the country, have helped me through the struggles of graduate school and made my time here happy and unforgettable. My parents, Brian and Susan Clark, have always been present to give me unconditional love, advice, and reminders that they are proud of me. My sisters Cassie and Maryssa Clark, along with many other members of my family, have encouraged and inspired me to continuously pursue my passions. My cat, Kirby, always cheered me up by curling up on my lap after hard days and making fun appearances in virtual calls. My fearless partner, Jeremiah Alford, has provided unwavering support in all stages of my PhD. Over the last five years, he has cooked and cleaned when I was unable, driven me home to and from work countless time, and stayed up to unreasonable hours with me to ensure I completed my work. I know I would have not been able to accomplish what I have without his support and sacrifices. I am eternally grateful for all my mentors, peers, family, and friends who have collectively believed in me more than I could ever believe in myself. I would not be the researcher or person I am today without all of their help along the way.

TABLE OF CONTENTS

CHAPTER 1: INTRODUCTION

1.1 Carbon Composite Electrodes

There are several forms of conductive carbon useful to sensing such as glassy carbon, boron doped diamond, and graphite. The most common type of carbon used for composite electrodes is graphitic carbon. Graphite is desirable for electrochemical applications because it is highly conductive but is more chemically inert than precious metals, resulting is less chemical fouling and unwanted side reactions.[1] The structure of graphite consists of graphene sheets (planar, sp^2 hybridized C) stacked on top of each other in a crystalline structure, shown in

Figure .[1] Graphite particles typically range from 0.5–150 μm.[2, 3] In the layers of graphite, there are basal planes and edge planes, shown in

Figure .[4] Basal planes are the layers that are parallel to the surface which consist of uninterrupted conjugation. Edge planes are perpendicular to the basal planes and are found at the end of graphitic planes and at surface defects. Basal and edge planes found in graphite have fundamentally different surface structure and chemistry.[2, 4] Electron transfer is generally considered much faster at the edge planes than at the basal plane, resulting in more efficient electrochemistry at the edge planes.[4] However, through Scanning Electrochemical Cell Microscopy (SECCM), it was shown that pristine basal plane have similar electroactivity but this activity decreases quickly with surface fouling.[5]

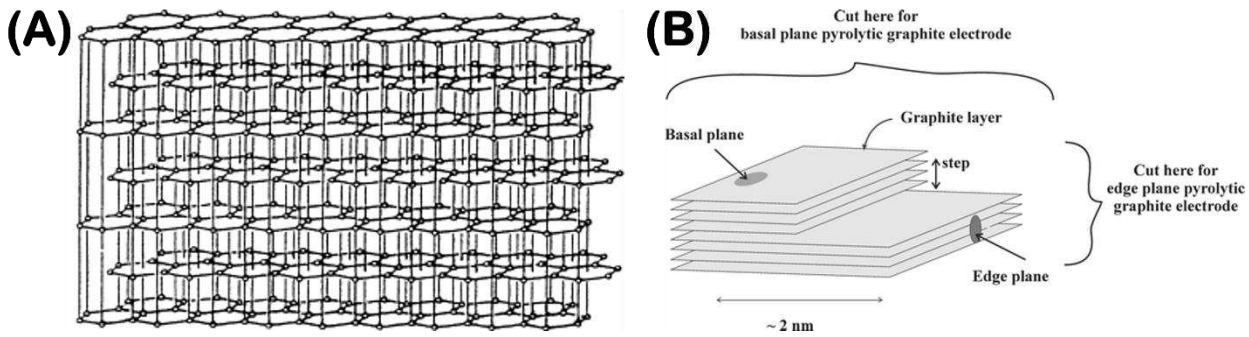

Figure 1.1 **(A)** Crystalline structure of graphite. Figure from Wissler.[1] **(B)** Simplified image depicting the structure of graphitic carbon and identifying edge planes, basal planes, and a "step" also categorized as a defect in the graphitic planes. Figure from Banks *et al*.[4]

Graphite and other carbon powders can be found both naturally and can be synthesized. Synthetic graphite is synthesized by thermal treatment of amorphous carbon. Petroleum coke, which is a byproduct of oil refining, is the most commonly used amorphous carbon for synthetic graphite. The amorphous carbon undergoes temperatures from 2300-3000 °C at ambient pressure to provide the carbon atoms with the mobility necessary to rearrange from an amorphous carbon to graphitic lattice. Natural graphite forms in the earth's crust where the temperature is only about 750 °C, however, it is at a pressure of approximately 75,000 psi for millions of years. Natural graphite can be mined, purified, and micronized by milling or grinding.[1, 6] Carbon black is a type of carbon that is similar to graphite but has a significantly smaller particle size of about 50 nm. It is produced through the thermal decomposition of acetylene gas.[7] Natural and synthetic graphite have similar crystalline structures that are effective for use in composite electrodes. However, natural graphite crystals are typically oriented in the same direction and synthetic graphite crystals are more randomly oriented.[1]

Carbon composite electrodes are an attractive option for sensing due to their low cost, easy fabrication, ability to be miniaturized, biocompatibility, and wide potential window.[8] Carbon composite electrodes are electrodes where a conductive carbon material is dispersed in an

insulating matrix.[9] Carbon composites were first introduced in 1958 when Adams reported mixing carbon and bromoform to make carbon paste electrodes (CPEs).[10] The field has grown immensely encompassing many different types of carbon composite electrodes including CPEs, screen-printed carbon electrodes (SPCEs), and epoxy-based composite electrodes.[11-13] CPEs are now categorized as composites made with organic liquids, most commonly paraffin or mineral oils.[14] CPEs have been applied towards the detection of analytes from RNA to small biomolecules to metals.[14] SPCEs use screens or meshes, typically made from silk or nylon, with different types of conductive carbon inks to print patterns of working, reference, and counter electrodes to the surface of a substrate.[15] The development of SPCEs has been accelerated due to their valuable application for cheap, disposable enzyme test strips for the commercialization of glucose sensors.[2] Since the introduction of carbon composite electrodes, researchers have utilized a creative variety of binders mixed with graphite including Teflon,[16] epoxy resin,[17] sol-gels,[18] ionic liquids,[19] wax,[20] natural rubber,[21] and conducting polymers.[22]

Due to the complexity of the graphite used, carbon composite electrodes tend to have many functional groups on the surface and therefore have much more complex surface chemistry than metal electrodes. When edges of graphene sheets are cleaved during fabrication or polishing, they react with oxygen and water forming various oxygen functional groups to complete the valences. Surface oxides include carbonyls, hydroxyls, carboxyls, ethers, and lactones. Some of these can be seen in **Figure 1.2**.[23] Surface oxides can affect adsorption, electron transfer kinetics, and electrocatalysis.[2] The surface of composite electrodes can often be tuned or renewed with pretreatments such as polishing and/or anodic/cathodic polarization.[24] Depending on the analyte being detected, the surface can be activated to be more favorable for electron transfer. For example, a negatively charged carbon electrode surface would more easily attract a positively charged

molecule (e.g. dopamine) and therefore be more sensitive to it and vice versa with a negatively charged analyte like uric acid.[2] Similarly, the carbon electrode can be treated with oxygen plasma, making the surface more hydrophilic, which allows aqueous analytes to better interact with the electrode surface.[25, 26] Also, composite electrodes can often mix electrocatalysts, enzymes, and chemical recognition agents directly into the electrode material for simple modification to better detect the analyte of interest.[2] Unfortunately in some composite electrodes, the binder material can coat and block electron transfer of the graphite which causes a decrease in electrocatalytic activity. Many composite electrode materials also suffer from limited ability to pattern and mold into complex designs necessary for some sensing applications.

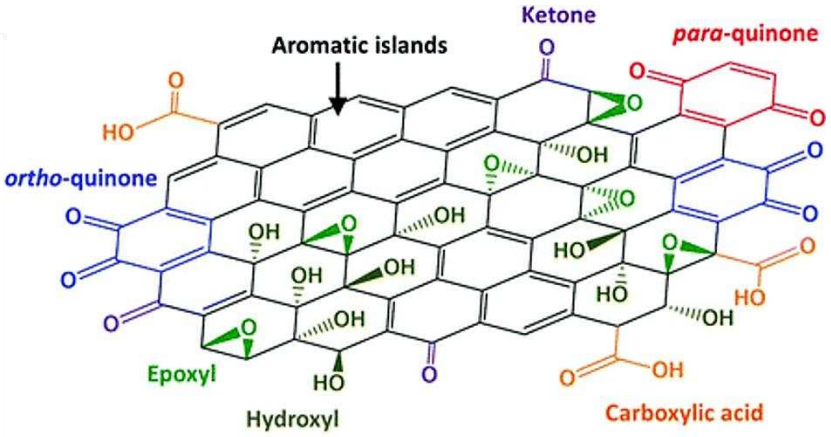

Figure 1.2 Image depicting examples of oxygen groups that can be found on the surface of graphitic planes. Figure adapted from Eng *et al*.[23]

1.2 Thermoplastic Electrodes

Thermoplastic electrodes (TPEs) were first introduced in a publication by the Henry Group (Klunder *et al.*) in 2017 as a easily moldable, highly electroactive carbon composite material.[27] Thermoplastics are polymers that become soft and moldable when heated and harden when cooled. Thermoplastics can be melted and cooled repeatedly without degrading or changing the plastic properties.[28] Polymethyl methacrylate (PMMA) has a melting point of 160 °C and was used as

the binder material for the electrodes in the original work.[27] There are very few reported uses of PMMA as an electrode binder in the literature; however, those that do use PMMA involve complicated processes such as in situ polymerization,[29-31] radiation-curing,[32] or lengthy and repetitive heating and cooling.[33] The method reported by Klunder, et. al. requires only simple mixing and heat pressing as shown in **Figure (A)**.[27] The TPEs retain similar mechanical properties to the thermoplastic used which enables the fabrication of intricate electrode designs, limited only by the conductive carbon particle size and resolution of the template fabrication.[27, 34] Composite carbon electrodes have been described to have "high enough" graphite loading with over 50% graphite to polymer.[2] TPEs can load carbon up to 10 times or more the weight of the polymer allowing for much higher conductivity. TPEs have conductivities of up to ~1000 S/m, which is over 100x higher than what typically reported for SPCEs.[34, 35]

The PMMA TPEs have shown improved electrochemical activity over traditional carbon composite electrodes such as screen-printed electrodes and comparable electrochemical activity to that of conventional electrodes such as glassy carbon and platinum (**Figure (B)**). The electrodes can be altered by changing the carbon type and ratio of carbon:PMMA and present a very attractive choice in electrode material due to their tunable mechanical and electrochemical properties.

The fabrication of the PMMA TPEs is relatively simple compared to some carbon composite fabrications, which can involve complex processes and conditions such as high temperatures, *in situ* synthesis, or electropolymerization.[36] However, due to its melting point of ~160 °C, it requires the material to be partially solvated in a "gum-like" state while pressing the material into templates. This process can cause the formation of gaps or cracks in the material if there is too much or too little organic solvent present when pressed. Furthermore, pressing requires several hours to ensure the solvent is fully evaporated. To eliminate the need for the material to be

partially solvated, the thermoplastic polycaprolactone (PCL) has been used as the binder, which will be further discussed in this dissertation.[34] PCL has a melting point of 60 °C which allows the electrode material to be easily molded while completely dry into patterns with more intricate details. Overall since TPEs introduction, a variety of thermoplastic binders have been used including polymethyl methacrylate (PMMA),[27, 37] polycaprolactone (PCL),[34, 37-40] cyclic olefin copolymer (COC),[37, 41, 42] and polystyrene (PS).[43, 44] Additionally, the moldability of TPEs has enabled them to be incorporated into a variety of fluidic devices.[34, 37, 38, 41] Due to their increased electrochemical activity and improved physical properties, TPEs have promising potential for application in a variety of fields.

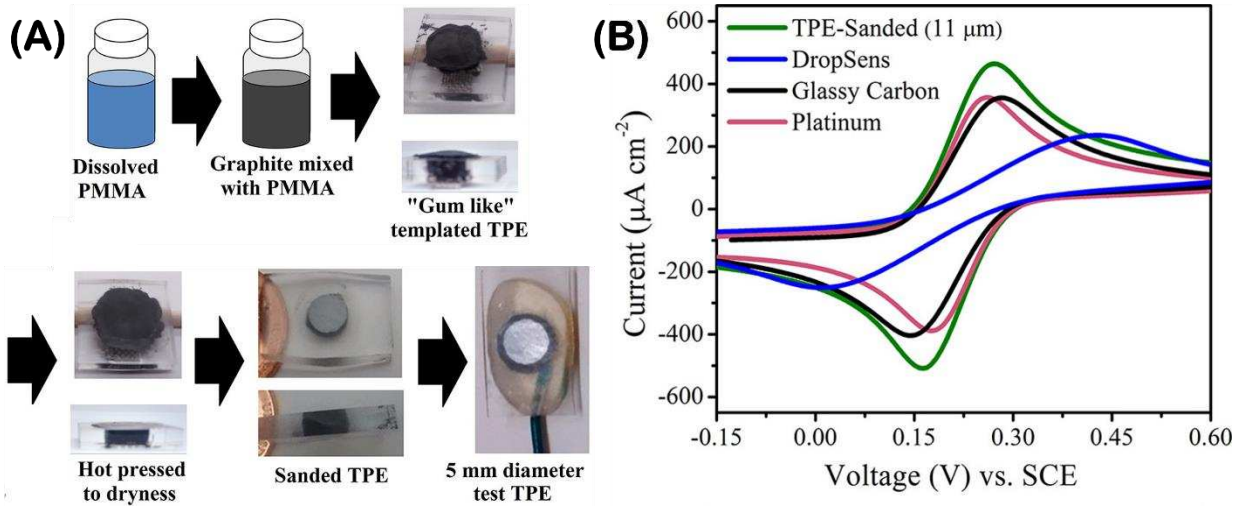

Figure 1.3 (A) Fabrication schematic for PMMA TPE's. **(B)** Cyclic voltammograms (CVs) of 10 mM potassium ferricyanide on PMMA TPE, DropSens screen printed electrode, glassy carbon electrode, and platinum electrode. Figure adapted from Klunder *et al*.[27]

1.3 Electrochemical Biosensors

Biosensors have countless applications including clinical, food, environmental, and national defense.[45] In clinical applications, use of biosensors can be used to understand and monitor health. Unfortunately, many medical tests rely on specialized laboratory techniques and

instruments such as high-performance liquid chromatography (HPLC), electrophoresis, spectrophotometry, or mass spectrometry.[46-49] The expensive instruments and trained personnel required makes many of these diagnostic and monitoring tools inaccessible or unaffordable.[50, 51] Access to effective medical tests is crucial because early diagnosis and accurate monitoring has been shown to greatly improve health outcomes of many diseases.[52] Unfortunately, many available point-of-care (POC) biosensors are qualitative visual tests that lack sensitivity and rely on interpretation of results from the end-user.[53-55] As a result, the development of simpler, faster, and more affordable biosensors is critical.[49, 50, 52, 56]

Biosensors are a specific subgroup of chemical sensor that uses a biochemical mechanism to translate chemical information into an analytical signal.[57] The purpose of a biosensor is to produce a signal that is proportional to the analyte concentration.[58] All biosensors have a receptor or biological sensing element, which translates the biological part of the system (often a concentration of an analyte) into a chemical output, and a transducer, which translates the chemical output produced into a quantifiable signal. In a biosensor, the transducer (i.e. electrode material in the case of electrochemical detection) determines the sensitivity, and the receptor determines selectivity and specificity for the analyte. [59] Examples of receptors for a biosensor include enzymes, antibodies, and specific ligands for protein binding. Common transducers are optical, electrochemical, or thermal-based.[57] Electrochemical biosensors are a favorable option due to their speed, sensitivity, specificity, low sample volumes required, and ability for real-time analysis.[50, 58, 60] The electrochemical signal measured by an electrochemical biosensor is directly proportional to the concentration of the electroactive species in the bulk solution.[57] A schematic of the components of a biosensor can be seen in **Figure 1.4**.

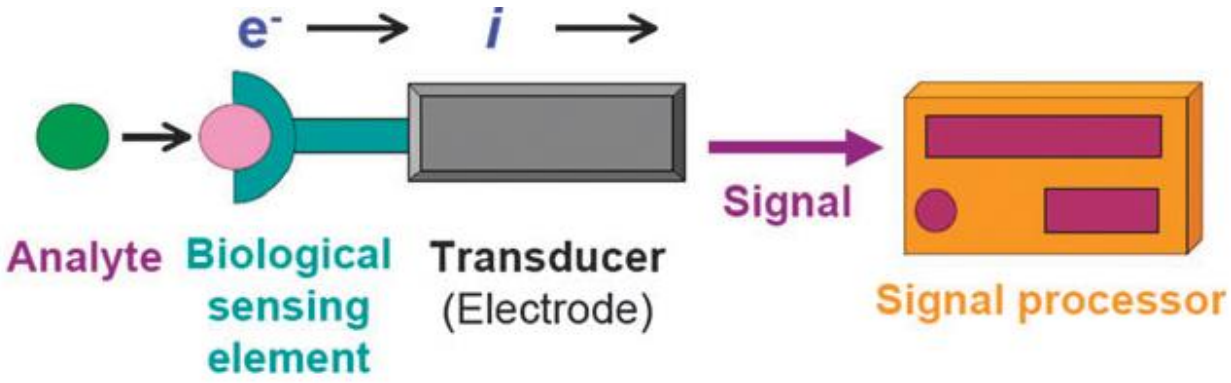

Figure 1.4 Simple schematic of a biosensor with an electrochemical transducer. Figure from Ronkainen *et al*.[45]

One of the most common and well known receptor types uses enzymes. Enzymes allow the conversion of electroinactive substrates of interest into electroactive products that can be more easily quantified.[15] The first enzymatic sensor was reported by Clark and Lyons in 1962. They used an oxygen electrode with glucose oxidase entrapped on its surface to measure concentrations of glucose.[61] This work prompted the start the new field of research leading to great advances in biosensing, resulting in the commercialization of easy-to-use POC blood sugar testing. In 2018, glucose biosensors accounted for 73.4% of the entire global biosensor market, so glucose is very commonly used as the analyte to develop new biosensing concepts.[62]

Effective immobilization of enzymes on electrode surfaces is crucial to developing effective enzymatic biosensors.[63] The immobilization process, however, will inevitably cause a loss in enzyme activity so minimizing the loss through the immobilization technique is a priority. Immobilization also has an effect on the biosensor's lifetime, linear range, sensitivity, selectivity, response time, stability, and anti-interferent.[58, 64, 65] There are a wide variety of immobilization techniques, such as physical adsorption, entrapment in a semipermeable membrane, covalent bonding to the electrode surface, covalent crosslinking, and electrochemical polymerization of an enzyme-containing monomer.[58]

Another common electrochemical biosensor receptor uses affinity-based receptors such as an antibody, aptamer, or molecularly imprinted polymer. Affinity-based receptors selectively recognize and capture the analyte through binding, resulting in a change in electrochemical signal.[66] Immunoassays are a well-established type of affinity-based assay that use antibodies, and traditionally, immunoassays employ optical detection methods such as colorimetry or fluorimetry.[67] Enzyme linked immunosorbent assays (ELISA) are a common immunoassay scheme that is frequently used as a diagnostic tool.[47] Unfortunately, traditional ELISAs still need to be performed in a laboratory setting, require many tedious steps or complicated robotics, and can take several hours to complete.[68] Electrochemical immunoassays were first introduced by Heineman in the 1980s using glassy carbon, carbon paste, and gold electrodes.[69-72] Since then, ELISA has become a popular detection scheme for electrochemical immunoassays where an enzymatic label on the antibody generates an electroactive product from the antibody-antigen interaction.[47, 73] "Sandwich" ELISAs are a subcategory where the analyte is captured with a primary antibody then "sandwiched" between an additional enzyme-labeled antibody that also binds to the analyte. A simplified schematic of a sandwich ELISA is shown in **Figure 1.5**. For electrochemical ELISA, the sandwich complex is introduced to a substrate to react with the enzyme to produce electroactive product.[74-76]

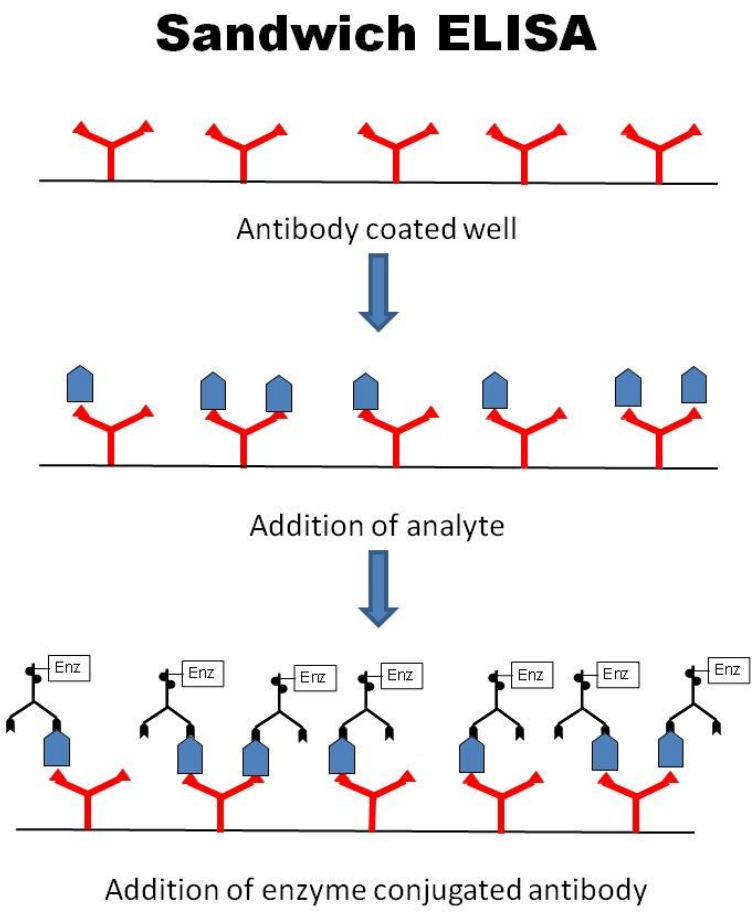

Figure 1.5 Simple schematic of a traditional sandwich ELISA. Figure from Cox *et al*.[77]

Similar to enzymatic electrochemical biosensors, antibody immobilization on the electrode surface is a key part of developing an effective electrochemical immunoassay-based biosensors. Antibody immobilization on electrodes is achieved through passive adsorption or chemical binding.[78-82] Passive adsorption relies on the intermolecular forces between proteins and the electrode surface for the antibody to spontaneously bind to the electrode.[83] Chemical binding often involves pretreatment of the electrode surface and includes techniques such as carbodiimide chemistry,[78] gold-thiol bonds,[84] and π-π stacking.[85] All of the immobilization techniques referenced can be effective, but many also require long incubation times, involve harsh chemicals, and can lack stability and reproducibility.[60, 81, 85]

Overall, with recent technological developments, electrochemical biosensors are a practical option for more clinical applications. There is still a need for improvement of inexpensive electrode materials and sensor performance from biosensing element optimization.[50, 66] Other major challenges facing electrochemical biosensors are the incompatibility in biofluids or in the body for implantable devices, miniaturization, long-term stability of the biological receptor and transducer, *in vivo* calibration, short stabilization times, and baseline drift.[15, 86] Additionally, the biosensing field is shifting towards developing materials and biosensors that can be easily incorporated into arrays and fluidic devices.[66, 87]

1.4 Electrochemistry in Flow

An obstacle in the biosensing field is that many analytes of interest are present at low concentrations. In low concentration samples, signal often must be amplified to have the sensitivity needed. Electrical current measured during electrochemical experiments can be increased by improving the mass transport to the electrode through flow, as discussed below.[88] Static electrochemical measurements rely on diffusion of the analyte to the electrode surface. As the electrochemical reaction occurs at the electrode, a concentration gradient occurs, and the analyte molecules move from a region of high concentration to lower concentration.[89] A depiction of mass transport in a static solution is shown in **Figure 1.6(A)**. While static measurements are simple, they are ineffective at measuring more than the comparatively small number of molecules near the electrode surface.

A common way to mechanically encourage mass transport of the analyte to the electrode surface by forcing the solution to flow (also referred to as convection). The more the solution is perturbed, the higher the probability of analyte reaching the electrode surface.[89] This can be done through stirring and the rate of mass transport can be increased by increasing the stir speed. The

effect of stirring a solution is shown in **Figure 1.6(B)**. Stirring allows more of the analyte to reach the surface in a shorter amount of time than it would in a static solution. For more precise control of mass transport, electrodes can be incorporated into a fluidic device. All solution (and therefore analyte) is forced to flow over the electrode exposed in the fluidic channel as seen in **Figure 1.6(C)**. While there is still diffusional element in the z direction, the flow eliminates the need for diffusion in the x-y direction. Similarly to stirring, transport of the analyte to the electrode can be manipulated through changing the flow rate in the device.[88] Both stirring and flow have been effectively applied to increase current response of electrochemical sensors and achieve lower limits of detection.[88, 90, 91]

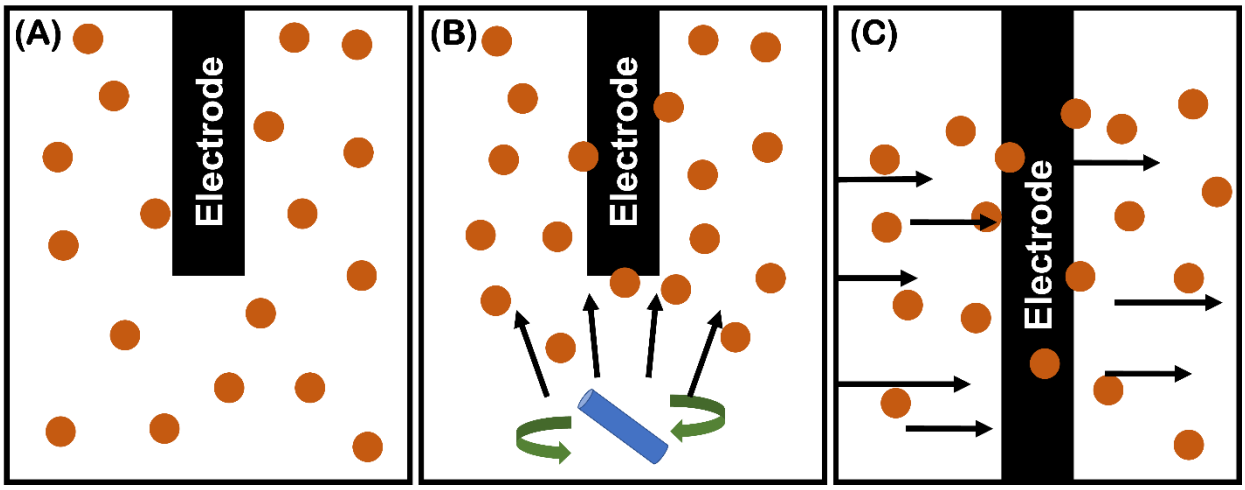

Figure 1.6 Depiction of mass transport in **(A)** a static solution, **(B)** a stirred solution, and **(C)** a fluidic channel.

In addition to increasing the sensitivity of the sensors, integrating electrodes into microfluidic devices can decrease analysis time, allow higher throughput, and automate complex multistep techniques. Processes that traditionally require multiple hours or days for analysis can be reduced to seconds or minutes without loss of sensitivity.[92] Microfluidics also can analyze small sample volumes and limit reagent consumption resulting in lower analyses cost.[90] Due to these

advantages, electrochemical fluidic devices have been used to detect a variety of analytes from small molecules, proteins, and whole cells for applications in numerous fields including biosensing, environmental analysis, point-of-care diagnostics, and electrochemical synthesis.[59, 93-99]

Poly(dimethylsiloxane) (PDMS) was one of the first microfluidic substrates used to incorporate electrochemical sensors and is still commonly used. PDMS allows for quick prototyping for new device designs; however, PMDS microfluidic fabrication process is not very transferable to commercial applications due to its inability to be mass produced.[92] Reports of electrodes incorporated into PDMS channels also often suffer from diminished electrochemical activity.[90, 100, 101] Now, electrodes have been incorporated into fluidic channels defined by paper, wax, 3D printing, laser ablation, and molding, among others.[59, 102]

In recent trends, many fluidic devices are moving toward modular devices or fully integrated microfluidic biosensor platforms.[59] The modular devices can easily exchange and incorporate different biosensors into the fluidic portion of the device.[103-107] These types of devices are useful for applications that might require affordable and/or simultaneous testing of multiple analytes.[59] Fully integrated microfluidic biosensor platforms, while lacking the flexibility of the modular devices, may be able to be better optimized for each specific application and might be particularly useful for health monitoring.[59] The integrated devices are applicable as wearable devices and *in vivo* real-time monitoring.[108-111]

This dissertation aims to improve carbon composite materials for biosensing applications and integration of electrochemical sensors into fluidic devices. In Chapter 2, the development and characterization of polycaprolactone (PCL)-based thermoplastic carbon composite electrodes is introduced. The new electrode material presented in this work is able to be patterned and molded

easily into templates by simple heat-pressing. This overcomes a major challenge of carbon composite electrodes by allowing fabrication of intricate shapes without use of solvent. The electrochemical properties of this material were found to be comparable or superior to other carbon composite electrode materials, while only using inexpensive materials and without the need for complicated syntheses or fabrication. Another barrier in electrochemical sensing with carbon composite electrodes is the difficult and tedious integration into flow devices. Chapter 2 also demonstrates a simple carbon composite electrode integration method for microfluidics using PCL to seal the devices.

Chapter 3 demonstrates the application of the PCL-based TPEs discussed in Chapter 2 as enzymatic sensors. The work introduces a simple bulk-modification technique for electrocatalysts, enzymes, and other additives. Glucose sensing is demonstrated as a proof-of-concept. Typically, these modifications are done on the electrode surface and can be easily damaged, lack stability, or become unusable due to fouling. Through the bulk-modification of the TPEs demonstrated in this chapter, the surface can be renewed via sanding and reused for months. Therefore, these electrodes maintain the cost-effectiveness of carbon composite electrodes while having the long term service life of more traditional electrode materials.

Chapter 4 continues the characterization of TPEs started in Chapter 2 with a focus on measuring H_2O_2 and O_2 as important molecules for sensing. In addition to PCL-based TPEs, it also explores polystyrene (PS)-based TPEs and compares the two materials. With the same graphite, PCL- and PS-based TPEs behave very electrochemically different. The work characterizes the material with techniques including XPS and SEM to gain a better understanding of the properties that make successful carbon composite electrodes and subsequently biosensors. The work applies unmodified PS-based TPEs to molecules that are traditionally very difficult to detect on carbon

composite electrodes without extensive modification, including dopamine, O_2, and H_2O_2. The PS-based TPEs were also integrated into an easily assembled/disassembled fluidic sensor module device in which detection of H_2O_2 demonstrated in flow. The sensor module allows for easy integration of reusable electrochemical sensors into flow as well as the ability to swap the sensors if needed. The detection of H_2O_2 in flow is an important step working towards a larger system for simple enzymatic detection of various biomolecules in complex biological environments.

Finally, Chapter 5 presents an electrochemical immunoassay for the detection of SARS-CoV-2. This work combines the concept and relative sensitivity of a sandwich ELISA with speed and ease-of-use of a lateral flow assay. SPCEs are modified with antibodies for SARS-CoV-2 with a quick drying method that uses passive adsorption. The modified SPCEs are then incorporated into a fluidic device that provides sequential reagent delivery to the electrode with one user step and without need for an external pump. The device is made from inexpensive materials which makes it affordable and therefore in the long-term more accessible. The many tedious steps of a traditional sandwich ELISA, which take trained personnel hours to complete, are eliminated through the automated reagent delivery. The methods used for device fabrication and electrode modification demonstrate a promising step towards manufacturing of similar devices.

Overall, this dissertation presents work on improved and affordable carbon composite electrodes, their modification, and integration into fluidic devices for simpler and more sensitive detection of biologically relevant analytes. Furthermore, small changes to the electrodes and devices in these works, such as exchanging the enzymes or antibodies used, to detect different analytes. This work provides materials, methods, and platforms to continue to bridge the gap towards improved, affordable electrochemical biosensing.

REFERENCES

1. Wissler, M., Graphite and carbon powders for electrochemical applications. *Journal of power sources* **2006,** *156* (2), 142-150.

2. McCreery, R. L., Advanced carbon electrode materials for molecular electrochemistry. *Chemical reviews* **2008,** *108* (7), 2646-2687.

3. Pumera, M., Graphene-based nanomaterials and their electrochemistry. *Chemical Society Reviews* **2010,** *39* (11), 4146-4157.

4. Banks, C. E.; Compton, R. G., New electrodes for old: from carbon nanotubes to edge plane pyrolytic graphite. *Analyst* **2006,** *131* (1), 15-21.

5. Lai, S. C.; Patel, A. N.; McKelvey, K.; Unwin, P. R., Definitive evidence for fast electron transfer at pristine basal plane graphite from high-resolution electrochemical imaging. *Angewandte Chemie International Edition* **2012,** *51* (22), 5405-5408.

6. Tamashausky, A. V. Graphite. A Closer Look.

7. Bigg, D., An investigation of the effect of carbon black structure, polymer morphology, and processing history on the electrical conductivity of carbon-black-filled thermoplastics. *Journal of Rheology* **1984,** *28* (5), 501-516.

8. O'Hare, D.; Macpherson, J. V.; Willows, A., On the microelectrode behaviour of graphite–epoxy composite electrodes. *Electrochemistry Communications* **2002,** *4* (3), 245-250.

9. Corb, I.; Manea, F.; Radovan, C.; Pop, A.; Burtica, G.; Malchev, P.; Picken, S.; Schoonman, J., Carbon-based composite electrodes: Preparation, characterization and application in electroanalysis. *Sensors* **2007,** *7* (11), 2626-2635.

10. Adams, R. N., Carbon paste electrodes. *Analytical chemistry* **1958,** *30* (9), 1576-1576.

11. Taleat, Z.; Khoshroo, A.; Mazloum-Ardakani, M., Screen-printed electrodes for biosensing: a review (2008–2013). *Microchimica Acta* **2014,** *181* (9-10), 865-891.

12. Antiochia, R.; Lavagnini, I.; Magno, F.; Valentini, F.; Palleschi, G., Single-wall carbon nanotube paste electrodes: a comparison with carbon paste, platinum and glassy carbon electrodes via cyclic voltammetric data. *Electroanalysis: An International Journal Devoted to Fundamental and Practical Aspects of Electroanalysis* **2004,** *16* (17), 1451-1458.

13. Manea, F.; Radovan, C.; Pop, A.; Corb, I.; Burtica, G.; Malchev, P.; Picken, S.; Schoonman, J., Carbon composite electrodes applied for electrochemical sensors. In *Sensors for Environment, Health and Security*, Springer: 2009; pp 179-189.

14. Švancara, I.; Vytřas, K.; Kalcher, K.; Walcarius, A.; Wang, J., Carbon paste electrodes in facts, numbers, and notes: a review on the occasion of the 50-years jubilee of carbon paste in electrochemistry and electroanalysis. *Electroanalysis: An International Journal Devoted to Fundamental and Practical Aspects of Electroanalysis* **2009,** *21* (1), 7-28.

15. Wang, J., Electrochemical glucose biosensors. *Chemical reviews* **2008,** *108* (2), 814-825.

16. Wang, J.; Musameh, M., Carbon nanotube/teflon composite electrochemical sensors and biosensors. *Analytical chemistry* **2003,** *75* (9), 2075-2079.

17. Céspedes, F.; Martínez-Fàbregas, E.; Alegret, S., Amperometric glucose biosensor based on an electrocatalytically bulk-modified epoxy-graphite biocomposite. *Analytica chimica acta* **1993,** *284* (1), 21-26.

18. Rabinovich, L.; Lev, O., Sol-Gel Derived Composite Ceramic Carbon Electrodes. *Electroanalysis: An International Journal Devoted to Fundamental and Practical Aspects of Electroanalysis* **2001,** *13* (4), 265-275.

19. Maleki, N.; Safavi, A.; Tajabadi, F., High-performance carbon composite electrode based on an ionic liquid as a binder. *Analytical Chemistry* **2006,** *78* (11), 3820-3826.

20. Wang, J.; Naser, N., Modified carbon-wax composite electrodes. *Analytica chimica acta* **1995,** *316* (2), 253-259.

21. Kampioti, K.; Matos, C. F.; Galembeck, F.; Jaillet, C. l.; Derré, A.; Zarbin, A. J.; Pénicaud, A., Highly Conducting, Sustainable, Nanographitic Rubber Composites. *ACS Omega* **2018,** *3* (2), 1367-1373.

22. Deshmukh, M. A.; Shirsat, M. D.; Ramanaviciene, A.; Ramanavicius, A., Composites based on conducting polymers and carbon nanomaterials for heavy metal ion sensing. *Critical reviews in analytical chemistry* **2018,** *48* (4), 293-304.

23. Eng, A. Y. S.; Chua, C. K.; Pumera, M., Refinements to the structure of graphite oxide: absolute quantification of functional groups via selective labelling. *Nanoscale* **2015,** *7* (47), 20256-20266.

24. Ramírez-García, S.; Alegret, S.; Céspedes, F.; Forster, R. J., Carbon composite electrodes: surface and electrochemical properties. *Analyst* **2002,** *127* (11), 1512-1519.

25. Wang, S.; Chang, K.; Yuan, C.-J., Enhancement of electrochemical properties of screen-printed carbon electrodes by oxygen plasma treatment. *Electrochimica Acta* **2009,** *54* (21), 4937-4943.

26. Akkarachanchainon, N.; Rattanawaleedirojn, P.; Chailapakul, O.; Rodthongkum, N., Hydrophilic graphene surface prepared by electrochemically reduced micellar graphene oxide as a platform for electrochemical sensor. *Talanta* **2017,** *165*, 692-701.

27. Klunder, K. J.; Nilsson, Z.; Sambur, J. B.; Henry, C. S., Patternable solvent-processed thermoplastic graphite electrodes. *Journal of the American Chemical Society* **2017,** *139* (36), 12623-12631.

28. Bîrcă, A.; Gherasim, O.; Grumezescu, V.; Grumezescu, A. M., Introduction in thermoplastic and thermosetting polymers. In *Materials for Biomedical Engineering*, Elsevier: 2019; pp 1-28.

29. Dai, H.; Xu, H.; Lin, Y.; Wu, X.; Chen, G., A highly performing electrochemical sensor for NADH based on graphite/poly (methylmethacrylate) composite electrode. *Electrochemistry Communications* **2009,** *11* (2), 343-346.

30. Yao, X.; Xu, X.; Yang, P.; Chen, G., Carbon nanotube/poly (methyl methacrylate) composite electrode for capillary electrophoretic measurement of honokiol and magnolol in Cortex Magnoliae Officinalis. *Electrophoresis* **2006,** *27* (16), 3233-3242.

31. Yao, X.; Wu, H.; Wang, J.; Qu, S.; Chen, G., Carbon nanotube/poly (methyl methacrylate)(CNT/PMMA) composite electrode fabricated by in situ polymerization for microchip capillary electrophoresis. *Chemistry–A European Journal* **2007,** *13* (3), 846-853.

32. McLaren, K.; Batley, G., Radiation-cured polymer-impregnated graphite electrodes for anodic stripping voltammetry. *Journal of Electroanalytical Chemistry and Interfacial Electrochemistry* **1977,** *79* (1), 169-178.

33. Regel, A.; Lunte, S., Integration of a graphite/poly (methyl-methacrylate) composite electrode into a poly (methylmethacrylate) substrate for electrochemical detection in microchips. *Electrophoresis* **2013,** *34* (14), 2101-2106.

34. Klunder, K. J.; Clark, K. M.; McCord, C.; Berg, K. E.; Minteer, S. D.; Henry, C. S., Polycaprolactone-enabled sealing and carbon composite electrode integration into electrochemical microfluidics. *Lab on a Chip* **2019,** *19* (15), 2589-2597.

35. Randviir, E. P.; Brownson, D. A.; Metters, J. P.; Kadara, R. O.; Banks, C. E., The fabrication, characterisation and electrochemical investigation of screen-printed graphene electrodes. *Physical Chemistry Chemical Physics* **2014,** *16* (10), 4598-4611.

36. Wang, D.-W.; Li, F.; Zhao, J.; Ren, W.; Chen, Z.-G.; Tan, J.; Wu, Z.-S.; Gentle, I.; Lu, G. Q.; Cheng, H.-M., Fabrication of graphene/polyaniline composite paper via in situ anodic electropolymerization for high-performance flexible electrode. *ACS nano* **2009,** *3* (7), 1745-1752.

37. Pradela-Filho, L. A.; Noviana, E.; Araujo, D. A.; Takeuchi, R. M.; Santos, A. L.; Henry, C. S., Rapid analysis in continuous-flow electrochemical paper-based analytical devices. *ACS sensors* **2020,** *5* (1), 274-281.

38. Berg, K. E.; Clark, K. M.; Li, X.; Carter, E. M.; Volckens, J.; Henry, C. S., High-throughput, semi-automated dithiothreitol (DTT) assays for oxidative potential of fine particulate matter. *Atmospheric Environment* **2020,** *222*, 117132.

39. Ozer, T.; McCord, C.; Geiss, B. J.; Dandy, D.; Henry, C. S., Thermoplastic Electrodes for Detection of Escherichia coli. *Journal of The Electrochemical Society* **2021,** *168* (4), 047509.

40. Clark, K. M.; Henry, C. S., Thermoplastic Electrode (TPE)-based Enzymatic Glucose Sensor Using Polycaprolactone-graphite Composites. *Electroanalysis* **2021**.

41. Noviana, E.; Klunder, K. J.; Channon, R. B.; Henry, C. S., Thermoplastic electrode arrays in electrochemical paper-based analytical devices. *Analytical chemistry* **2019,** *91* (3), 2431-2438.

42. Berg, K. E.; Leroux, Y. R.; Hapiot, P.; Henry, C. S., Increasing Applications of Graphite Thermoplastic Electrodes with Aryl Diazonium Grafting. *ChemElectroChem* **2019,** *6* (18), 4811-4816.

43. McCord, C. P.; Summers, B.; Henry, C. S., Redox behavior and surface morphology of polystyrene thermoplastic electrodes. *Electrochimica Acta* **2021,** *393*, 139069.

44. McCord, C. P.; Summers, B.; Henry, C., Simultaneous Analysis of Ascorbic Acid, Uric Acid, and Dopamine at Bare Polystyrene Thermoplastic Electrodes. *ChemElectroChem* **2022**.

45. Ronkainen, N. J.; Halsall, H. B.; Heineman, W. R., Electrochemical biosensors. *Chemical Society Reviews* **2010,** *39* (5), 1747-1763.

46. Dhara, K.; Debiprosad, R. M., Review on nanomaterials-enabled electrochemical sensors for ascorbic acid detection. *Analytical biochemistry* **2019,** *586*, 113415.

47. Weissleder, R.; Lee, H.; Ko, J.; Pittet, M. J., COVID-19 diagnostics in context. *Science translational medicine* **2020,** *12* (546), eabc1931.

48. Lakshmi, D.; Whitcombe, M. J.; Davis, F.; Sharma, P. S.; Prasad, B. B., Electrochemical detection of uric acid in mixed and clinical samples: a review. *Electroanalysis* **2011,** *23* (2), 305-320.

49. Liu, D.; Wang, J.; Wu, L.; Huang, Y.; Zhang, Y.; Zhu, M.; Wang, Y.; Zhu, Z.; Yang, C., Trends in miniaturized biosensors for point-of-care testing. *TrAC Trends in Analytical Chemistry* **2020,** *122*, 115701.

50. Campuzano, S.; Pedrero, M.; Yáñez-Sedeño, P.; Pingarrón, J. M., New challenges in point of care electrochemical detection of clinical biomarkers. *Sensors and Actuators B: Chemical* **2021,** *345*, 130349.

51. Bernabé-Ortiz, A.; Zafra-Tanaka, J. H.; Moscoso-Porras, M.; Sampath, R.; Vetter, B.; Miranda, J. J.; Beran, D., Diagnostics and monitoring tools for noncommunicable diseases: a missing component in the global response. *Globalization and health* **2021,** *17* (1), 1-5.

52. Bai, Y.; Xu, T.; Zhang, X., Graphene-based biosensors for detection of biomarkers. *Micromachines* **2020,** *11* (1), 60.

53. Abraham, R. S.; Barnidge, D. R., Protein Analysis in the Clinical Immunology Laboratory. *Manual of Molecular and Clinical Laboratory Immunology* **2016**, 26-45.

54. Unic, A.; Nikolac Gabaj, N.; Miler, M.; Culej, J.; Lisac, A.; Horvat, A.; Vrkic, N., Ascorbic acid—A black hole of urine chemistry screening. *Journal of Clinical Laboratory Analysis* **2018,** *32* (5), e22390.

55. Park, H.-D., Current status of clinical application of point-of-care testing. *Archives of Pathology & Laboratory Medicine* **2021,** *145* (2), 168-175.

56. Morais, A. L.; Rijo, P.; Batanero Hernan, M. B.; Nicolai, M., Biomolecules and electrochemical tools in chronic non-communicable disease surveillance: a systematic review. *Biosensors* **2020,** *10* (9), 121.

57. Thevenot, D. R.; Toth, K.; Durst, R. A.; Wilson, G. S., Electrochemical biosensors: recommended definitions and classification. *Pure and applied chemistry* **1999,** *71* (12), 2333-2348.

58. Wang, X.; Uchiyama, S., Polymers for biosensors construction. In *State of the art in biosensors-general aspects*, IntechOpen: 2013.

59. Schmidt-Speicher, L. M.; Länge, K., Microfluidic integration for electrochemical biosensor applications. *Current Opinion in Electrochemistry* **2021,** *29*, 100755.

60. Ahmed, M. U.; Hossain, M. M.; Safavieh, M.; Wong, Y. L.; Rahman, I. A.; Zourob, M.; Tamiya, E., Toward the development of smart and low cost point-of-care biosensors based on screen printed electrodes. *Critical reviews in biotechnology* **2016,** *36* (3), 495-505.

61. Clark Jr, L. C.; Lyons, C., Electrode systems for continuous monitoring in cardiovascular surgery. *Annals of the New York Academy of sciences* **1962,** *102* (1), 29-45.

62. *Biosensors Market*; Global Market Insights: 2018.

63. Putzbach, W.; Ronkainen, N. J., Immobilization techniques in the fabrication of nanomaterial-based electrochemical biosensors: A review. *Sensors* **2013,** *13* (4), 4811-4840.

64. Nery, E. W.; Kubota, L. T., Evaluation of enzyme immobilization methods for paper-based devices—a glucose oxidase study. *Journal of Pharmaceutical and Biomedical Analysis* **2016,** *117*, 551-559.

65. Prakash, P. A.; Yogeswaran, U.; Chen, S.-M., A review on direct electrochemistry of catalase for electrochemical sensors. *Sensors* **2009,** *9* (3), 1821-1844.

66. Noviana, E.; McCord, C. P.; Clark, K. M.; Jang, I.; Henry, C. S., Electrochemical paper-based devices: Sensing approaches and progress toward practical applications. *Lab on a Chip* **2020,** *20* (1), 9-34.

67. Wisdom, G. B., Enzyme-immunoassay. *Clinical chemistry* **1976,** *22* (8), 1243-1255.

68. Carter, L. J.; Garner, L. V.; Smoot, J. W.; Li, Y.; Zhou, Q.; Saveson, C. J.; Sasso, J. M.; Gregg, A. C.; Soares, D. J.; Beskid, T. R., Assay techniques and test development for COVID-19 diagnosis. ACS Publications: 2020.

69. Eggers, H. M.; Halsall, H.; Heineman, W., Enzyme immunoassay with flow-amperometric detection of NADH. *Clinical chemistry* **1982,** *28* (9), 1848-1851.

70. Heineman, W. R.; Halsall, H. B., Strategies for electrochemical immunoassay. *Analytical chemistry* **1985,** *57* (12), 1321A-1331A.

71. Wehmeyer, K. R.; Halsall, H.; Heineman, W., Heterogeneous enzyme immunoassay with electrochemical detection: competitive and" sandwich"-type immunoassays. *Clinical chemistry* **1985,** *31* (9), 1546-1549.

72. Tang, H. T.; Lunte, C. E.; Halsall, H. B.; Heineman, W. R., P-Aminophenyl phosphate: An improved substrate for electrochemical enzyme immnoassay. *Analytica Chimica Acta* **1988,** *214*, 187-195.

73. Ricci, F.; Adornetto, G.; Palleschi, G., A review of experimental aspects of electrochemical immunosensors. *Electrochimica Acta* **2012,** *84*, 74-83.

74. Singh, B.; Flampouri, E.; Dempsey, E., Electrochemical enzyme-linked immunosorbent assay (e-ELISA) for parasitic nematode Ostertagia ostertagi (brown stomach worm) infections in dairy cattle. *Analyst* **2019,** *144* (19), 5748-5754.

75. Rossier, J. S.; Girault, H. H., Enzyme linked immunosorbent assay on a microchip with electrochemical detection. *Lab on a Chip* **2001,** *1* (2), 153-157.

76. Bhimji, A.; Zaragoza, A. A.; Live, L. S.; Kelley, S. O., Electrochemical enzyme-linked immunosorbent assay featuring proximal reagent generation: detection of human immunodeficiency virus antibodies in clinical samples. *Analytical chemistry* **2013,** *85* (14), 6813-6819.

77. Cox, K. L.; Devanarayan, V.; Kriauciunas, A.; Manetta, J.; Montrose, C.; Sittampalam, S., Immunoassay methods. *Assay Guidance Manual [Internet]* **2019**.

78. Booth, M. A.; Kannappan, K.; Hosseini, A.; Partridge, A., In-depth electrochemical investigation of surface attachment chemistry via carbodiimide coupling. *Langmuir* **2015,** *31* (29), 8033-8041.

79. Welch, N. G.; Scoble, J. A.; Muir, B. W.; Pigram, P. J., Orientation and characterization of immobilized antibodies for improved immunoassays. *Biointerphases* **2017,** *12* (2), 02D301.

80. Svalova, T.; Malysheva, N.; Bubekova, A.; Saigushkina, A.; Medvedeva, M.; Kozitsina, A., Effect of the Method for Immobilizing Receptor Layer on the Analytical Characteristics of a Label-Free Electrochemical Immunosensor for the Determination of Measles Antibodies. *Journal of Analytical Chemistry* **2020,** *75* (2), 254-261.

81. Yáñez-Sedeño, P.; Campuzano, S.; Pingarrón, J. M., Integrated affinity biosensing platforms on screen-printed electrodes electrografted with diazonium salts. *Sensors* **2018,** *18* (2), 675.

82. Wan, Y.; Su, Y.; Zhu, X.; Liu, G.; Fan, C., Development of electrochemical immunosensors towards point of care diagnostics. *Biosensors and Bioelectronics* **2013,** *47*, 1-11.

83. Shen, M.; Rusling, J. F.; Dixit, C. K., Site-selective orientated immobilization of antibodies and conjugates for immunodiagnostics development. *Methods* **2017,** *116*, 95-111.

84. Frasconi, M.; Mazzei, F.; Ferri, T., Protein immobilization at gold–thiol surfaces and potential for biosensing. *Analytical and bioanalytical chemistry* **2010,** *398* (4), 1545-1564.

85. Cao, M.; Fu, A.; Wang, Z.; Liu, J.; Kong, N.; Zong, X.; Liu, H.; Gooding, J. J., Electrochemical and theoretical study of π–π stacking interactions between graphitic surfaces and pyrene derivatives. *The Journal of Physical Chemistry C* **2014,** *118* (5), 2650-2659.

86. Pumera, M.; Sanchez, S.; Ichinose, I.; Tang, J., Electrochemical nanobiosensors. *Sensors and Actuators B: Chemical* **2007,** *123* (2), 1195-1205.

87. Nontawong, N.; Amatatongchai, M.; Wuepchaiyaphum, W.; Chairam, S.; Pimmongkol, S.; Panich, S.; Tamuang, S.; Jarujamrus, P., Fabrication of a three-dimensional electrochemical paper-based device (3D-ePAD) for individual and simultaneous detection of ascorbic acid, dopamine and uric acid. *Int. J. Electrochem. Sci* **2018,** *13*, 6940-6957.

88. Brownlee, B. J.; Marr, K. M.; Claussen, J. C.; Iverson, B. D., Improving sensitivity of electrochemical sensors with convective transport in free-standing, carbon nanotube structures. *Sensors and Actuators B: Chemical* **2017,** *246*, 20-28.

89. Bard, A. J.; Faulkner, L. R., Electrochemical Methods: Fundamentals and Applications. *Surface Technology* **1983,** *20* (1), 91-92.

90. Chikkaveeraiah, B. V.; Liu, H.; Mani, V.; Papadimitrakopoulos, F.; Rusling, J. F., A microfluidic electrochemical device for high sensitivity biosensing: Detection of nanomolar hydrogen peroxide. *Electrochemistry communications* **2009,** *11* (4), 819-822.

91. Musameh, M.; Wang, J.; Merkoci, A.; Lin, Y., Low-potential stable NADH detection at carbon-nanotube-modified glassy carbon electrodes. *Electrochemistry communications* **2002,** *4* (10), 743-746.

92. Bange, A.; Halsall, H. B.; Heineman, W. R., Microfluidic immunosensor systems. *Biosensors and Bioelectronics* **2005,** *20* (12), 2488-2503.

93. Dincer, C.; Bruch, R.; Kling, A.; Dittrich, P. S.; Urban, G. A., Multiplexed Point-of-Care Testing - xPOCT. *Trends in biotechnology* **2017,** *35* (8), 728-742.

94. Sameenoi, Y.; Koehler, K.; Shapiro, J.; Boonsong, K.; Sun, Y.; Collett, J.; Volckens, J.; Henry, C. S., Microfluidic Electrochemical Sensor for On-Line Monitoring of Aerosol Oxidative Activity. *Journal of the American Chemical Society* **2012,** *134* (25), 10562-10568.

95. Rackus, D. G.; Shamsi, M. H.; Wheeler, A. R., Electrochemistry, biosensors and microfluidics: a convergence of fields. *Chemical Society Reviews* **2015,** *44* (15), 5320-5340.

96. Kudr, J.; Zitka, O.; Klimanek, M.; Vrba, R.; Adam, V., Microfluidic electrochemical devices for pollution analysis–A review. *Sensors and Actuators B: Chemical* **2017,** *246*, 578-590.

97. Pletcher, D.; Green, R. A.; Brown, R. C. D., Flow Electrolysis Cells for the Synthetic Organic Chemistry Laboratory. *Chemical Reviews* **2018,** *118* (9), 4573-4591.

98. Folgueiras-Amador, A. A.; Wirth, T., Perspectives in Flow Electrochemistry. *Journal of Flow Chemistry* **2017,** *7* (3), 94-95.

99. Azeredo, N. F. B.; Santos, M. S. F.; Sempionatto, J. R.; Wang, J.; Angnes, L., Screen-printed technologies combined with flow analysis techniques: moving from benchtop to everywhere. *Analytical chemistry* **2022,** *94* (1), 250-268.

100. Sameenoi, Y.; Mensack, M. M.; Boonsong, K.; Ewing, R.; Dungchai, W.; Chailapakul, O.; Cropek, D. M.; Henry, C. S., Poly(dimethylsiloxane) cross-linked carbon paste electrodes for microfluidic electrochemical sensing. *Analyst* **2011,** *136* (15), 3177-3184.

101. Sia, S. K.; Whitesides, G. M., Microfluidic devices fabricated in poly (dimethylsiloxane) for biological studies. *Electrophoresis* **2003,** *24* (21), 3563-3576.

102. del Campo, F. J., Miniaturization of electrochemical flow devices: a mini-review. *Electrochemistry communications* **2014,** *45*, 91-94.

103. Erkal, J. L.; Selimovic, A.; Gross, B. C.; Lockwood, S. Y.; Walton, E. L.; McNamara, S.; Martin, R. S.; Spence, D. M., 3D printed microfluidic devices with integrated versatile and reusable electrodes. *Lab on a Chip* **2014,** *14* (12), 2023-2032.

104. Shin, K.-H.; Moon, C.-R.; Lee, T.-H.; Lim, C.-H.; Kim, Y.-J., Flexible wireless pressure sensor module. *Sensors and Actuators A: Physical* **2005,** *123*, 30-35.

105. Kara, A.; Rouillard, C.; Mathault, J.; Boisvert, M.; Tessier, F.; Landari, H.; Melki, I.; Laprise-Pelletier, M.; Boisselier, E.; Fortin, M.-A., Towards a multifunctional electrochemical sensing and niosome generation lab-on-chip platform based on a plug-and-play concept. *Sensors* **2016,** *16* (6), 778.

106. Roley, A.; Clark, K.; Richardson, A.; Martinez, B.; Tobet, S.; Henry, C., User-friendly, magnetically sealed plug-and-play sensor module for online electrochemical sensing for fluidic devices. **2021**.

107. Lin, Y.; Timchalk, C. A.; Matson, D. W.; Wu, H.; Thrall, K. D., Integrated microfluidics/electrochemical sensor system for monitoring of environmental exposures to lead and chlorophenols. *Biomedical microdevices* **2001,** *3* (4), 331-338.

108. Sanati, A.; Esmaeili, Y.; Bidram, E.; Shariati, L.; Rafienia, M.; Mahshid, S.; Parlak, O., Recent advancement in electrode materials and fabrication, microfluidic designs, and self-powered systems for wearable non-invasive electrochemical glucose monitoring. *Applied Materials Today* **2022,** *26*, 101350.

109. Tu, J.; Torrente-Rodríguez, R. M.; Wang, M.; Gao, W., The era of digital health: A review of portable and wearable affinity biosensors. *Advanced Functional Materials* **2020,** *30* (29), 1906713.

110. Gao, W.; Emaminejad, S.; Nyein, H. Y. Y.; Challa, S.; Chen, K.; Peck, A.; Fahad, H. M.; Ota, H.; Shiraki, H.; Kiriya, D., Fully integrated wearable sensor arrays for multiplexed in situ perspiration analysis. *Nature* **2016,** *529* (7587), 509-514.

111. Chung, M.; Fortunato, G.; Radacsi, N., Wearable flexible sweat sensors for healthcare monitoring: a review. *Journal of the Royal Society Interface* **2019,** *16* (159), 20190217.

CHAPTER 2: POLYCAPROLACTONE-BASED THERMOPLASTIC ELECTRODES AND SIMPLE CARBON COMPOSITE ELECTRODE INTEGRATION INTO ELECTROCHEMICAL MICROFLUIDICS

2.1 Chapter Overview

Combining electrochemistry with microfluidics is attractive for a wide array of applications including multiplexing, automation, and high-throughput screening. Electrochemical instrumentation is low-cost and can be easily miniaturized, yet still enables high analytical sensitivity. For many electrochemical microfluidic applications, carbon electrodes are more desirable than precious metals because they are inexpensive, resistant to biological fouling, and have large electrochemical solvent windows. However, fabrication of electrochemical microfluidic devices with integrated carbon electrodes remains a challenge. This work introduces a simple technique for integrating polycaprolactone (PCL) and carbon composite electrodes into microfluidics. The PCL:carbon composites have excellent electrochemical activity towards a wide range of analytes as well as high electrical conductivity. The presented electrode-integrated microfluidic devices are quickly fabricated with a laser cutter using PCL as a bonding layer. As a proof-of-concept application, water-in-oil droplets are electrochemically analyzed. The work in this chapter was published in *Lab on a Chip* entitled "Polycaprolactone-Enabled Sealing and Carbon Composite Electrode Integration into Electrochemical Microfluidics." This was a multi-author work with additional data in the paper that is not included in this dissertation. The data included in this chapter was collected and processed by myself unless otherwise denoted in the figure caption.

2.2 Introduction

Integrating electrodes into microfluidics is an attractive platform for chemical analyses. Electrochemical microfluidic devices have been applied in biosensing, environmental monitoring, point-of-care diagnostics, and electrochemical synthesis.[1-6] Integrating electrodes into microfluidic chips can allow for faster detection, higher throughput, and automation of multistep analysis. However, in practice, these devices can be challenging and tedious to fabricate. Precious metal electrodes are often used but typically require expensive and complicated fabrication methods,[3] have raised features that can prevent full sealing of channels and are prone to fouling.[7]

Carbon composite electrodes are an attractive alternative to precious metals because they are low cost, less prone to fouling, and have large potential windows.[8-10] Even with these advantages, it is still very challenging to effectively integrate carbon electrodes into microfluidics due to their similarly raised features,[11-13] extensive fabrication with harsh chemicals,[14, 15] and/or inability to for integration until after the microfluidic device is sealed.[16] Epoxy-based carbon electrodes have been incorporated into in microfluidics but need to be mixed and cast into a template quickly to create the correct geometry.[17-19] Poly(dimethylsiloxane) (PDMS) has been a common microfluidic platform and PDMS-based electrodes have been incorporated often but suffer from low conductivity and diminished electrochemical activity.[20] Electrodes are sometimes placed in the waste area of the fluidic device to avoid integration altogether, but the sample dispersion results in reduced signal.[21]

Polycaprolactone (PCL) is an inexpensive thermopolymer that melts at 60 ºC.[22] PCL is also FDA approved for use in drug delivery, prosthetics, and other medical applications providing the long-term potential for integration into wearable devices.[23, 24] To our knowledge PCL has not been

demonstrated previously for electrochemical applications and here is presented as a novel binder material for creating carbon composite electrodes.

This work reports the first use of PCL carbon composite electrodes and a simple method for their integration into microfluidic devices. PCL:carbon ratios were optimized, and the electrochemistry of the composites was characterized. Microfluidic devices were fabricated using PCL as a bonding layer defining channels with a CO_2 laser. Finally, as a proof-of-concept, an electrochemical droplet generator is demonstrated. The work presented here demonstrated a new strategy to easily assemble low-cost, high-end microfluidics with fully integrated carbon composites for enhanced electrochemical detection.

2.3 Experimental Section

Reagents

Polycaprolactone (PCL) was purchased from ThermoMorph® (Toledo, OH). ^{1}H-NMR characterization of the PCL was performed to confirm its structure, shown in **Figure 2.1**. Solutions were prepared using 18.2 MΩ・cm water purified using a Milli-Q system (MilliporeSigma, USA). Different graphite were purchased from various vendors: MG-1599 (~15 μm) from Great Lakes Graphite, Inc. (Toronto, Canada), 7-11 micron graphite from Fisher Scientific (Waltham, MA), 3569 ($\leq$150 μm) from Asbury Carbon (Asbury, NJ), carbon black (~50 nm) from STREM Chemicals, Inc. (Newburyport, MA). Properties and details of the carbons are summarized in **Table 2.1**. Fluorescein isothiocyanate was purchased from Thermo Fisher Scientific (Waltham, MA). ACS grade dichloromethane and redox molecules used were purchased from Sigma-Aldrich (Saint Louis, MO). $FcTMA^+$ was synthesized in house via the metathesis of the corresponding iodide salt with ammonium hexafluorophosphate.

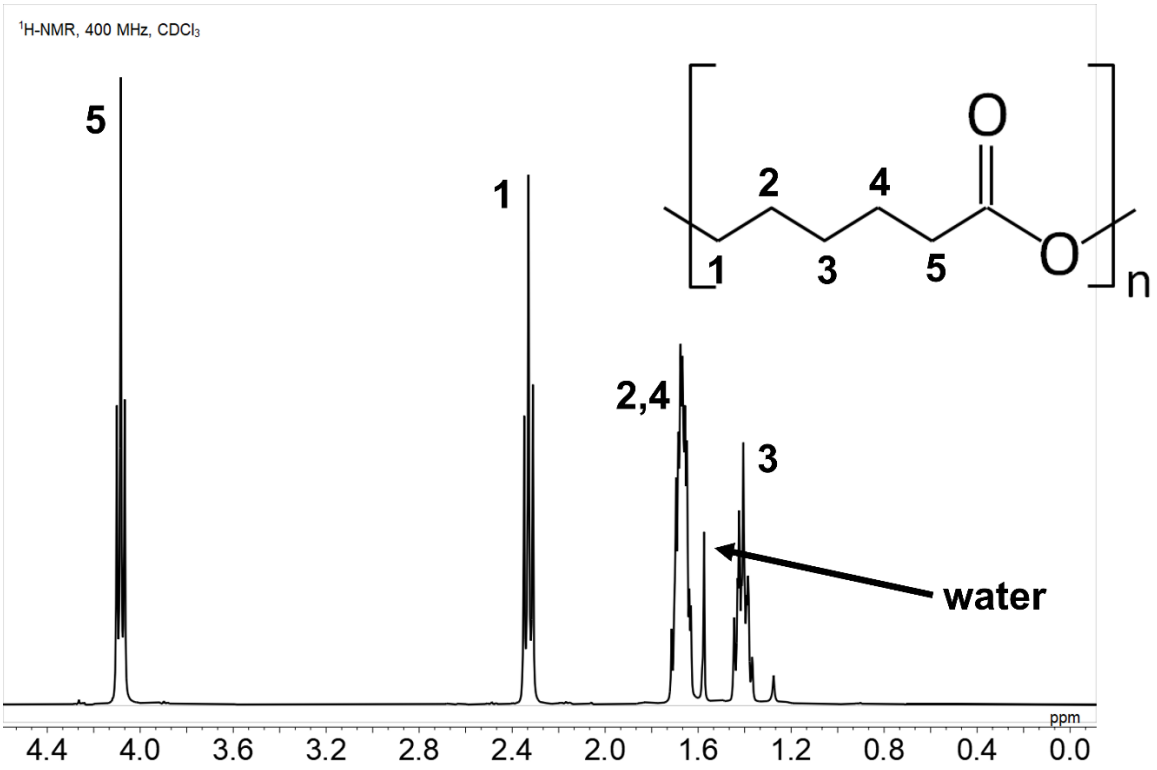

Figure 2.1 ^{1}H-NMR spectra of ThermoMorph polymer in $CDCl_3$ and (inset) structure according to the spectrum.

Table 2.1 Carbon type particle size, purity, synthesis, and source.[25-27]

Carbon Type	Average Particle Size	Purity	Impurities- if available (ppm)	Production	Company
11 micron (graphite)	7-11 μm	99%		Synthesized through thermal treatment of petroleum coke	Alfa Aesar
MG-1599 (graphite)	16 μm	99.7%	Al (0.10), Ca(<0.50), Co (<0.05), Cr (<0.50), Cu (<0.10), Fe (0.32), Mo (1.20), Ni (<0.05), Pb (<0.10), Sb (<0.10), Si (16.00), V (0.81), S (0.81), Zn (<0.10)	Micronized natural flake	Great Lakes Graphite
3569 (graphite)	150 μm	99.8%		Natural flake	Asbury Carbon
Acetylene Carbon Black	50 nm	99.9%		Thermal decomposition of acetylene gas	Strem Chemicals

Conductivity and Capacitance Measurements

Through-plane conductivity measurements were performed measuring resistance with a two-point probe (Fluke 187 multimeter, accuracy of 0.01 Ω) following the method previously reported.[28] The capacitance was measured with cyclic voltammetry in 0.5 M KNO_3 using the current response at 0.2 V vs. following the method previously reported.[28] In this work, 2.5 mm disks of the composite that were typically 3 mm thick were used.

Electrochemistry

All electrochemistry was performed with a CH Instruments 660b potentiostat. A saturated calomel electrode (SCE) reference was used for all experiments. The counter electrode was a composite plate of TPE with at least 10x the working area of the working electrode.

Flow cell experiments used PCL:Carbon in the same composition as the working, counter, and reference electrodes. The electrolyte for droplet generation was 0.5 M KCl with 1% Tween20 surfactant, and light weight mineral oil. The voltage was held at -0.4 V vs. carbon pseudo-reference electrode.

Fabrication of Microfluidics

Microfluidic devices were fabricated using the following method. Pressure was applied for 1 min until the dichloromethane (DCM) was mostly evaporated. After 15 min, the plate was removed from the silicon wafer with a razorblade by scoring around the edges. After PCL coating the polymethyl methacrylate (PMMA) plate, an Epilog Zing (30 W) with 25% speed and 30% power was used to create the channels. More detail on the fabrication can be found in the **Results and Discussion** section.

2.4 Results and Discussion

Fabrication of PCL Thermoplastic Electrodes

Integrated electrodes into microfluidics requires patterning the electrode material onto or into a substrate. Patterned PCL TPEs were assembled as shown in **Figure 2.2**. First, PCL is dissolved in dichloromethane (DCM) followed by mixing graphite powder with the dissolved plastic. The graphite, solvent, and plastic mixture is then poured onto a Si wafer and mixed until it starts to solidify. Finally, the material is allowed to fully dry in a fume hood, which typically takes less than 10 minutes. Once solvent free, the material can be stored for later use. Although formal stability studies were not performed, no change was seen in the materials properties after 6 months of storage in a glass vial in ambient conditions.

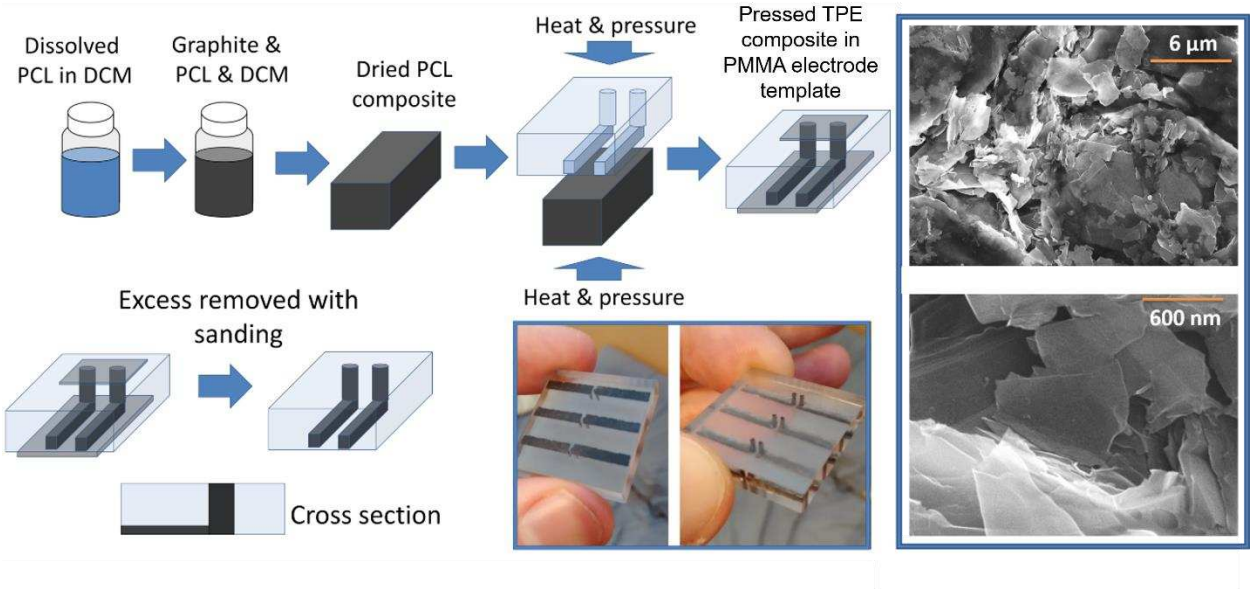

Figure 2.2 CO_2 laser-enabled fabrication of 3-dimensional patterned PCL composite electrodes, and (right) SEM images at 5,000x and 50,000x of a 1:2 MG PCL:carbon composite after sanding. Schematic was created by Kevin Klunder.

The PCL TPEs were patterned electrodes using a traditional hydraulic heated press at ~70 ºC to press the material into templates. However, any technique which delivers pressure and heat could be used to make the electrodes, such as a hot plate and large weight, or clamps and an oven.

Templates were cut from poly(methyl methacrylate) (PMMA) sheets using a CO_2 laser to define patterns. As shown in **Figure 2.2**, the electrodes can also be patterned in 3 dimensions, which allows for a well-defined electrode area and the ability to make easy electrical contact from the backside to a given piece of instrumentation. After the material was pressed into the templates, the excess material was removed, and the electrode surface was smoothed with sandpaper. Rougher (600 grit) sandpaper was initially used followed by finer (1200 grit) sandpaper to ensure a smooth surface which is important for integration into microfluidics.

Figure 2.2 also contains SEM images of a PCL composite electrode with MG-1599 graphite. SEM Images for the other carbon types can be found in **Figure 2.3**. In general, the different graphites had similar surface structure, except carbon black, which appeared to be composed of small nm-sized spherical particles. For the TPE material with graphitic carbon, a high density of exposed graphitic flakes is seen in the SEM images. The surface at the nm-scale is heterogeneous, containing folded and randomly oriented graphitic domains. At higher magnification, numerous exposed graphitic edge sites are clearly present and some are translucent suggesting very thin layers which could present graphene-like behavior. Edge plane graphite is reportedly the most electrochemically active, and the high density of these sites on the PCL composites should be favorable for performing electrochemical measurements.[29] Even though much of the images show conductive regions, there is significant charging in the images as well, likely from the insulating PCL binder. The charging areas are especially present in the carbon black TPE. Carbon black has a significantly smaller particle size than the other graphites (~50 nm) which could cause the PCL to coat the particles more than other carbons as it is being heat-pressed.

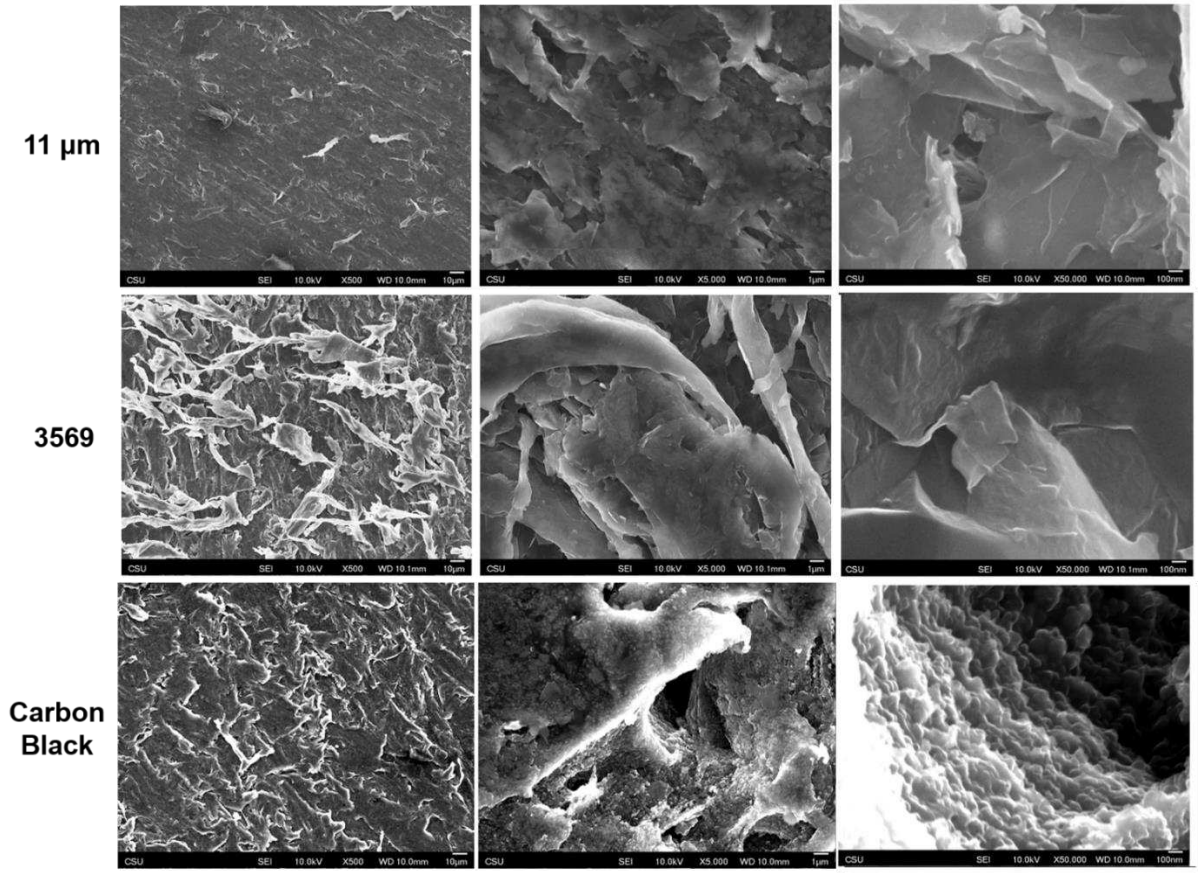

Figure 2.3 SEM images at (from left to right) 500x, 5,000x, and 50,000x magnification of a (top) 1:2 PCL:11 µm electrode, (middle) 1:2 PCL:3569 electrode, and (bottom) 3:4 PCL:Carbon Black electrode.

Conductivity and Capacitance

A proper balance of conductivity and capacitance is critical to electrode performance. Highly resistive electrodes can cause ohmic drop in an electrochemical cell and lead to errors in applied potential, while large capacitance values increase background signal.[30] Conductivity and capacitance measurements were taken on four carbon types at various ratios of PCL to graphite. **Table 2.1** contains information on the supplier and particle size. As expected, conductivity increases with increasing carbon content (**Figure 2.4(A)**). Below ~40 S m^{-1}, an electrode has undesirable resistance for use in a microfluidic device, and any composition that had a value below this was considered unusable. The conductivity values near the 1:2 PCL:carbon ratio for the

graphitic carbons are all above this value. The carbon black electrode could not support more than a 1:1 ratio without losing mechanical stability. In general, the conductivity values and trends are similar to other high-end composite materials.[28]

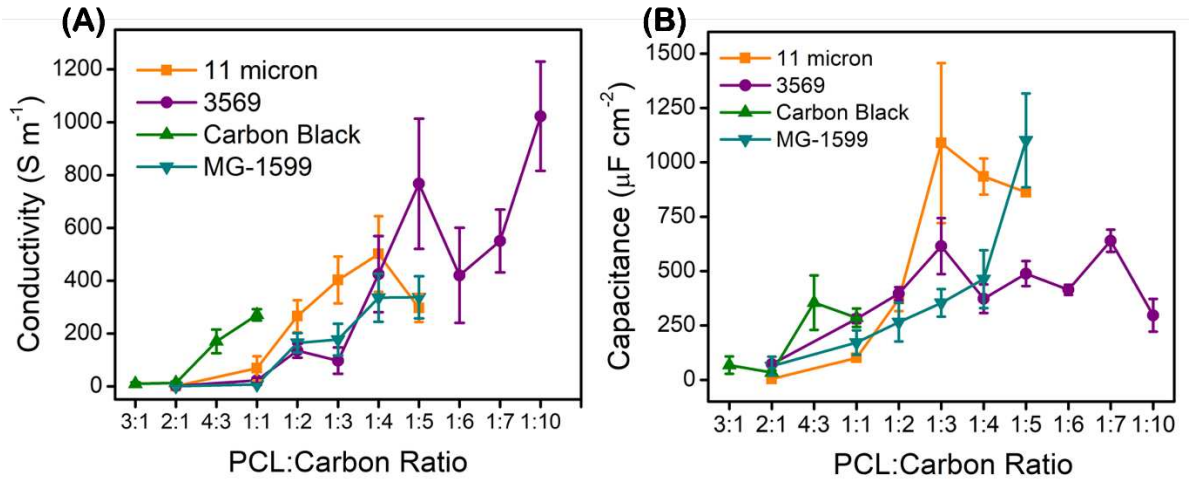

Figure 2.4 Measured conductivity and capacitance values of various PCL:carbon ratios of different carbon types. Symbols and error bars represent average and standard deviation of n=3 for each ratio and carbon type.

The capacitance of these TPE electrodes, shown in **Figure 2.4(B)**, is higher than other reported planar graphite electrodes. Basal and edge plane graphitic electrodes have capacitance values of ≤2 and ~60 µF cm^{-2}, respectively.[31] The PCL-based composites had capacitance values in the range of 200 to 1000 µF cm^{-2}. This implies that the PCL composites have at least 3x the surface area than flat graphitic electrodes, which is confirmed from the heterogeneity observed in the SEM images. The 1:2 PCL:carbon ratio has the best balance of low capacitance and favorable conductivity. Also, the fabrication method is typically easier with increased PCL content due to the composites' lower melting points. Given the results in **Figure 2.4**, the MG-1599, 3569, and 11 µm graphites at high and low ratios were chosen for further electrochemical characterization. Carbon black was not studied further as it had higher capacitance at lower ratios and overall lower conductivity.

Electrochemical Characterization

The electrochemical activity of the new PCL carbon composites was characterized to determine differences in carbon electroactivity and how the ratio of carbon affects the electrochemistry. Initially, the electrodes were examined with ferri-ferrocyanide ($Fe(CN)_6^{3-/4-}$) and ferrocenylmethyl trimethylammonium ($FcTMA^+$) which are commonly used for electrode characterization.[31-33] These molecules typically have fast kinetics, and in the case of ferricyanide, charge transfer rate constants are known for a variety of carbon electrodes. The rate constant can be used as a gauge of the electrochemical activity of the electrodes to compare carbon materials. Cyclic voltammograms (CVs) for $FcTMA^+$ and $Fe(CN)_6^{3-/4-}$ at varying scan rates are shown in **Figure 2.5(A)** and **(B)**, respectively. Differences in the shapes of the CVs can be attributed to the faster electron transfer for $FcTMA^+$. $Fe(CN)_6^{3-/4-}$ is more surface sensitive $FcTMA^+$ than so this is expected, especially considering all the surface defects seen in the SEM (**Figure 2.2** and **2.3**). The effects of scan rate on ΔE for the TPEs in $FcTMA^+$ and $Fe(CN)_6^{3-/4-}$ are summarized in **Table 2.2** and **2.3**.

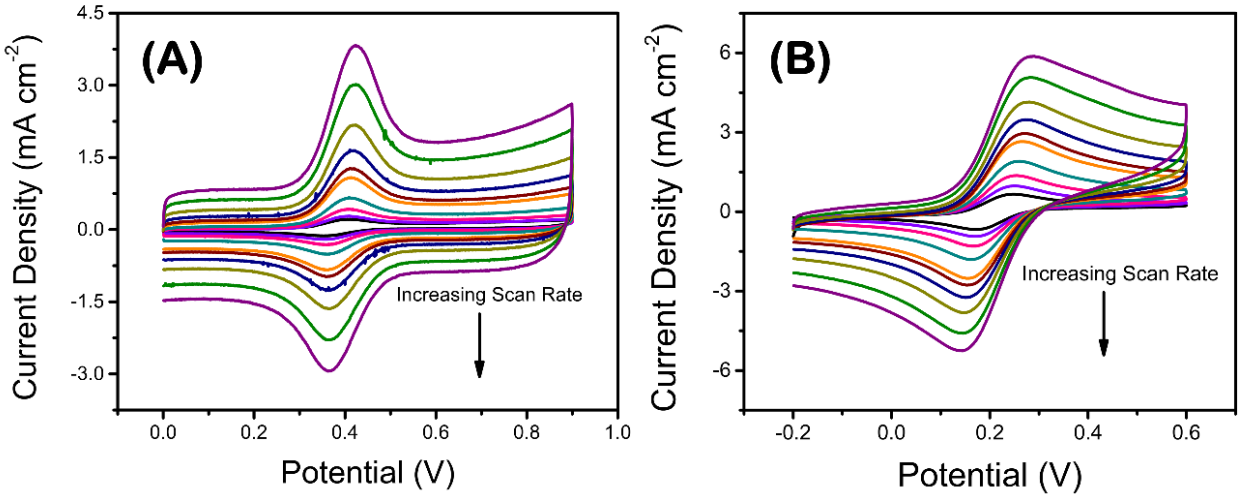

Figure 2.5 Representative CVs for scan rate study for 1 mM **(A)** $FcTMA^+$ and **(B)** ferri-ferrocyanide in 0.5 M KNO_3 on 1:2 PCL:MG-1599 electrode (v = 25, 50, 100, 200, 400, 500, 700, 1000, 1500, 2000 mV/s). Ferri-ferrocyanide data was collected by Cynthia McCord.

Table 2.2 Scan rate study for 1 mM $FcTMA^+$ in 0.5 M KNO_3. ΔE is the average of the calculated difference between oxidation and reduction peak potential and the error is from standard deviation of 3 different electrodes.

Scan Rate (mV/s)	ΔE (mV)					
	1:2 PCL: 11 micron	1:4 PCL: 11 micron	1:2 PCL: 3569	1:4 PCL: 3569	1:2 PCL: MG-1599	1:4 PCL: MG-1599
25	56 ± 5	54 ± 2	50 ± 5	53 ± 3	55 ± 8	57 ± 6
50	53 ± 4	55 ± 0	53 ± 8	58 ± 8	53 ± 5	56 ± 4
100	56 ± 2	52 ± 6	53 ± 5	56 ± 1	46 ± 2	51 ± 5
200	49 ± 2	52 ± 3	52 ± 9	54 ± 3	47 ± 3	51 ± 5
400	54 ± 5	57 ± 4	51 ± 10	54 ± 4	55 ± 5	56 ± 2
500	55 ± 3	58 ± 4	54 ± 10	59 ± 2	56 ± 3	59 ± 1
700	56 ± 7	59 ± 1	51 ± 2	59 ± 2	55 ± 6	59 ± 1
1000	63 ± 3	64 ± 4	59 ± 5	59 ± 4	56 ± 4	60 ± 2
1500	61 ± 3	70 ± 1	61 ± 6	67 ± 1	55 ± 3	65 ± 2
2000	61 ± 1	70 ± 3	70 ± 4	64 ± 3	58 ± 1	66 ± 4

Table 2.3 Scan rate study for 1 mM $Fe(CN)_6^{3-/4-}$ in 0.5 M KNO_3. ΔE is the average of the calculated difference between oxidation and reduction peak potential and the error is from standard deviation of 3 different electrodes. Data collected and processed by Cynthia McCord.

Scan Rate (mV/s)	ΔE (mV)					
	1:2 PCL:11 micron	1:4 PCL:11 micron	1:2 PCL:3569	1:4 PCL:3569	1:2 PCL:MG-1599	1:4 PCL:MG-1599
25	72 ± 5	74 ± 4	77 ± 7	69 ± 2	75 ± 2	75 ± 7
50	79 ± 7	76 ± 6	81 ± 8	73 ± 2	79 ± 3	79 ± 5
100	85 ± 6	81 ± 5	88 ± 11	77 ± 2	84 ± 3	88 ± 6
200	95 ± 6	86 ± 8	94 ± 14	83 ± 6	95 ± 5	98 ± 10
400	107 ± 10	100 ± 8	103 ± 13	93 ± 6	106 ± 7	116 ± 10
500	115 ± 9	103 ± 10	107 ± 13	97 ± 8	111 ± 10	119 ± 12
700	121 ± 5	108 ± 7	111 ± 13	101 ± 9	119 ± 9	127 ± 13
1000	131 ± 8	119 ± 8	110 ± 13	108 ± 10	128 ± 9	140 ± 15
1500	136 ± 11	131 ± 6	116 ± 9	115 ± 15	132 ± 8	155 ± 19
2000	142 ± 10	143 ± 9	124 ± 11	119 ± 19	135 ± 9	163 ± 17

Further investigation of the electrode kinetics was investigated by calculating the heterogeneous electron transfer rate constants (k^0) using the Nicholson method.[40] The following equation was used:

$$\psi = k^0[\pi DnFv/RT]^{-1/2}$$

The kinetic parameters (ψ) from the average ΔEs of the ferri/ferrocyanide peaks for each scan rate were plotted versus $[\pi DnFv/RT]^{-1/2}$ where D is the diffusion coefficient, F is Faraday's constant, v is the scan rate, R is the ideal gas constant, and T is temperature. The rate constants were determined from the slopes of the regression lines and the error shown is the standard error of the slope.

Attempts to calculate the rate constants for $FcTMA^+$ were performed; however, the electrodes were too active to measure kinetics with traditional methods. **Table 2.4** lists the electrochemical rate constant k^o for a variety of electrode compositions towards ferri-ferrocyanide. The rate constants are similar between high and low ratios of carbon, except in the case of the larger particle size 3569-based composite where the rate constant is 2x larger for the higher ratio. Larger graphite particles have been shown to lower electrochemical activity due to a decrease in edge plane graphite.[34] The 3569 particles are 10-20x the size of the other studied graphites so it is likely to have fewer active edge plane sites. Overall, the rate constants are consistent with polished glassy carbon surfaces (0.005 cm s^{-1}),[31] which is promising for utility integrated into microfluidic devices. Moving forward, the 1:2 PCL:carbon ratio was used to balance fabrication ease and favorable electrochemistry.

Table 2.4 Electrochemical rate constants, k^o, of 1 mM ferri-ferrocyanide in 0.5 M KNO_3 in relation to differing electrode compositions.

Carbon Type	Calculated electrochemical rate constant, k^o ($x10^{-3}$ cm·s^{-1})	
	1:2 PCL:Carbon	1:4 PCL:Carbon
3569	6.5 ± 0.2	12.7 ± 0.3
MG-1599	8.3 ± 0.3	8.5 ± 0.3
11 μm	8.8 ± 0.7	9.7 ± 0.2

Ascorbic acid, p-aminophenol, uric acid, and benzoquinone are biological molecules that often used for lab-on-a-chip applications.[31-33] CVs for these biologically relevant redox molecules is shown in **Figure 2.6**. For the oxidation of ascorbic acid (AA), the different carbons gave similar electrochemistry. The peak potentials for AA oxidation are about -0.05 V vs. SCE which is similar to that of a carbon nanotube and an electrochemically pre-treated carbon electrodes.[35] The CV of 3569 carbon shows a slightly lower peak current and a peak shift to a higher potential. This potential shift is likely related to lower activity from the larger particle size discussed previously.

Uric acid (UA) oxidation for all three carbons occurred at 0.3 V vs. SCE which is similar to a report using graphene on glassy carbon with a peak at 0.4 V vs. SCE.[36] In contrast to the results with AA, 3569 carbon resulted in the highest peak current for UA. This difference suggests that different biomolecules interact uniquely with different types of carbon and therefore carbon type should be considered when optimizing assays for different analytes. The electrocatalytic activity of the PCL composites was similar to a glassy carbon electrode for the reversible electrochemical reaction of 1,4-benzoquinone.[37] Once again, the CV of 3569 carbon has a higher peak current relative to the other carbons. Another theory for this could be an increase in surface area due to

the larger particles. The PCL TPEs gave well defined and reversible peaks for p-aminophenol that are similar to a highly active reduced graphene electrode.[38] Overall, the PCL graphite composites show electrochemical activity similar to more carbon materials that require more extensive synthesis, fabrication, and modification such as carbon nanotubes or graphene. This excellent electrochemical activity most likely results from the sanding step which is hypothesized to activate and exfoliate the electrode surface by exposing freshly cleaved graphite.[28]

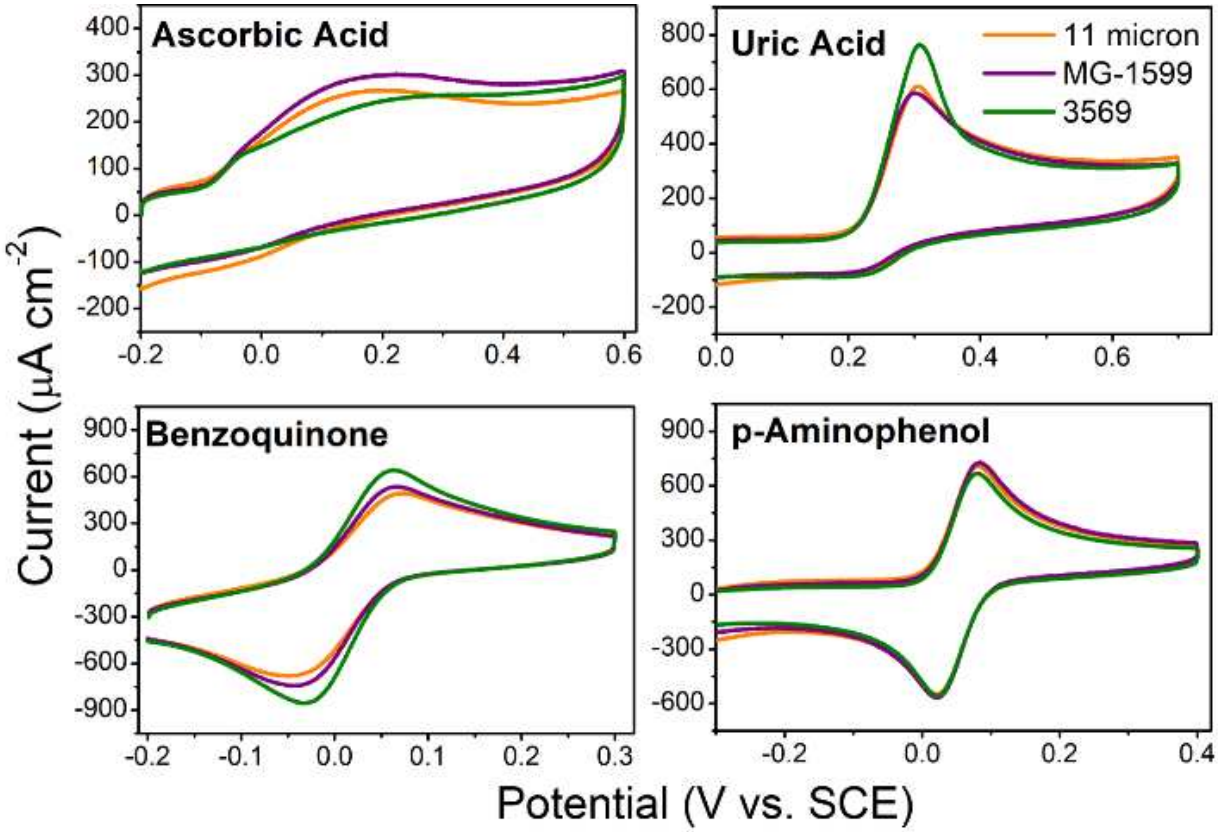

Figure 2.6 Cyclic voltammetry of 1 mM substrate in 0.1 M phosphate buffer (pH 7.4), scan rate was 100 mV s^{-1}. All electrodes are in a 1:2 PCL:carbon ratio.

Fabrication of PCL-sealed Microfluidics with Integrated Electrodes

After electrochemical characterization of the composites, 1:2 PCL:MG-1599 was chosen for integration into microfluidic devices. The 1:2 ratio has a significant percentage of PCL within the composite, which may help with sealing the electrodes in devices. It was also observed that

TPEs with lower percentages of carbon pressed into templates easier than higher ratios, simplifying fabrication. PMMA was chosen as a base material to fabricate microfluidics due to previous reports in microfluidic device fabrication with a CO_2 laser in particular.[39-42]

Sealing PMMA-based microfluidics has been done with a variety of techniques,[43] including thermal bonding,[44] plasma treatment,[45] plastisizers,[46] microwave treatment,[47] ultrasonic assisted bonding,[48] or solvent bonding.[49, 50] Other reports have used a thin adhesive layer to join the two halves.[51, 52] Here, the devices assembled here were sealed by applying a thin layer of PCL. PCL has a lower melting temperature than PMMA and, when heated under pressure, can bond two pieces without deforming the PMMA.[53] Prior to this work, there was only a single report on the use of PCL as a sealing layer from the Remcho group.[54] This report required a spin coater to apply the PCL layer onto a substrate.[54] To simplify the coating process and eliminate the need for specialized equipment, a "push coating" method was developed, which had previously been used for creating patterned thin film transistors.[55]

Figure 2.7 shows the fabrication process of PCL sealed devices. First, a small amount of PCL:DCM solution (1:100 by mass) was poured onto a silicon wafer. Next, a blank PMMA slide was firmly pressed by hand onto the PCL:DCM solution (**Figure 2.7(A)**). After the PMMA was removed, there was an average PCL coating thickness of 3 ± 1 µm (n=9). The microfluidic channel was then generated with a CO_2 laser operating in raster mode, shown in **Figure 2.7(B)**. In contrast to previous PCL-sealed microfluidics,[54] the channel was cut into the plate containing the PCL film. Channel dimensions were defined by the optics of the laser used and typical channel dimensions were 150 µm deep and 300 µm wide; however, these could theoretically be made smaller with a more precise laser.

To seal the device, the two PMMA halves per placed in a heated press at 85 ºC for 5 min. Alternatively, halves could be clamped and heated in an 85 ºC oven, although this method required longer times. The chip needed to be cooled under pressure to maintain the seal. The electrode layer was reusable many times over by heating the chip above 70 ^{0}C and prying apart the layers. The electrode layer could then be sanded resulting in a renewed surface.

Connecting pumps to microfluidic devices can be problematic.[37] Here, connections to the chips were made with a unique laser cut PMMA and O-ring detachable interface. The reusable connection pieces are labelled "interface layer" in **Figure 2.7(C)**. PMMA was rastered (ablated) to accommodate an O-ring and then tapped to accept threaded standard microfluidic fittings. The interface layer is simply bolted to the sealed chip.

Electrochemistry of PCL Composites in a Droplet Generator

Electrochemical measurements in droplets was first reported in 2008.[56] Since then, there are only a handful of examples of electrochemistry in droplets within microfluidic devices.[57-62] There are many different configurations for microfluidic droplet generators.[63] In this work, a pinching droplet generator was selected. **Figure 2.8(A)** shows droplets being generated in the device. PMMA is not sufficiently hydrophobic to create water-in-oil droplets so the channels were silanized, as previously reported.[64]

The device used 3 inlets and the total flow rate of the oil and the aqueous phase was kept a constant 8 µL min^{-1}. Representative amperometry results sensing ferricyanide in water droplets is shown in **Figure 2.8(B)**. **Figure 2.8(C)** shows a smaller interval of time where the signal is very consistent and stable. However, it can be seen in **Figure 2.8(B)** that the peak currents are decreasing. The drop in signal is most likely a result of the non-conductive oil phase coating the electrode surface with an insulating layer that deactivates the surface.[62]

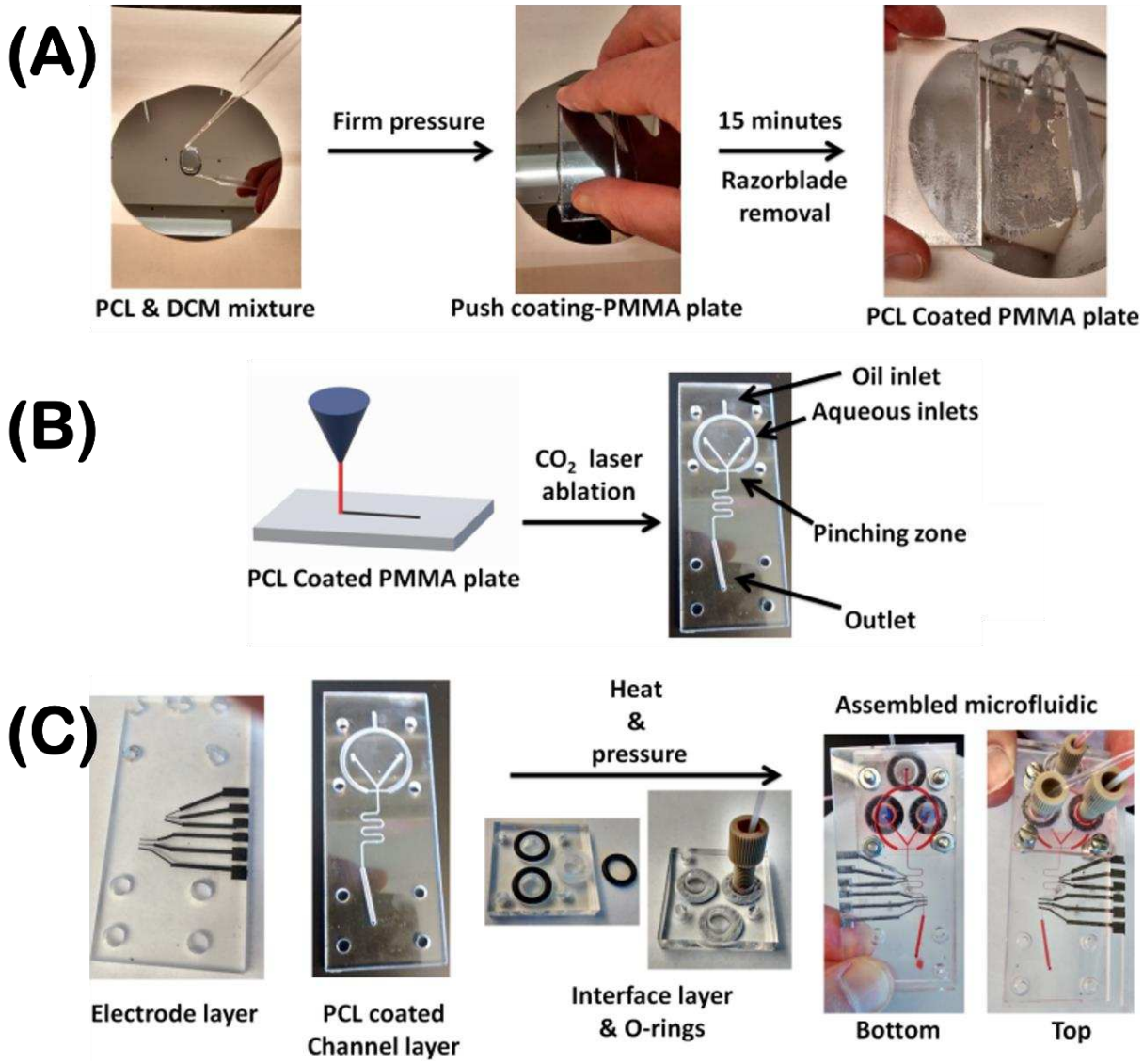

Figure 2.7 General procedure for assembling PCL enabled carbon composite electrochemical microfluidics. **(A)** The PMMA slide is coated with PCL. **(B)** Microfluidic channels are defined using a CO_2 laser. **(C)** Device is assembled and interface layer is added to connect pump. This figure was adapted from a schematic created by Kevin Klunder.

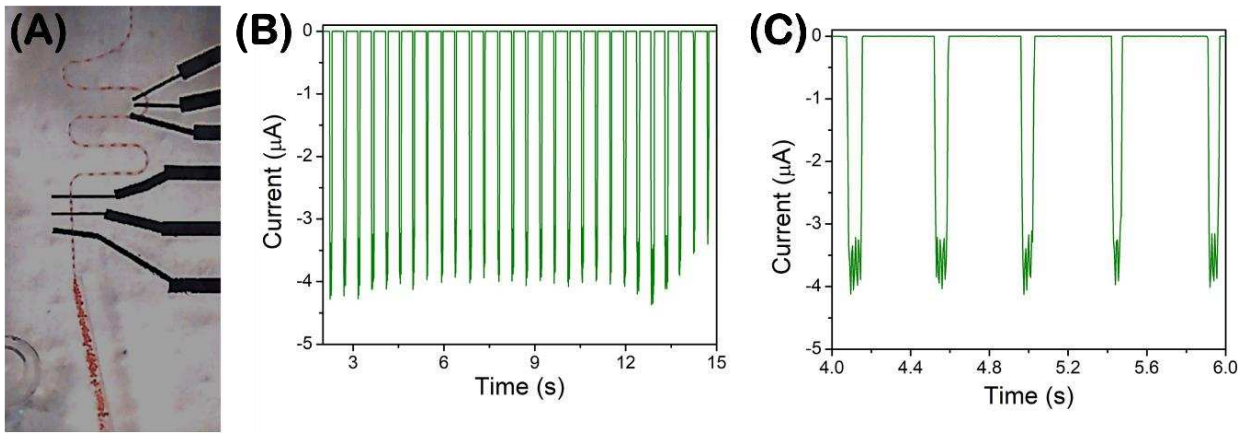

Figure 2.8 **(A)** Image of PCL electrodes interfaced to a channel in a sealed device and water-in-oil droplets visualized with red dye. Representative amperogram of detection of droplets containing 1 mM of ferricyanide in 0.5 M KCl with the sealed device over **(B)** 15 s and zoomed in on a **(C)** 2 s interval. Potential was held at -0.4 V vs. carbon. These data were collected by Kevin Klunder.

2.5 Conclusions

In conclusion, PCL has enabled the integration of carbon composite electrodes into complex microfluidics through a simple process. The new PCL composite electrodes are quickly and easily fabricated and have electrocatalytic activity that is comparable to much more complex composite electrodes as well as traditional carbon electrodes such as glassy carbon. This work demonstrates the ability to tune the electrochemical characteristics of the electrodes by altering PCL:carbon ratios and changing carbon type. Additionally, the use of a CO_2 laser cutter has also enabled a fast and highly robust assembly of the microfluidic devices. The techniques proposed enable quickly prototyping new electrochemical microfluidic designs, overcoming the challenges often presented with electrode integration. Because of the ease of fabrication and promising proof-of-concept, this work has significant impact for a wide range of fields relating to electroanalytical chemistry, or other applications requiring intricate, well-integrated electrodes placed within microfluidic devices.

REFERENCES

1. Dincer, C.; Bruch, R.; Kling, A.; Dittrich, P. S.; Urban, G. A., Multiplexed Point-of-Care Testing - xPOCT. *Trends in biotechnology* **2017,** *35* (8), 728-742.

2. Sameenoi, Y.; Koehler, K.; Shapiro, J.; Boonsong, K.; Sun, Y.; Collett, J.; Volckens, J.; Henry, C. S., Microfluidic Electrochemical Sensor for On-Line Monitoring of Aerosol Oxidative Activity. *Journal of the American Chemical Society* **2012,** *134* (25), 10562-10568.

3. Rackus, D. G.; Shamsi, M. H.; Wheeler, A. R., Electrochemistry, biosensors and microfluidics: a convergence of fields. *Chemical Society Reviews* **2015,** *44* (15), 5320-5340.

4. Kudr, J.; Zitka, O.; Klimanek, M.; Vrba, R.; Adam, V., Microfluidic electrochemical devices for pollution analysis–A review. *Sensors and Actuators B: Chemical* **2017,** *246*, 578-590.

5. Pletcher, D.; Green, R. A.; Brown, R. C. D., Flow Electrolysis Cells for the Synthetic Organic Chemistry Laboratory. *Chemical Reviews* **2018,** *118* (9), 4573-4591.

6. Folgueiras-Amador, A. A.; Wirth, T., Perspectives in Flow Electrochemistry. *Journal of Flow Chemistry* **2017,** *7* (3), 94-95.

7. Tujunen, N.; Kaivosoja, E.; Protopopova, V.; Valle-Delgado, J. J.; Österberg, M.; Koskinen, J.; Laurila, T., Electrochemical detection of hydrogen peroxide on platinum-containing tetrahedral amorphous carbon sensors and evaluation of their biofouling properties. *Materials Science and Engineering: C* **2015,** *55*, 70-78.

8. Kuhnline, C. D.; Gangel, M. G.; Hulvey, M. K.; Martin, R. S., Detecting thiols in a microchip device using micromolded carbon ink electrodes modified with cobalt phthalocyanine. *Analyst* **2006,** *131* (2), 202-207.

9. Villalba, M. M.; Davis, J., New directions for carbon-based detectors: exploiting the versatility of carbon substrates in electroanalysis. *Journal of Solid State Electrochemistry* **2008,** *12* (10), 1245-1254.

10. Peltola, E.; Sainio, S.; Holt, K. B.; Palomäki, T.; Koskinen, J.; Laurila, T., Electrochemical Fouling of Dopamine and Recovery of Carbon Electrodes. *Analytical Chemistry* **2018,** *90* (2), 1408-1416.

11. Hamedi, M. M.; Unal, B.; Kerr, E.; Glavan, A. C.; Fernandez-Abedul, M. T.; Whitesides, G. M., Coated and uncoated cellophane as materials for microplates and open-channel microfluidics devices. *Lab on a Chip* **2016,** *16* (20), 3885-3897.

12. Pereira, S. V.; Bertolino, F. A.; Fernandez-Baldo, M. A.; Messina, G. A.; Salinas, E.; Sanz, M. I.; Raba, J., A microfluidic device based on a screen-printed carbon electrode with electrodeposited gold nanoparticles for the detection of IgG anti-Trypanosoma cruziantibodies. *Analyst* **2011,** *136* (22), 4745-4751.

13. Kovarik, M. L.; Torrence, N. J.; Spence, D. M.; Martin, R. S., Fabrication of carbon microelectrodes with a micromolding technique and their use in microchip-based flow analyses. *Analyst* **2004,** *129* (5), 400-405.

14. Moore, C. M.; Minteer, S. D.; Martin, R. S., Microchip-based ethanol/oxygen biofuel cell. *Lab on a Chip* **2005,** *5* (2), 218-225.

15. Chen, C.-H.; Lin, Y.-T.; Lin, M.-S., Fabrication of a totally renewable off-channel amperometric platform for microchip electrophoresis. *Analytica Chimica Acta* **2015,** *874*, 33-39.

16. Erkal, J. L.; Selimovic, A.; Gross, B. C.; Lockwood, S. Y.; Walton, E. L.; McNamara, S.; Martin, R. S.; Spence, D. M., 3D Printed Microfluidic Devices with Integrated Versatile and Reusable Electrodes. *Lab on a chip* **2014,** *14* (12), 2023-2032.

17. Selimovic, A.; Johnson, A. S.; Kiss, I. Z.; Martin, R. S., Use of epoxy-embedded electrodes to integrate electrochemical detection with microchip-based analysis systems. *ELECTROPHORESIS* **2011,** *32* (8), 822-831.

18. Johnson, A. S.; Selimovic, A.; Martin, R. S., Integration of microchip electrophoresis with electrochemical detection using an epoxy-based molding method to embed multiple electrode materials. *ELECTROPHORESIS* **2011,** *32* (22), 3121-3128.

19. Xu, X.; Weber, S. G., Carbon fiber/epoxy composite ring–disk electrode: Fabrication, characterization and application to electrochemical detection in capillary high performance liquid chromatography. *Journal of Electroanalytical Chemistry* **2009,** *630* (1), 75-80.

20. Sameenoi, Y.; Mensack, M. M.; Boonsong, K.; Ewing, R.; Dungchai, W.; Chailapakul, O.; Cropek, D. M.; Henry, C. S., Poly(dimethylsiloxane) cross-linked carbon paste electrodes for microfluidic electrochemical sensing. *Analyst* **2011,** *136* (15), 3177-3184.

21. Wang, J.; Pumera, M.; Chatrathi, M. P.; Escarpa, A.; Konrad, R.; Griebel, A.; Dörner, W.; Löwe, H., Towards disposable lab-on-a-chip: Poly(methylmethacrylate) microchip electrophoresis device with electrochemical detection. *ELECTROPHORESIS* **2002,** *23* (4), 596-601.

22. Labet, M.; Thielemans, W., Synthesis of polycaprolactone: a review. *Chemical Society Reviews* **2009,** *38* (12), 3484-3504.

23. Malikmammadov, E.; Tanir, T. E.; Kiziltay, A.; Hasirci, V.; Hasirci, N., PCL and PCL-based materials in biomedical applications. *Journal of Biomaterials Science, Polymer Edition* **2018,** *29* (7-9), 863-893.

24. Woodruff, M. A.; Hutmacher, D. W., The return of a forgotten polymer—Polycaprolactone in the 21st century. *Progress in Polymer Science* **2010,** *35* (10), 1217-1256.

25. Tamashausky, A. V. Graphite. A Closer Look.

26. NovoCarbon High Purity Graphites.

27. Bigg, D., An investigation of the effect of carbon black structure, polymer morphology, and processing history on the electrical conductivity of carbon-black-filled thermoplastics. *Journal of Rheology* **1984,** *28* (5), 501-516.

28. Klunder, K. J.; Nilsson, Z.; Sambur, J. B.; Henry, C. S., Patternable Solvent-Processed Thermoplastic Graphite Electrodes. *Journal of the American Chemical Society* **2017,** *139* (36), 12623-12631.

29. Lowe, E. R.; Banks, C. E.; Compton, R. G., Edge Plane Pyrolytic Graphite Electrodes for Halide Detection in Aqueous Solutions. *Electroanalysis* **2005,** *17* (18), 1627-1634.

30. Aller Pellitero, M.; Guimerà, A.; Villa, R.; del Campo, F. J., iR Drop Effects in Self-Powered and Electrochromic Biosensors. *The Journal of Physical Chemistry C* **2018,** *122* (5), 2596-2607.

31. McCreery, R. L., Advanced Carbon Electrode Materials for Molecular Electrochemistry. *Chemical Reviews* **2008,** *108*, 2646-2687.

32. Asadian, E.; Ghalkhani, M.; Shahrokhian, S., Electrochemical sensing based on carbon nanoparticles: A review. *Sensors and Actuators B: Chemical* **2019,** *293*, 183-209.

33. Niwa, O.; Xu, Y.; Halsall, H. B.; Heineman, W. R., Small-volume voltammetric detection of 4-aminophenol with interdigitated array electrodes and its application to electrochemical enzyme immunoassay. *Analytical Chemistry* **1993,** *65* (11), 1559-1563.

34. Slate, A. J.; Brownson, D. A. C.; Abo Dena, A. S.; Smith, G. C.; Whitehead, K. A.; Banks, C. E., Exploring the electrochemical performance of graphite and graphene paste electrodes composed of varying lateral flake sizes. *Physical Chemistry Chemical Physics* **2018**.

35. Musameh, M.; Lawrence, N. S.; Wang, J., Electrochemical activation of carbon nanotubes. *Electrochemistry Communications* **2005,** *7* (1), 14-18.

36. Argüello, J.; Leidens, V. L.; Magosso, H. A.; Ramos, R. R.; Gushikem, Y., Simultaneous voltammetric determination of ascorbic acid, dopamine and uric acid by methylene blue adsorbed on a phosphorylated zirconia–silica composite electrode. *Electrochimica Acta* **2008,** *54* (2), 560-565.

37. Quan, M.; Sanchez, D.; Wasylkiw, M. F.; Smith, D. K., Voltammetry of Quinones in Unbuffered Aqueous Solution: Reassessing the Roles of Proton Transfer and Hydrogen Bonding in the Aqueous Electrochemistry of Quinones. *J. Am. Chem. Soc.* **2007,** *129* (42), 12847-12856.

38. Vilian, A. T. E.; Veeramani, V.; Chen, S.-M.; Madhu, R.; Huh, Y. S.; Han, Y.-K., Preparation of a reduced graphene oxide/poly-l-glutathione nanocomposite for electrochemical detection of 4-aminophenol in orange juice samples. *Analytical Methods* **2015,** *7* (13), 5627-5634.

39. Davim, J. P.; Barricas, N.; Conceição, M.; Oliveira, C., Some experimental studies on CO2 laser cutting quality of polymeric materials. *Journal of Materials Processing Technology* **2008,** *198* (1), 99-104.

40. Choudhury, I. A.; Shirley, S., Laser cutting of polymeric materials: An experimental investigation. *Optics & Laser Technology* **2010,** *42* (3), 503-508.

41. Shashi, P.; Subrata, K., Profile and depth prediction in single-pass and two-pass CO 2 laser microchanneling processes. *Journal of Micromechanics and Microengineering* **2015,** *25* (3), 035010.

42. Yuan, D.; Das, S., Experimental and theoretical analysis of direct-write laser micromachining of polymethyl methacrylate by CO2 laser ablation. *Journal of Applied Physics* **2007,** *101* (2), 024901.

43. Temiz, Y.; Lovchik, R. D.; Kaigala, G. V.; Delamarche, E., Lab-on-a-chip devices: How to close and plug the lab? *Microelectronic Engineering* **2015,** *132*, 156-175.

44. Zhu, X.; Liu, G.; Guo, Y.; Tian, Y., Study of PMMA thermal bonding. *Microsyst Technol* **2007,** *13* (3), 403-407.

45. Liu, J.; Qiao, H.; Liu, C.; Xu, Z.; Li, Y.; Wang, L., Plasma assisted thermal bonding for PMMA microfluidic chips with integrated metal microelectrodes. *Sensor. Actuat. B-Chem.* **2009,** *141* (2), 646-651.

46. Duan, H.; Zhang, L.; Chen, G., Plasticizer-assisted bonding of poly(methyl methacrylate) microfluidic chips at low temperature. *Journal of Chromatography A* **2010,** *1217* (1), 160-166.

47. Toossi, A.; Moghadas, H.; Daneshmand, M.; Sameoto, D., Bonding PMMA microfluidics using commercial microwave ovens. *Journal of Micromechanics and Microengineering* **2015,** *25* (8), 085008.

48. Luo, Y.; Zhang, Z.; Wang, X.; Zheng, Y., Ultrasonic bonding for thermoplastic microfluidic devices without energy director. *Microelectronic Engineering* **2010,** *87* (11), 2429-2436.

49. Arshya, B.; Alireza, N.; Hossein, K., A new simple and fast thermally-solvent assisted method to bond PMMA–PMMA in micro-fluidics devices. *Journal of Micromechanics and Microengineering* **2016,** *26* (6), 065017.

50. Gan, Z.; Zhang, L.; Chen, G., Solvent bonding of poly(methyl methacrylate) microfluidic chip using phase-changing agar hydrogel as a sacrificial layer. *Electrophoresis* **2011,** *32* (23), 3319-3323.

51. Tsao, C.-W.; DeVoe, D., Bonding of thermoplastic polymer microfluidics. *Microfluid Nanofluid* **2009,** *6* (1), 1-16.

52. Wasay, A.; Sameoto, D., Gecko gaskets for self-sealing and high-strength reversible bonding of microfluidics. *Lab on a Chip* **2015,** *15* (13), 2749-2753.

53. Yu, H.; Chong, Z. Z.; Tor, S. B.; Liu, E.; Loh, N. H., Low temperature and deformation-free bonding of PMMA microfluidic devices with stable hydrophilicity via oxygen plasma treatment and PVA coating. *RSC Advances* **2015,** *5* (11), 8377-8388.

54. Myra, T. K.; Jintana, N.; Yuanyuan, W.; Ryan, T. F.; Vincent, T. R., Cost-efficient fabrication techniques for microchips and interconnects enabled by polycaprolactone. *Journal of Micromechanics and Microengineering* **2012,** *22* (11), 115030.

55. Ikawa, M.; Yamada, T.; Matsui, H.; Minemawari, H.; Tsutsumi, J. y.; Horii, Y.; Chikamatsu, M.; Azumi, R.; Kumai, R.; Hasegawa, T., Simple push coating of polymer thin-film transistors. *Nature Communications* **2012,** *3*, 1176.

56. Liu, S.; Gu, Y.; Le Roux, R. B.; Matthews, S. M.; Bratton, D.; Yunus, K.; Fisher, A. C.; Huck, W. T. S., The electrochemical detection of droplets in microfluidic devices. *Lab on a Chip* **2008,** *8* (11), 1937-1942.

57. Wu, C.; Shah, A.; Ye, H.; Chen, X.; Ye, J.; Jiang, H.; Chen, B.; Wang, X.; Yan, H., Droplet electrochemical study of the pH dependent redox behavior of novel ferrocenyl-carborane derivatives and its application in specific cancer cell recognition. *Analytica Chimica Acta* **2015,** *857*, 39-45.

58. Rattanarat, P.; Suea-Ngam, A.; Ruecha, N.; Siangproh, W.; Henry, C. S.; Srisa-Art, M.; Chailapakul, O., Graphene-polyaniline modified electrochemical droplet-based microfluidic sensor for high-throughput determination of 4-aminophenol. *Analytica Chimica Acta* **2016,** *925*, 51-60.

59. Gu, S.; Lu, Y.; Ding, Y.; Li, L.; Song, H.; Wang, J.; Wu, Q., A droplet-based microfluidic electrochemical sensor using platinum-black microelectrode and its application in high sensitive glucose sensing. *Biosensors and Bioelectronics* **2014,** *55*, 106-112.

60. Lin, X.; Hu, X.; Bai, Z.; He, Q.; Chen, H.; Yan, Y.; Ding, Z., A microfluidic chip capable of switching W/O droplets to vertical laminar flow for electrochemical detection of droplet contents. *Analytica Chimica Acta* **2014,** *828*, 70-79.

61. Abadie, T.; Sella, C.; Thouin, L., Electrochemical detection of droplet content in microfluidic devices: Evidence of internal recirculating convection within droplets. *Electrochemistry Communications* **2017,** *80*, 55-59.

62. Liu, H.; Crooks, R. M., Highly reproducible chronoamperometric analysis in microdroplets. *Lab on a Chip* **2013,** *13* (7), 1364-1370.

63. Teh, S.-Y.; Lin, R.; Hung, L.-H.; Lee, A. P., Droplet microfluidics. *Lab on a Chip* **2008,** *8* (2), 198-220.

64. Subramanian, B.; Kim, N.; Lee, W.; Spivak, D. A.; Nikitopoulos, D. E.; McCarley, R. L.; Soper, S. A., Surface Modification of Droplet Polymeric Microfluidic Devices for the Stable and Continuous Generation of Aqueous Droplets. *Langmuir* **2011,** *27* (12), 7949-7957.

CHAPTER 3: THERMOPLASTIC ELECTRODE (TPE)-BASED ENZYMATIC GLUCOSE SENSOR USING POLYCAPROLACTONE-GRAPHITE COMPOSITES

3.1 Chapter Overview

Monitoring biomolecules, such as glucose, is essential to the management and treatment of many diseases. Electrochemical detection allows for highly sensitive and selective, continuous measurements of molecules with fast response times. Carbon composite electrodes are an attractive option for electrochemical detection due to their low cost, easy fabrication, and ability to be patterned. Enzymatic electrodes use enzymes as a detection scheme for biomolecules and are a crucial portion of today's biosensor market. Carbon composite electrodes are commonly used for enzymatic electrodes; they often underperform compared to traditional metallic electrodes or other carbon-based electrodes like glassy carbon. Our group has recently developed new carbon composite electrodes called thermoplastic electrodes (TPEs) that use a thermopolymer. Because of the binder, the electrode material can be easily molded into intricate structures without extensive use of organic solvents. TPEs demonstrate comparable electrochemical performance to traditional metallic electrodes with the advantages of carbon electrodes like resistance to fouling and large potential window. The simple fabrication also allows catalysts and enzymes to be mixed directly into the material to enhance detection. Here, we report the first use of polycaprolactone (PCL) as the thermopolymer binder to make TPE glucose sensors. The TPE material is bulk-modified with cobalt phthalocyanine, an electrocatalyst, and glucose oxidase, resulting in a robust sensor that maintains a stable current response for over 100 minutes. These sensors can be molded into intricate shapes and sanded for surface renewal (without requiring additional steps to maintain the modification), allowing the sensors to be continuously reused even if damaged or fouled. The work from this chapter was published in *Electroanalysis* entitled "Thermoplastic Electrode (TPE)-Based

Enzymatic Glucose Sensor Using Polycaprolactone-Graphite Composites." I was the sole author on this work and performed all experiments in this chapter.

3.2 Introduction

Carbon composite electrodes are an attractive option for sensing due to their low cost, easy fabrication, biocompatibility, and wide potential windows.[1] A major disadvantage of the typical carbon composite electrodes, i.g. screen-printed electrodes, is that the electron transfer kinetics and other electrochemical properties are lacking relative to metallic electrodes and other carbon-based electrodes such as glassy carbon.[2] Enzymatic electrodes are one of the most widely used versions of carbon composite electrodes. Enzymatic electrodes use immobilized enzymes on the electrode surface to convert electroinactive substrates of interest into electroactive products that can be electrochemically quantified.[3]

The first enzymatic-electrochemical sensor was reported by Clark and Lyons in 1962.[4] Now, enzymatic glucose sensors are still a vital research field and a $12.64 billion market in 2020 because of the growing demand for diabetes management.[5-8] In addition to glucose, enzymatic sensors are used to detect hundreds of other biologically relevant molecules such as lactate, acetylcholine, glutamate, and malate.[9] Effective immobilization of enzymes on electrode surfaces is crucial to developing effective biosensors. There are a wide variety of immobilization techniques including physical adsorption,[10] entrapment in a semipermeable membrane,[11] covalent bonding,[12] crosslinking,[13] and electrochemical polymerization.[14] Many of these techniques can be tedious, complicated, or the modification can be easily damaged.[8]

Many enzymatic sensors rely on hydrogen peroxide (H_2O_2) quantification to detect biomolecules of interest because it is produced in glucose oxidase and all oxidase reactions.

Carbon composite electrodes often require an electrocatalyst for H_2O_2 redox chemistry due to inferior electron transfer capabilities compared to traditional metallic electrodes. CoPC is widely used for H_2O_2 detection because it is nontoxic, biocompatible, and inexpensive.[15-17] In previous reports, dropcasting CoPC directly onto an electrode surface has been demonstrated effectively, although dispersion on the electrode surface is often heterogenous and reproducibility can be an issue.[18] Also, CoPC-modified electrode surfaces often have relatively low conductivity and can detach from the electrode surface over time.[16] To overcome these limitations, CoPC has been successfully incorporated into reduced graphene oxide electrodes as opposed to being adsorbed on the electrode surface; however, this often involves multistep time-consuming syntheses.[16, 17] To simplify the modification even further, CoPC has been directly mixed into carbon composite electrode materials to avoid synthesis steps altogether.[19] Incorporating CoPC directly into carbon inks has allowed for the production of reproducible and mass-produced screen-printed electrodes, yet these electrodes still underperform relative to traditional metallic and glassy carbon electrodes.[18]

Thermoplastic electrodes (TPEs), first introduced in 2017, use thermopolymer binders that become soft and moldable when heated and harden when cooled.[20] TPEs present a very attractive alternative electrode material due to their tunable mechanical and electrochemical properties. TPEs have been demonstrated as effective electrodes for basic electrochemistry and immunosensors, comparable to traditional glassy carbon electrodes.[20-25] Polycaprolactone (PCL) has been demonstrated as an effective TPE binder and has a melting point of 60°C which allows the electrode material to be molded into patterns with fine details more easily.[21]

Here, TPEs were successfully applied as enzymatic glucose sensors using PCL as the thermoplastic binder. The low melting point of PCL enables the electrode material to be

manipulated into molds without high temperature that could denature the enzymes. The presented sensors directly incorporate cobalt phthalocyanine (CoPC) and glucose oxidase (GOx) directly into the material for bulk-modification. The TPE glucose electrodes wield the advantages of traditional enzymatic carbon composite electrodes (biocompatible, inexpensive, etc.) with the added advantages of TPEs (moldable, reusable, renewable surface, etc.) to create robust enzymatic sensors. The simple fabrication of the glucose TPEs show promise for various applications in the biomolecule sensing field.

3.3 Experimental Section

Reagents

Solutions were prepared using 18.2 M Ω · cm water purified using a Milli-Q system (MilliporeSigma, USA). Graphite (MG-1599, size ~15 μm) was purchased from Great Lakes Graphite, Inc. (Toronto, Canada). Polycaprolactone (PCL) was purchased from ThermoMorph® (Toledo, OH). ACS grade dichloromethane, cobalt phthalocyanine, D-glucose, and dimethylformamide were purchased from Sigma-Aldrich (Saint Louis, MO). Fluorescein isothiocyanate was purchased from Thermo Fisher Scientific (Waltham, MA). Glucose oxidase from Aspergillus Niger (crude, 5,730 units/g solid) was purchased from Sigma-Aldrich (Saint Louis, MO).

Fabrication of Bulk-Modified Electrodes

Polycaprolactone (PCL) was first dissolved in dichloromethane (DCM). PCL and graphite (MG-1599) were weighed to make a 1:2 PCL:carbon ratio by mass. Then, 10% CoPC and 10% GOx (by weight of the carbon) were hand-mixed into graphite. For CoPC modified electrodes, no GOx was added at this step. This mixture was added directly to the dissolved PCL, mixed using a

glass rod or wooden applicator, and poured onto a Si wafer to continue mixing and drying. Once the electrode material is completely dry (typically less than 10 minutes), it can be stored in vials in ambient conditions for later use or incorporated into electrode templates. Polymethyl methacrylate templates were designed using CorelDRAW (Corel, Ontario, Canada) and cut using a CO_2 laser cutter (Zing 10000, Epilog Laser), similar to previous work.[20, 21] For the purposes of this work, simple 1.5 mm diameter/3 mm thick disk electrodes were used; however, the ability to mold the electrodes into intricate designs are shown in **Figure 3.1** and in our previous reports.[20-22] The electrode material was then pressed into the templates using a hydraulic heat press at 60°C and 1500-2000 psi. Excess material was then polished away with 600 grit sandpaper, and electrical connections were attached with silver paint. Further polishing to achieve more uniform or regenerate surface was done with finer 1200 grit sandpaper.

Figure 3.1 Image of PCL TPEs pressed in various templates with different shapes and designs.

Surface Imaging

Fluorescence images were taken using a fluorescent Dino-Lite digital microscope (Dino-Lite AM4115T-YFGW) with excitation = 470 nm, emission = 510 nm. 2 mg/mL Fluorescein isothiocyanate (FITC) in dimethylformamide (DMF) was diluted 100x to 20 μg/mL in 0.1 M sodium carbonate (pH 9.5). CoPC and CoPC/GOx electrode material were incubated in the described FITC solution at 5 °C covered in foil overnight and then rinsed before imaging. Surface images were taken of the electrode material using scanning electron microscope (JEOL JSM-6500F). Elemental maps were obtained with dispersive X-ray spectroscopy (EDS) using an Oxford silicon drift detector energy.

Electrochemical Measurements

Electrochemical measurements were recorded using CHI1242 and CHI660b potentiostats (CH Instruments, Inc., Austin, TX). All experiments were performed with a three-electrode system using the CoPC and GOx modified electrodes as the working electrode, a saturated calomel electrode (SCE) as a reference electrode, and larger surface area TPE (with PCL and graphite) as the counter electrode. All solutions were prepared and diluted in 0.05 M phosphate buffer (pH 7.4) prior to measurements. Cyclic voltammetry (CV) to characterize H_2O_2 detection with CoPC-modified TPEs was performed scanning from -1.6 V to +1.6 V at a scan rate of 100 mV/s. CV to characterize glucose detection with CoPC/GOx-modified TPEs was performed scanning from -0.2 V to +0.6 V at a scan rate of 100 mV/s. Potential was held at +0.6 V for amperometry experiments for H_2O_2 and glucose. Analytes were added (~10 μM H_2O_2 aliquots and ~0.5 mM glucose aliquots) into stirred 0.05 M phosphate buffer (pH 7.4) allowing the current to stabilize before adding the next aliquot. For measurements with the TPE glucose sensor, an apple juice sample was diluted 200x in buffer. Standard addition measurements were performed by adding ~0.5 mM glucose

aliquots into the stirred apple juice standard. The currents were plotted and then a best fit line was extrapolated to determine the glucose concentration. Replicate measurements for all CVs and amperometry were recorded by rinsing and reusing the same TPE sensor.

Glucose Assay Kit

The commercial Glucose Assay Kit used to validate the real sample measurements in apple juice was purchased from Sigma Aldrich (Saint Louis, MO). The kit included reagents, standard solutions, and specific instructions to produce a colorimetric reaction to quantify the sample. The kit reacts the sample glucose oxidase, and subsequently reacts the hydrogen peroxide side product with o-dianisidine in the presence of peroxidase to form a colored product. The absorbance of this product was then measured at 540 nm using a traditional UV-Vis spectrometer and the concentration of glucose was determined using a calibration curve made from the provided glucose standards. The apple juice was diluted 12000x in 0.05 M phosphate buffer (pH 7.4) to get the sample into the appropriate range for the assay.

3.4 Results and Discussion

Fabrication of Bulk-Modified Glucose Oxidase Electrodes

Moldable electrodes have been shown to be vital for progress in applications such as non-invasive medical sensors,[26, 27] integrated sensors in microfluidic devices,[28, 29] force sensors,[30] and neural microsensors.[31] Bulk-modification steps for electrocatalysts can require complicated synthesis,[16, 32, 33] while others do not display great electrocatalytic activity.[34] Many enzymatic sensors use surface modifications to incorporate the enzyme,[35] which can be tedious, easily damaged, and often only single-use. This work introduces a simple fabrication method (shown in **Figure 3.2**) to produce bulk-modified, moldable enzymatic electrodes for glucose sensing, that

eliminates the need for complicated modification steps. Similar to previously reported work in our group, polycaprolactone (PCL) is used as a binder because of its low melting point which allows for molding the material easily without excessive heat that could negatively affect the enzyme activity.[21] CoPC and GOx are added directly into the material for modification to increase catalytic activity and allow for detection of glucose, respectively. Mixing and drying the electrode material takes typically less than 10 minutes, and it can be stored in bulk for later use or incorporated directly into electrode templates. The moldable nature of the electrode material is unique and useful allowing electrode geometry to not be limited by the fabrication. Because the material is bulk-modified, these TPE enzymatic electrodes can simply be sanded down to renew the surface if it is damaged or fouled. The sanding removes any residue on the electrode surface and a layer of PCL and graphite to expose more graphitic flakes and fresh GOx. This makes them reusable multiple times, which is a great advantage for many applications, including clinical.

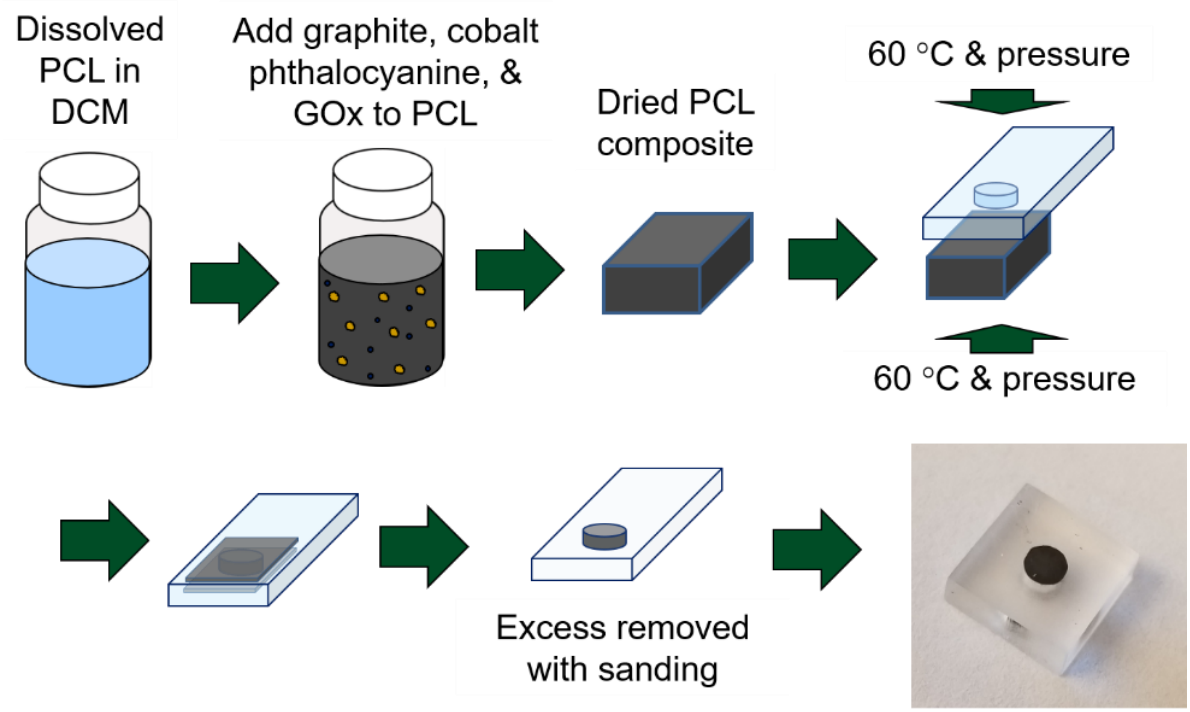

Figure 3.2 Simple fabrication of bulk-modified GOx/CoPC PCL composite electrodes, using templates cut using a CO_2 laser.

Cyclic Voltammetry for Characterization

PCL TPEs are modified with CoPC by mixing it directly into the electrode material, similarly to that of other carbon composite materials.[18, 19] **Figure 3.3(A)** shows CVs obtained with unmodified and bulk modified CoPC TPEs in the presence of H_2O_2. For the unmodified electrodes, the CV in buffer with and without H_2O_2 are nearly identical, reinforcing the fact that H_2O_2 cannot be analyzed on the TPEs without the modification with CoPC. The CVs of CoPC-modified electrodes plotted on the same graph show a significant increase in both anodic current (1.3 mA cm^{-2} around +0.7 V) and cathodic current (2.2 mA cm^{-2} around -0.8 V) in the presence of H_2O_2. The cobalt central atom of the CoPC changes oxidation states from Co(II) to Co(III) at positive potentials, which facilitates electron transfer for the oxidation of H_2O_2. In reverse, at negative potentials the change from Co(II) to Co(I) facilitates electron transfer for the reduction of H_2O_2.[16] These increases in signal show that the CoPC PCL electrodes can be applied toward sensing H_2O_2. The results were further confirmed with amperometric measurements of H_2O_2, resulting in a linear current response with increasing concentration (**Figure 3.4(A)** and **3.4(B)**).

Figure 3.3(B) shows representative CVs (three replicates of the same two electrodes) on electrodes modified with CoPC and GOx and just with CoPC in the presence and absence of glucose. This plot is offset by 110 μA cm^{-2} for clarity. Without GOx modification, there is no signal difference between solutions with and without glucose. With the GOx modification, an increase in anodic current (approximately 70 μA cm^{-2}) is observed at higher positive potentials in the presence of glucose compared with phosphate buffer. This provides evidence that the GOx modification is effective for glucose detection. A difference in capacitance between the non-modified electrode and the electrode modified with GOx is observed on the CVs. The GOx-modified electrode CVs have higher baseline currents than the non-modified electrode CVs, both

in buffer and in glucose. This increased capacitance could be a result of increased surface roughness and broken electron pathways from GOx in the material.[36] The increased current in the CVs from the modified electrodes in glucose demonstrates the feasibility of the sensor to detect glucose.

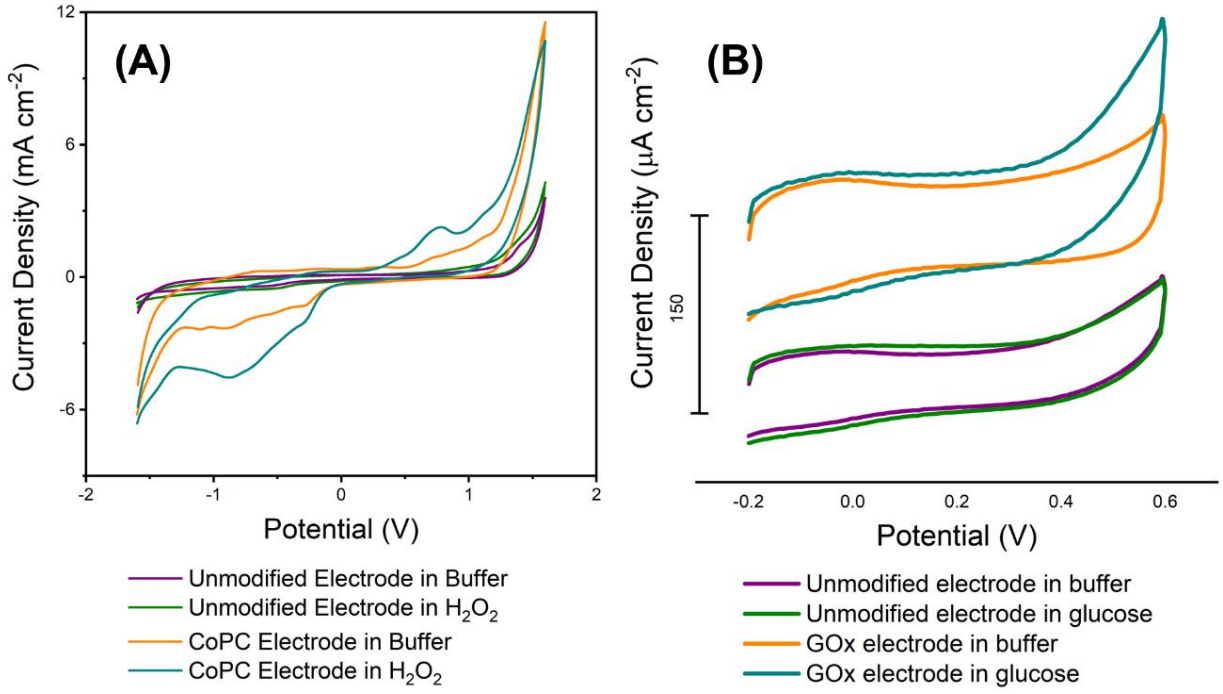

Figure 3.3 (A) Representative CVs (n=3) of an unmodified electrode and a CoPC-modified electrode, in 0.05 M phosphate buffer (pH 7.4) with and without H_2O_2 (5mM). **(B)** Representative CVs (n=3) of a CoPC-modified electrode and a CoPC/GOx-modified electrode in 0.05 M phosphate buffer (pH 7.4) with and without glucose (10 mM). CVs are offset for clarity. Potential was scanned vs. a SCE reference at a scan rate of 100 mV/s for both A and B.

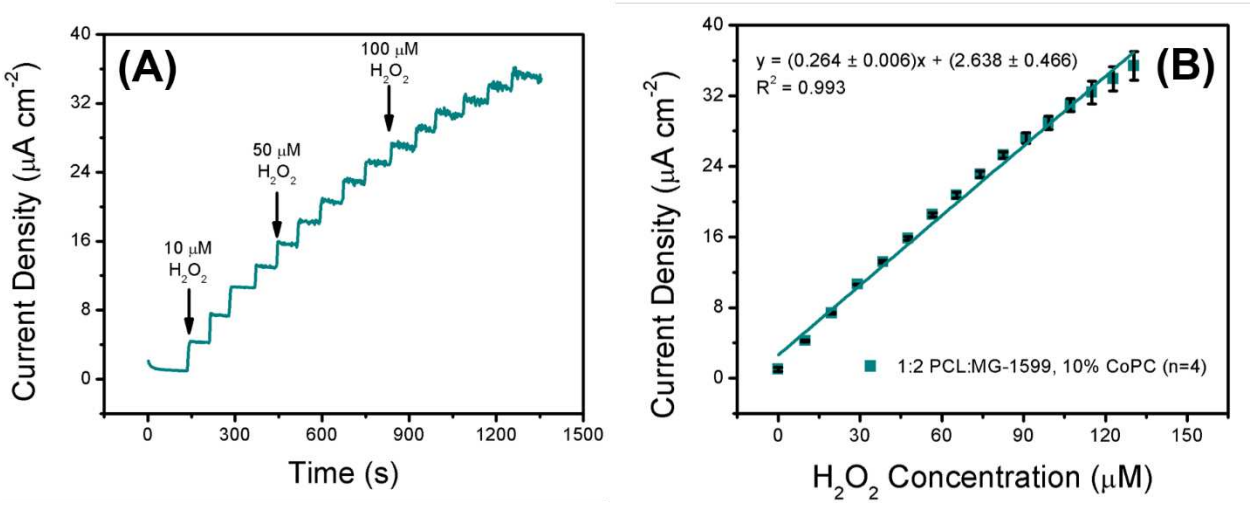

Figure 3.4 (A) Representative amperogram of detection of H_2O_2. Potential held at +0.6 V vs. a SCE reference on CoPC modified electrode adding equal aliquots of H_2O_2 in stirred 0.05 M phosphate buffer (pH 7.4) and **(B)** the resulting H_2O_2 calibration curve using the same electrode for replicates (n=4).

Surface Characterization of Electrode Material

Scanning electron microscopy (SEM) images were taken of the surface of CoPC/GOx modified (**Figure 3.5(A)**) and unmodified (**Figure 3.5(B)**) electrode material. Both images show graphitic flakes on the surface of the material. The exposed edge planes have been shown to increase conductivity and electrocatalytic activity of the electrode surface, which improves performance of this electrode material compared to other carbon composite electrodes in which the binder covers the graphitic edge planes.[2] These properties were explored in greater detail in previous publications.[21] The surface of the CoPC/GOx modified material, however, shows increased surface roughness and more graphitic edges, likely due to the CoPC and GOx interrupting the graphite/PCL composite, further confirming the cause previously discussed for increased capacitance shown in **Figure 3.3(B)**. While most of the images show the conductive graphite exposed from sanding, the lighter areas of the SEM images demonstrate charging which is likely due the PCL binder because it is insulating. There is significantly more charging in the

image without modification, indicating that the addition of CoPC and GOx also helped expose more of the graphite during the sanding process. The modification not only allows for the detection of glucose but also improves surface morphology of the electrode. The surface features shown in the SEM are irregular, which could account for some of the variation in signal across electrodes.

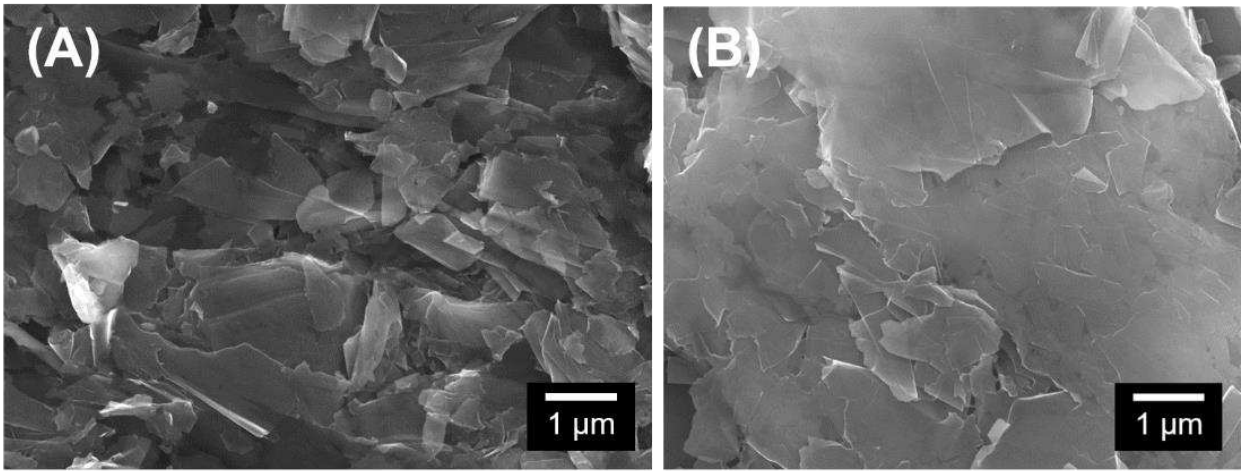

Figure 3.5 SEM image at 15,000x magnification of **(A)** CoPC/GOx modified and **(B)** unmodified electrode material.

In addition to electron images taken with SEM, energy dispersive X-ray spectroscopy (EDS) was used to characterize the elements present on the surface of the electrode material. The map of the Co distribution is shown in **Figure 3.6(A)**. The only source of Co in the electrode material is the CoPC electrocatalyst, so this map should be representative of the CoPC distribution on the surface of the electrode after bulk-modification. After the electrode is sanded, there is comprehensive, relatively even coverage of the CoPC on the surface with minimal aggregation. The background signal of material without CoPC to compare can be seen in **Figure 3.6(B)**. Carbon (originating from both graphite and PCL) coverage (**Figure 3.7(B)**) is consistent with the topography of the electrode material shown in the SEM image for that specific measurement (**Figure 3.7(A)**). The EDS also demonstrated an extensive coverage of oxygen suggesting a large

number of surface oxide groups (**Figure 3.7(C)**). Surface oxide groups have been shown to lead to increased electrocatalytic activity,[2] which is consistent with the excellent performance shown previously for TPE electrode material.[20, 21] Trace amounts of Si were detected on a few samples which likely is residue from sandpaper used for polishing (**Figure 3.7(D)**). EDS spectra can be found in SI for electrode material with (**Figure 3.6(C)**) and without (**Figure 3.6(D)**) CoPC. The spectra also show the calculated percentages of Co for CoPC modified material to be 1.1 ± 0.0 % Co and for unmodified to be 0.0 ± 0.0 % Co.

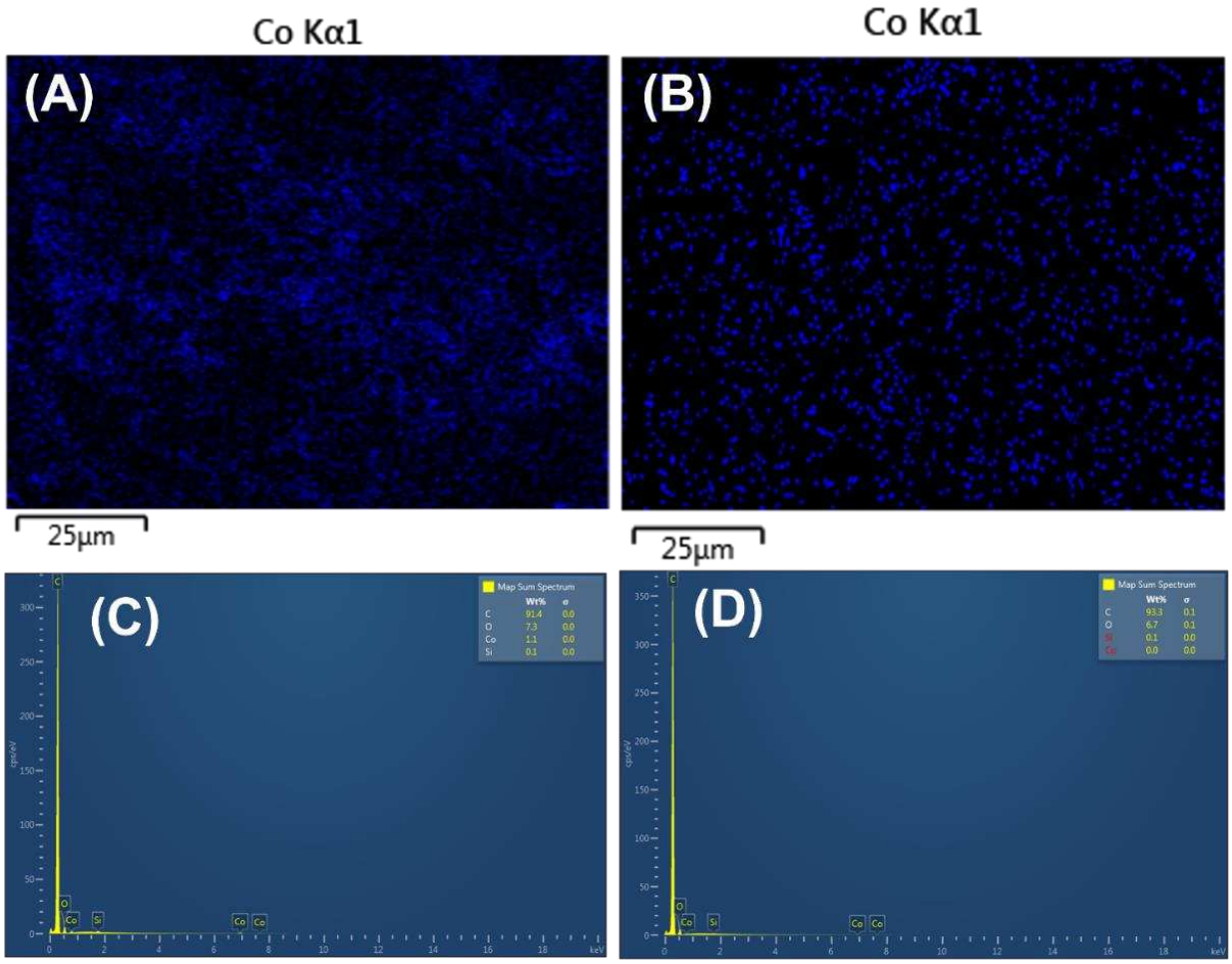

Figure 3.6 **(A)** SEM-EDS image of CoPC/GOx modified electrode material showing the element distribution of cobalt. **(B)** SEM-EDS image of unmodified electrode (no CoPC) material showing the background noise for distribution of cobalt. Representative spectra of elements present in **(C)** modified and **(D)** unmodified electrode material from SEM-EDS analysis.

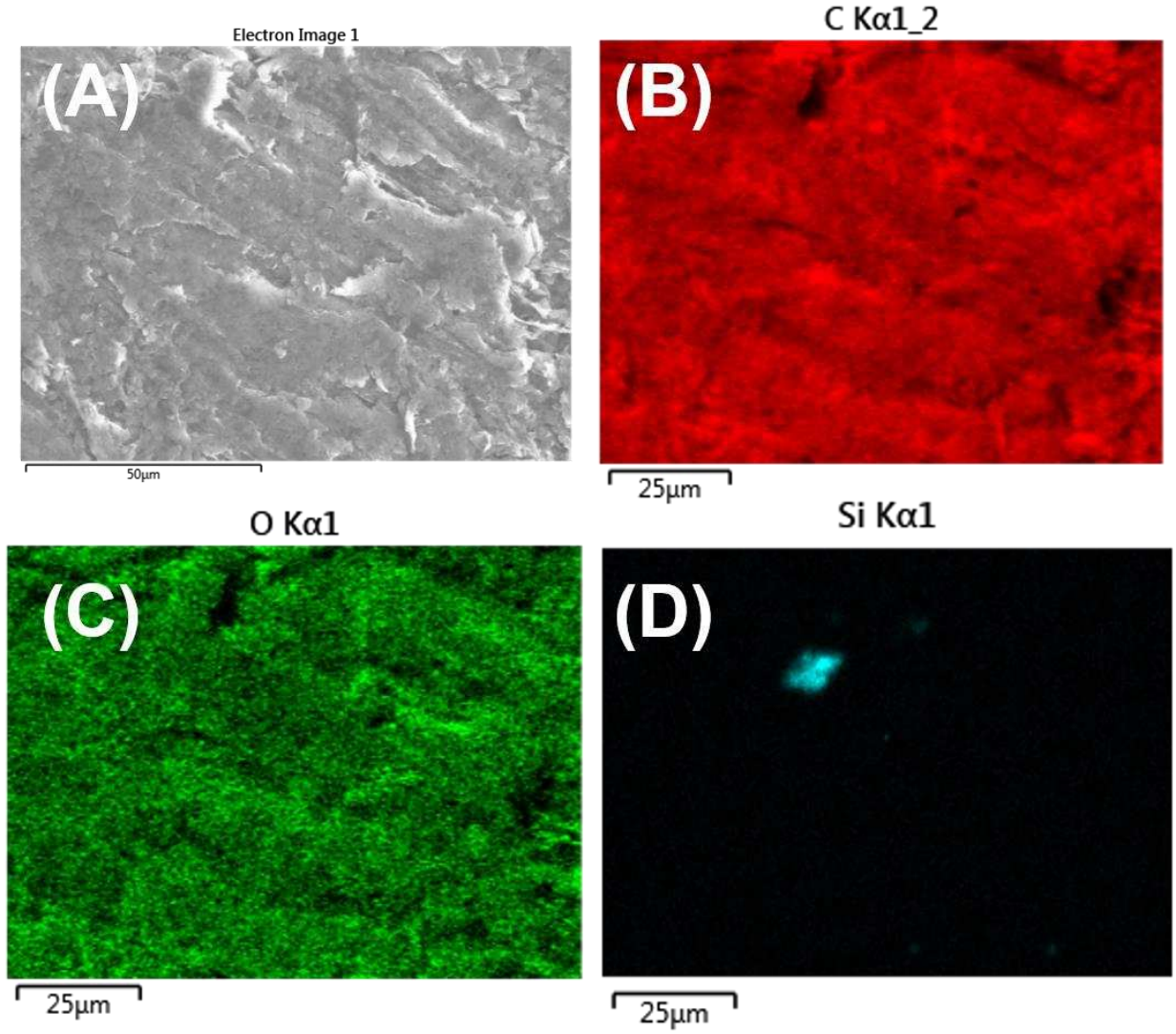

Figure 3.7 SEM-EDS images of 1:2 PCL:MG-1599 with 10% CoPC and 10% GOx showing the **(A)** electron image and element distribution of **(B)** carbon, **(C)** oxygen, and **(D)** silicon.

Fluorescein isothiocyanate (FITC) is an isomer commonly used to fluorescently label antibodies, enzymes, nucleic acids, and other proteins of interest for flow cytometry and immunofluorescence microscopy.[37-39] It is not selective and will couple to any protein due to a reaction with amine groups.[40] CoPC-modified and CoPC/GOx-modified electrode materials were incubated in FITC solutions and then fluorescent images were taken after rinsing (excitation: 470 nm, emission: 510 nm). A clear difference can be observed between the material modified without

(**Figure 3.8(A)**) and with (**Figure 3.8(B)**) GOx modification. While there is some non-specific adsorption on the unmodified material, the significant signal increase on the GOx modified material indicates presence of GOx on the surface after bulk modification. These images also show the non-uniformity of GOx distribution on the surface. The clusters of GOx shown from the FITC images (**Figure 3.8(B)** and **3.9**) explains the electrode variability. **Figure 3.10** shows sensor response for 3 different sensors. Because of the variation in current response across electrodes, for each individual experiment the same electrode was used multiple times for the replicates. Variation of responses from different electrodes is a common problem in electrochemical biosensors both in research and in manufacturing settings, and calibration is often required either in factory or by the end-user prior to use.[41, 42] In future studies with enzymatic TPE sensors, previously reported calibration methods could be employed to address this problem.[43-46]

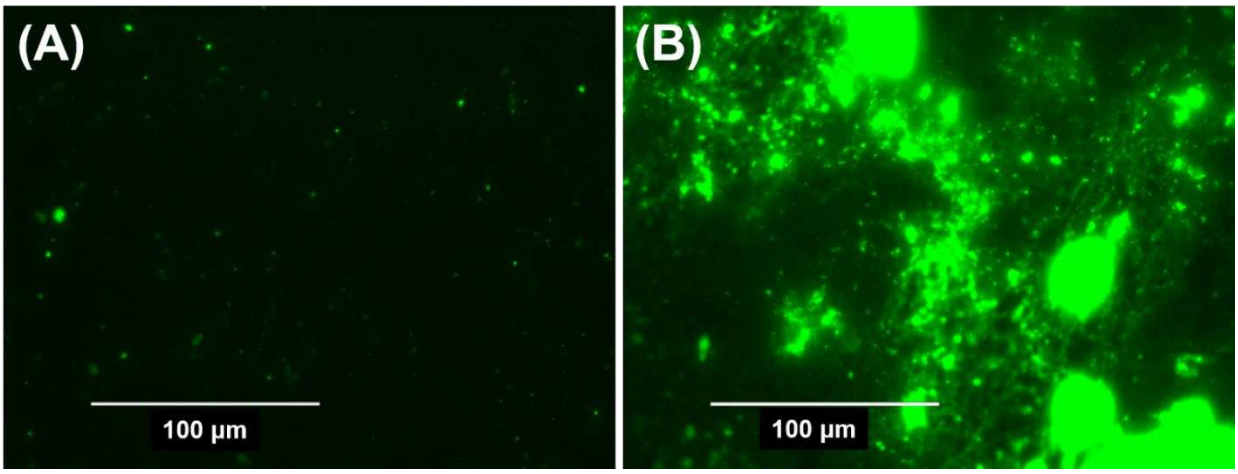

Figure 3.8 Fluorescent microscope images (excitation: 470 nm, emission: 510 nm) at 40x zoom of **(A)** CoPC-modified electrode material and **(B)** CoPC/GOx-modified electrode material, after incubation in 20 µg/mL FITC in 0.1 M sodium carbonate (pH 9.5).

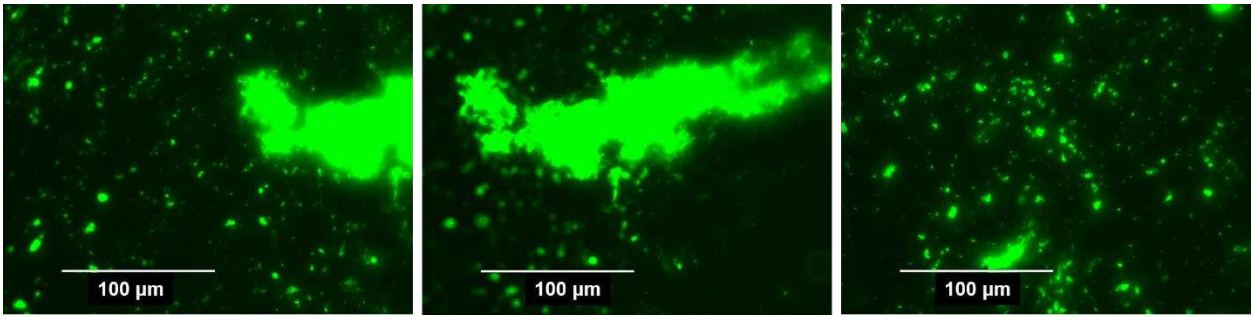

Figure 3.9 Fluorescent microscope images (excitation: 470 nm, emission: 510 nm) at 40x zoom of three different CoPC and GOx modified electrodes, after incubation in 20 µg/mL FITC in 0.1 M sodium carbonate (pH 9.5).

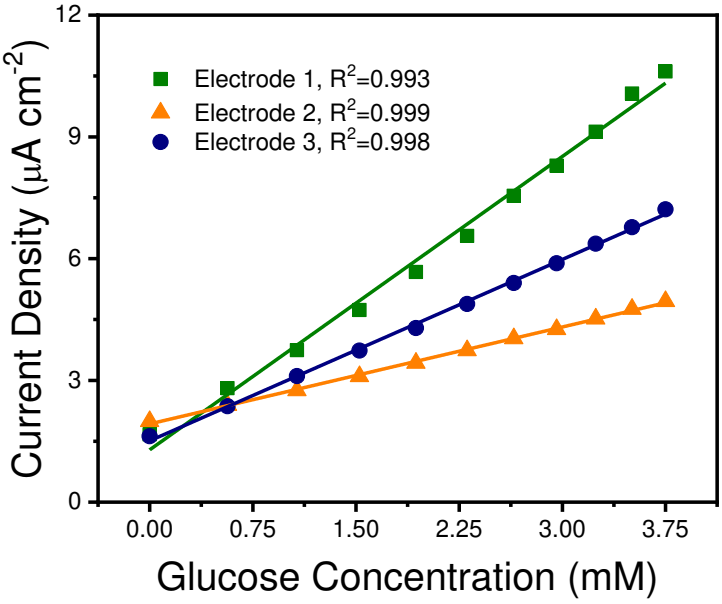

Figure 3.10 Glucose calibration curves of three different GOx/CoPC modified electrodes from amperograms, where potential was held at +0.6 V vs. a SCE reference in stirred 0.05 M phosphate buffer (pH 7.4) adding equal aliquots of glucose.

Glucose Detection

The glucose electrode responses were tested using amperometry at +0.6 V. This potential showed a significant current difference between solutions with and without glucose for the GOx modified electrode CVs in **Figure 3.3(B)**. **Figure 3.11(A)** shows the glucose sensor response to addition of glucose in phosphate buffer. As aliquots of glucose are added, step increases in current

are measured corresponding to the increase in glucose concentration. The resulting calibration curve (**Figure 3.11(B)**) was plotted by averaging a 5 s interval of the nominal current value of the plateau as is common in the literature,[32, 47-49] and it shows a linear response in the range from 0-3.75 mM glucose. The replicates for this data were done using the same glucose sensor six times in a row rinsing in between. The small error bars on the calibration curve from the subsequent continuous measurements with the same electrode show excellent stability over a period of 100+ minutes without signal degradation. Many glucose sensors require recalibration in much shorter periods of time.[50, 51] However, in **Figure 3.11(A)**, the response time begins to slow over the continuous measurement, which has been an issue for other reported biosensors at higher concentrations and should be addressed in future work.[52] Although a formal stability study has not been performed for electrode storage, the electrodes were stored in open air on a countertop at room temperature and reused for several months. If the sensors were reused, a calibration curve was performed on the same day. As an example, **Figure 3.12** demonstrates the successful performance of the same electrode after storage and sanding, showing calibration curves for the same electrode approximately 3 months apart. The difference in the electrode's response is likely due to the previously discussed heterogeneous nature of the material between sanding. Recents reports show storage stability from 10-120 days but often involve more complex modification for this stability or must be stored at lower temperatures (4° C) than the sensors presented in this work.[49, 53-55]

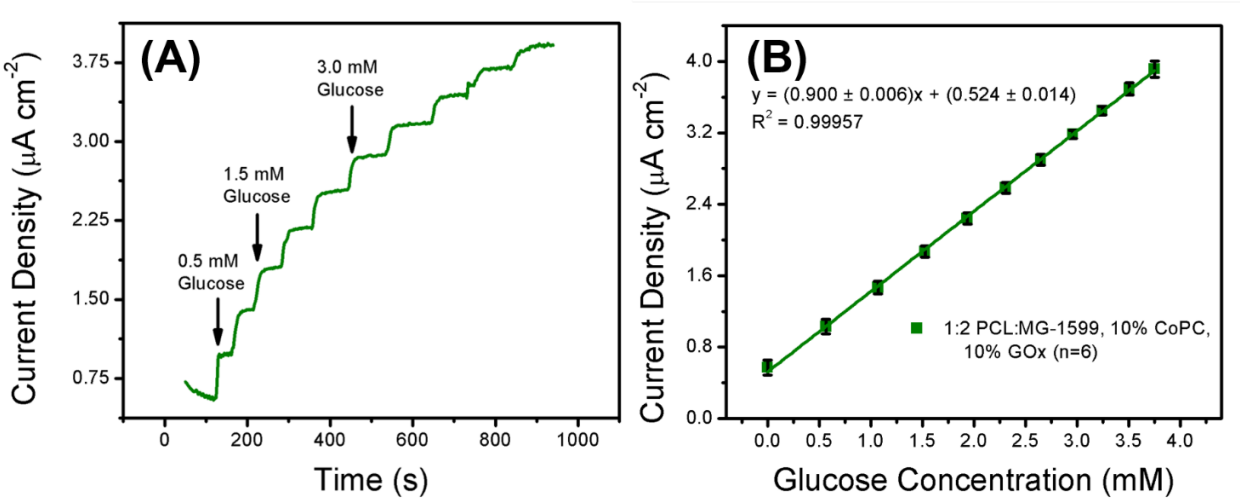

Figure 3.11 (A) Representative amperogram of glucose detection. Potential held at +0.6 V on GOx/CoPC modified electrode adding equal aliquots of glucose in stirred 0.05 M phosphate buffer (pH 7.4) **(B)** and the resulting glucose calibration curve using the same electrode for replicates (Markers and error bars show mean and sds, n=6).

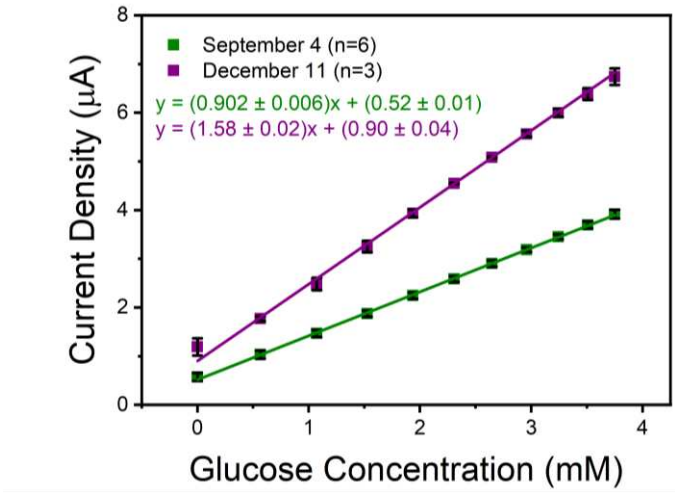

Figure 3.12 Glucose calibration curves of the same GOx/CoPC modified electrode on two days several months apart from amperograms, where potential was held at +0.6 V vs. a SCE reference in stirred 0.05 M phosphate buffer (pH 7.4) adding equal aliquots of glucose.

Figure 3.13(A) shows a representative amperogram measurement across the whole dynamic range of sensor. Current responses to corresponding glucose concentrations are plotted in **Figure 3.13(B)**. The curve shown in this plot shows that the enzymatic sensor follows Michaelis-Menten kinetics. A Lineweaver-Burke plot (**Figure 3.13(C)**) was used to calculate the

kinetic constants: Vmax = 52. ± 3., Km = 8.5 ± 0.9 mM. In any glucose sensor, the activity of the enzyme is limited due immobilization on the electrode. Previously published carbon-based glucose sensors report a wide range of Km values from 1-17 mM.[56-58] A lower Km value is desirable because it indicates a higher affinity of the enzyme for the substrate. The Km for this TPE sensor is more than sufficient for monitoring glucose levels in organ tissues. For example, the sensor's range fits well into the range needed for monitoring organs, such as kidneys, to assess viability before transplantation (3.6-5.5 mM) [59, 60] or monitoring a patient's brain after a traumatic brain injury (4.4-6.1 mM).[61] Additionally, the sensor is stable and robust, making it ideal for biological applications.

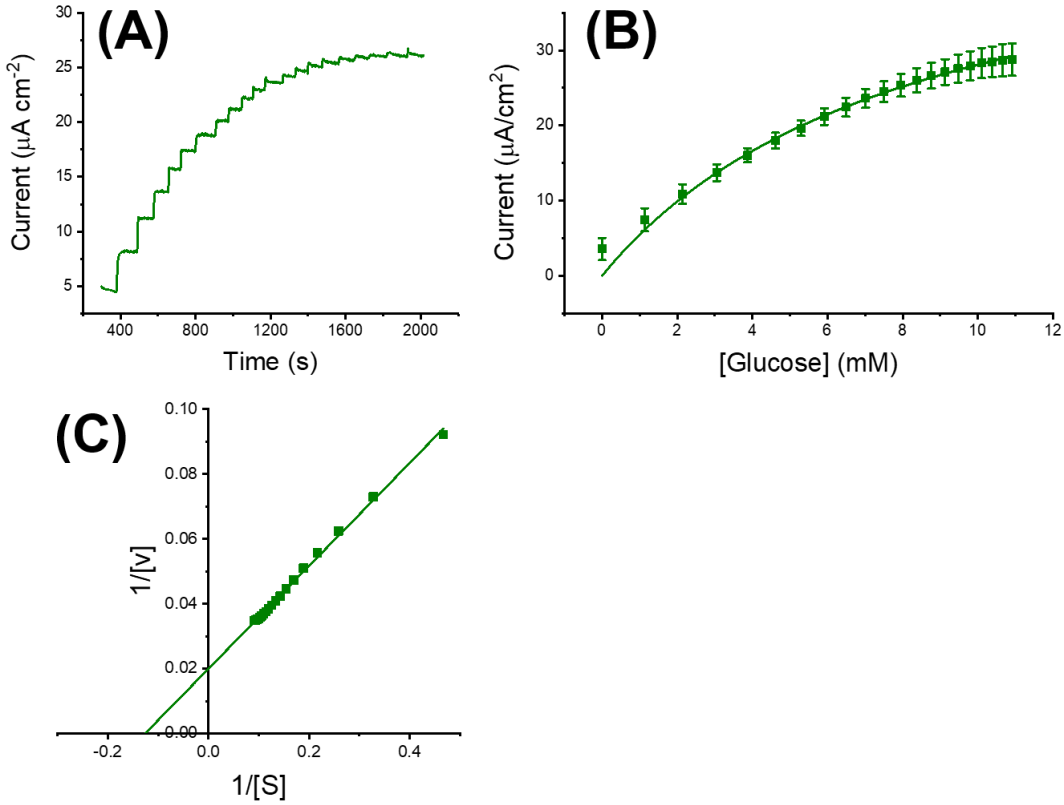

Figure 3.13 Michaelis-Menten kinetics **(A)** Representative amperogram holding potential at +0.6 V vs. a SCE reference on GOx/CoPC modified electrode adding aliquots of glucose in stirred 0.05 M phosphate buffer (pH 7.4) until saturation. **(B)** Plot of resulting current versus concentration of glucose (n=3 on same electrode). **(C)** Lineweaver-Burke plot of resulting data. Equation of line: y = (0.159 ± 0.002)x + (0.0199 ± 0.0004).

Application to a Real Juice Sample

As a proof of concept, the TPE glucose sensors were tested in diluted apple juice and verified using a commercial UV/Vis assay. The TPE sensor measurement was calculated using amperometry similarly to the method presented above and standard addition of known glucose amounts. The standard addition curve is shown in **Figure 3.14**. The calibration curve and measurements of the Glucose Assay Kit are recorded in **Figure 3.15** and **Table 3.1**. The responses of each method were extrapolated to calculate the full concentration of the juice tested. Results of the two assays agreed within error (**Table 3.2**). Notably, TPE glucose sensors showed high precision, as the error of the sensor developed here is far smaller than that of the commercial assay.

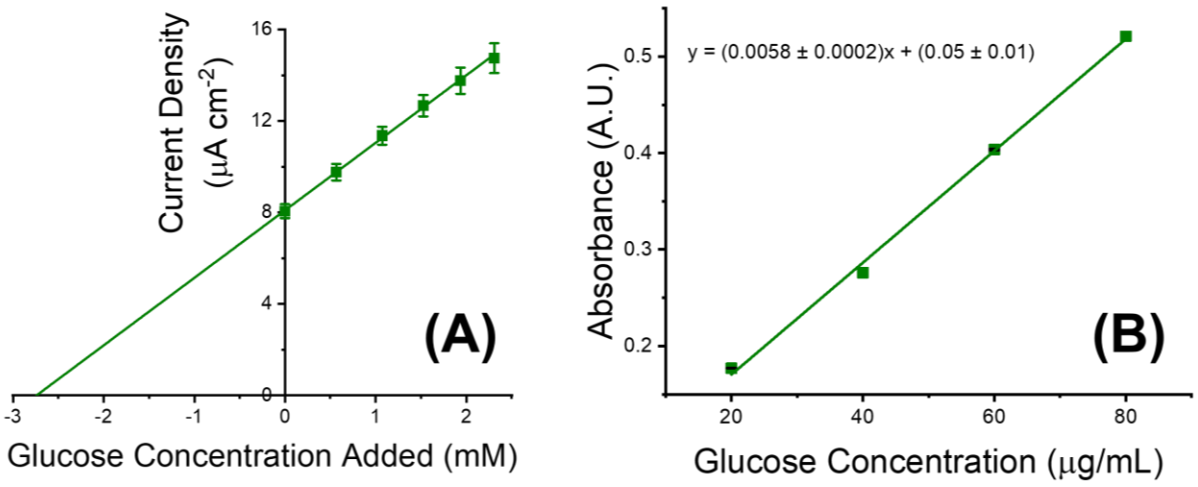

Apple Juice Aliquot	Average Absorbance (A.U.)	Diluted Calculated Concentration (μg/mL)	Diluted Calculated Concentration (mM)	Total Concentration (mM)
sample 1	0.112	9.917	0.0550	660.0
sample 2	0.101	8.077	0.0448	537.6
sample 3	0.101	8.020	0.0445	534.0
sample 4	0.098	7.502	0.0416	499.2

Figure 3.14 (A) Standard addition plot of 200x dilute apple juice in 0.05 M phosphate buffer (pH 7.4) from amperograms where potential held at +0.6 V vs. a SCE reference on GOx/CoPC modified electrode adding equal aliquots of glucose in stirred dilute apple juice (n=3 on same electrode). **(B)** Absorbance calibration curve from Sigma-Aldrich Glucose Assay Kit that was used to quantify the apple juice sample. (Below) Table of absorbance values and calculated concentration for apple juice measurements.

Table 3.2 Comparison of TPE glucose sensor to a UV/Vis Glucose Assay Kit on the market for measurement of apple juice. Apple juice was diluted 200x for measurement using the TPE sensor and 12000x for the Glucose Assay Kit.

Method	Calculated Concentration (mM)
Glucose Assay Kit (n=4)	558 ± 64
TPE Sensor (n=3)	549 ± 14

3.5 Conclusions

In summary, this work presents the use of TPEs to produce robust, bulk-modified glucose sensors as a proof-of-concept for enzymatic sensors. The reported method allows for simple, cheap, and quick fabrication of enzymatic sensors in bulk. The moldability of the TPE glucose electrode material makes it promising for various applications where electrode geometry is important and/or electrodes must be incorporated into complicated devices. The sensors can be used continuously with consistent and reproducible current response. The bulk-modification allows for the surface to be sanded down if the surface is damaged or fouled making the sensors reusable, which is useful in many applications such as clinical monitoring. With the current scheme, the enzyme incorporated into the material can be substituted for a variety of enzymes to sense different biomolecules, making enzymatic TPEs applicable to countless applications.

REFERENCES

1. O'Hare, D.; Macpherson, J. V.; Willows, A., On the microelectrode behaviour of graphite–epoxy composite electrodes. *Electrochemistry Communications* **2002,** *4* (3), 245-250.

2. McCreery, R. L., Advanced carbon electrode materials for molecular electrochemistry. *Chemical reviews* **2008,** *108* (7), 2646-2687.

3. Wang, J., Electrochemical glucose biosensors. *Chemical reviews* **2008,** *108* (2), 814-825.

4. Clark Jr, L. C.; Lyons, C., Electrode systems for continuous monitoring in cardiovascular surgery. *Annals of the New York Academy of sciences* **1962,** *102* (1), 29-45.

5. Niu, X.; Li, X.; Pan, J.; He, Y.; Qiu, F.; Yan, Y., Recent advances in non-enzymatic electrochemical glucose sensors based on non-precious transition metal materials: opportunities and challenges. *RSC advances* **2016,** *6* (88), 84893-84905.

6. GVR Report coverBlood Glucose Monitoring Devices Market Size, Share & Trends Report

Blood Glucose Monitoring Devices Market Size, Share & Trends Analysis Report By Product (Self-monitoring, Continuous), By End-use (Hospitals, Home Care, Diagnostic Centers), By Region, And Segment Forecasts, 2021 - 2028. https://www.grandviewresearch.com/industry-analysis/blood-glucose-monitoring-bgm-devices-market/methodology.

7. Sehit, E.; Altintas, Z., Significance of nanomaterials in electrochemical glucose sensors: An updated review (2016-2020). *Biosensors and Bioelectronics* **2020,** *159*, 112165.

8. Hassan, M. H.; Vyas, C.; Grieve, B.; Bartolo, P., Recent Advances in Enzymatic and Non-Enzymatic Electrochemical Glucose Sensing. *Sensors* **2021,** *21* (14), 4672.

9. Albareda-Sirvent, M.; Merkoci, A.; Alegret, S., Configurations used in the design of screen-printed enzymatic biosensors. A review. *Sensors and Actuators B: Chemical* **2000,** *69* (1-2), 153-163.

10. Lei, Y.; Yan, X.; Zhao, J.; Liu, X.; Song, Y.; Luo, N.; Zhang, Y., Improved glucose electrochemical biosensor by appropriate immobilization of nano-ZnO. *Colloids and surfaces B: Biointerfaces* **2011,** *82* (1), 168-172.

11. Salimi, A.; Compton, R. G.; Hallaj, R., Glucose biosensor prepared by glucose oxidase encapsulated sol-gel and carbon-nanotube-modified basal plane pyrolytic graphite electrode. *Analytical biochemistry* **2004,** *333* (1), 49-56.

12. Yang, X.; Hua, L.; Gong, H.; Tan, S. N., Covalent immobilization of an enzyme (glucose oxidase) onto a carbon sol–gel silicate composite surface as a biosensing platform. *Analytica Chimica Acta* **2003,** *478* (1), 67-75.

13. Burmeister, J. J.; Gerhardt, G. A., Self-referencing ceramic-based multisite microelectrodes for the detection and elimination of interferences from the measurement of L-glutamate and other analytes. *Analytical chemistry* **2001,** *73* (5), 1037-1042.

14. Kaya, H. Z.; Söylemez, S.; Udum, Y. A.; Toppare, L., Application of an Efficient Amperometric Glucose Sensing Electrode Based on a Bilayer Polymer Film Platform. *Journal of The Electrochemical Society* **2018,** *165* (16), B939.

15. Chen, W.; Cai, S.; Ren, Q.-Q.; Wen, W.; Zhao, Y.-D., Recent advances in electrochemical sensing for hydrogen peroxide: a review. *Analyst* **2012,** *137* (1), 49-58.

16. Hosu, I. S.; Wang, Q.; Vasilescu, A.; Peteu, S. F.; Raditoiu, V.; Railian, S.; Zaitsev, V.; Turcheniuk, K.; Wang, Q.; Li, M., Cobalt phthalocyanine tetracarboxylic acid modified

reduced graphene oxide: a sensitive matrix for the electrocatalytic detection of peroxynitrite and hydrogen peroxide. *RSC advances* **2015,** *5* (2), 1474-1484.

17. Wang, H.; Bu, Y.; Dai, W.; Li, K.; Wang, H.; Zuo, X., Well-dispersed cobalt phthalocyanine nanorods on graphene for the electrochemical detection of hydrogen peroxide and glucose sensing. *Sensors and Actuators B: Chemical* **2015,** *216*, 298-306.

18. Foster, C. W.; Pillay, J.; Metters, J. P.; Banks, C. E., Cobalt phthalocyanine modified electrodes utilised in electroanalysis: nano-structured modified electrodes vs. bulk modified screen-printed electrodes. *Sensors* **2014,** *14* (11), 21905-21922.

19. Wring, S. A.; Hart, J. P.; Birch, B. J., Voltammetric behaviour of ascorbic acid at a graphite—epoxy composite electrode chemically modified with cobalt phthalocyanine and its amperometric determination in multivitamin preparations. *Analytica chimica acta* **1990,** *229*, 63-70.

20. Klunder, K. J.; Nilsson, Z.; Sambur, J. B.; Henry, C. S., Patternable solvent-processed thermoplastic graphite electrodes. *Journal of the American Chemical Society* **2017,** *139* (36), 12623-12631.

21. Klunder, K. J.; Clark, K. M.; McCord, C.; Berg, K. E.; Minteer, S. D.; Henry, C. S., Polycaprolactone-enabled sealing and carbon composite electrode integration into electrochemical microfluidics. *Lab on a Chip* **2019,** *19* (15), 2589-2597.

22. Noviana, E.; Klunder, K. J.; Channon, R. B.; Henry, C. S., Thermoplastic electrode arrays in electrochemical paper-based analytical devices. *Analytical chemistry* **2019,** *91* (3), 2431-2438.

23. Ozer, T.; McCord, C.; Geiss, B. J.; Dandy, D.; Henry, C. S., Thermoplastic Electrodes for Detection of Escherichia coli. *Journal of The Electrochemical Society* **2021,** *168* (4), 047509.

24. Pradela-Filho, L. A.; Araújo, D. A.; Takeuchi, R. M.; Santos, A. L.; Henry, C. S., Thermoplastic electrodes as a new electrochemical platform coupled to microfluidic devices for tryptamine determination. *Analytica Chimica Acta* **2021,** *1147*, 116-123.

25. McCord, C. P.; Summers, B.; Henry, C. S., Redox behavior and surface morphology of polystyrene thermoplastic electrodes. *Electrochimica Acta* **2021,** *393*, 139069.

26. Fiedler, P.; Mühle, R.; Griebel, S.; Pedrosa, P.; Fonseca, C.; Vaz, F.; Zanow, F.; Haueisen, J., Contact pressure and flexibility of multipin dry EEG electrodes. *IEEE transactions on neural systems and rehabilitation engineering* **2018,** *26* (4), 750-757.

27. You, I.; Kong, M.; Jeong, U., Block copolymer elastomers for stretchable electronics. *Accounts of chemical research* **2018,** *52* (1), 63-72.

28. Chikkaveeraiah, B. V.; Liu, H.; Mani, V.; Papadimitrakopoulos, F.; Rusling, J. F., A microfluidic electrochemical device for high sensitivity biosensing: Detection of nanomolar hydrogen peroxide. *Electrochemistry communications* **2009,** *11* (4), 819-822.

29. Pegan, J. D.; Ho, A. Y.; Bachman, M.; Khine, M., Flexible shrink-induced high surface area electrodes for electrochemiluminescent sensing. *Lab on a Chip* **2013,** *13* (21), 4205-4209.

30. Xu, Y.; Wu, X.; Guo, X.; Kong, B.; Zhang, M.; Qian, X.; Mi, S.; Sun, W., The boom in 3D-printed sensor technology. *Sensors* **2017,** *17* (5), 1166.

31. Yang, C.; Cao, Q.; Puthongkham, P.; Lee, S. T.; Ganesana, M.; Lavrik, N. V.; Venton, B. J., 3D-Printed Carbon Electrodes for Neurotransmitter Detection. *Angewandte Chemie International Edition* **2018,** *57* (43), 14255-14259.

32. Cheng, C.; Zhang, C.; Gao, X.; Zhuang, Z.; Du, C.; Chen, W., 3D network and 2D paper of reduced graphene oxide/Cu2O composite for electrochemical sensing of hydrogen peroxide. *Analytical chemistry* **2017,** *90* (3), 1983-1991.

33. Zhang, X.; Zhao, N.; He, C., The superior mechanical and physical properties of nanocarbon reinforced bulk composites achieved by architecture design–a review. *Progress in Materials Science* **2020,** *113*, 100672.

34. Taleat, Z.; Khoshroo, A.; Mazloum-Ardakani, M., Screen-printed electrodes for biosensing: a review (2008–2013). *Microchimica Acta* **2014,** *181* (9-10), 865-891.

35. Sandhyarani, N., Surface modification methods for electrochemical biosensors. In *Electrochemical Biosensors*, Elsevier: 2019; pp 45-75.

36. Patrikar, R. M., Modeling and simulation of surface roughness. *Applied Surface Science* **2004,** *228* (1-4), 213-220.

37. Heimer, G.; Taylor, C., Improved mountant for immunofluorescence preparations. *Journal of Clinical Pathology* **1974,** *27* (3), 254.

38. Fei Liu, X.; Lin Guan, Y.; Zhi Yang, D.; Li, Z.; De Yao, K., Antibacterial action of chitosan and carboxymethylated chitosan. *Journal of applied polymer science* **2001,** *79* (7), 1324-1335.

39. Lombard, C.; Saulnier, J.; Wallach, J., Assays of matrix metalloproteinases (MMPs) activities: a review. *Biochimie* **2005,** *87* (3-4), 265-272.

40. Twining, S. S., Fluorescein isothiocyanate-labeled casein assay for proteolytic enzymes. *Analytical biochemistry* **1984,** *143* (1), 30-34.

41. Noble, M.; Rippeth, J.; Edington, D.; Rayman, G.; Brandon-Jones, S.; Hollowood, Z.; Kew, S., Clinical evaluation of a novel on-strip calibration method for blood glucose measurement. *Journal of diabetes science and technology* **2014,** *8* (4), 766-775.

42. Yue, X.-Y.; Zheng, Y.; Cai, Y.-H.; Yin, N.-N.; Zhou, J.-X., Real-time continuous glucose monitoring shows high accuracy within 6 hours after sensor calibration: a prospective study. *PLoS One* **2013,** *8* (3), e60070.

43. Li, H.; Dauphin-Ducharme, P.; Ortega, G.; Plaxco, K. W., Calibration-free electrochemical biosensors supporting accurate molecular measurements directly in undiluted whole blood. *Journal of the American Chemical Society* **2017,** *139* (32), 11207-11213.

44. Ishikawa, F. N.; Curreli, M.; Chang, H.-K.; Chen, P.-C.; Zhang, R.; Cote, R. J.; Thompson, M. E.; Zhou, C., A calibration method for nanowire biosensors to suppress device-to-device variation. *ACS nano* **2009,** *3* (12), 3969-3976.

45. Wilson, G. S.; Gifford, R., Biosensors for real-time in vivo measurements. *Biosensors and Bioelectronics* **2005,** *20* (12), 2388-2403.

46. Rinken, T.; Tenno, T., Dynamic model of amperometric biosensors. Characterisation of glucose biosensor output. *Biosensors and Bioelectronics* **2001,** *16* (1-2), 53-59.

47. Wang, B.; Li, B.; Deng, Q.; Dong, S., Amperometric glucose biosensor based on sol− gel organic− inorganic hybrid material. *Analytical Chemistry* **1998,** *70* (15), 3170-3174.

48. Zou, Y.; Xiang, C.; Sun, L.-X.; Xu, F., Glucose biosensor based on electrodeposition of platinum nanoparticles onto carbon nanotubes and immobilizing enzyme with chitosan-SiO2 sol–gel. *Biosensors and Bioelectronics* **2008,** *23* (7), 1010-1016.

49. Shan, D.; Zhu, M.; Xue, H.; Cosnier, S., Development of amperometric biosensor for glucose based on a novel attractive enzyme immobilization matrix: calcium carbonate nanoparticles. *Biosensors and Bioelectronics* **2007,** *22* (8), 1612-1617.

50. Rossetti, P.; Bondia, J.; Vehí, J.; Fanelli, C. G., Estimating plasma glucose from interstitial glucose: the issue of calibration algorithms in commercial continuous glucose monitoring devices. *Sensors* **2010,** *10* (12), 10936-10952.

51. Gowers, S. A.; Rogers, M. L.; Booth, M. A.; Leong, C. L.; Samper, I. C.; Phairatana, T.; Jewell, S. L.; Pahl, C.; Strong, A. J.; Boutelle, M. G., Clinical translation of microfluidic sensor devices: focus on calibration and analytical robustness. *Lab on a Chip* **2019,** *19* (15), 2537-2548.

52. Carelli, D.; Centonze, D.; Palermo, C.; Quinto, M.; Rotunno, T., An interference free amperometric biosensor for the detection of biogenic amines in food products. *Biosensors and Bioelectronics* **2007,** *23* (5), 640-647.

53. Temoçin, Z., Designing of a stable and selective glucose biosensor by glucose oxidase immobilization on glassy carbon electrode sensitive to H 2 O 2 via nanofiber interface. *Journal of Applied Electrochemistry* **2021,** *51* (2), 283-293.

54. Christwardana, M.; Frattini, D., Electrochemical study of enzymatic glucose sensors biocatalyst: Thermal degradation after long-term storage. *Chemosensors* **2018,** *6* (4), 53.

55. Zhang, B. L.; Jin, X.; Sun, L. H.; Guo, X. D., Needle-shaped glucose sensor based on polypyrrole doped with glucose oxidase. *Microchemical Journal* **2020,** *158*, 105217.

56. Rahman, M.; Ahammad, A.; Jin, J.-H.; Ahn, S. J.; Lee, J.-J., A comprehensive review of glucose biosensors based on nanostructured metal-oxides. *Sensors* **2010,** *10* (5), 4855-4886.

57. German, N.; Ramanavicius, A.; Voronovic, J.; Oztekin, Y.; Ramanaviciene, A., The effect of colloidal solutions of gold nanoparticles on the performance of a glucose oxidase modified carbon electrode. *Microchimica Acta* **2011,** *172* (1-2), 185-191.

58. Zhu, Z.; Garcia-Gancedo, L.; Flewitt, A. J.; Xie, H.; Moussy, F.; Milne, W. I., A critical review of glucose biosensors based on carbon nanomaterials: carbon nanotubes and graphene. *Sensors* **2012,** *12* (5), 5996-6022.

59. Hill, N. R.; Oliver, N. S.; Choudhary, P.; Levy, J. C.; Hindmarsh, P.; Matthews, D. R., Normal reference range for mean tissue glucose and glycemic variability derived from continuous glucose monitoring for subjects without diabetes in different ethnic groups. *Diabetes technology & therapeutics* **2011,** *13* (9), 921-928.

60. Booth, M. A.; Gowers, S. A.; Leong, C. L.; Rogers, M. L.; Samper, I. C.; Wickham, A. P.; Boutelle, M. G., Chemical monitoring in clinical settings: recent developments toward real-time chemical monitoring of patients. **2018**.

61. Rostami, E., Glucose and the injured brain-monitored in the neurointensive care unit. *Frontiers in neurology* **2014,** *5*, 91.

CHAPTER 4: COMPARISON OF THERMOPLASTIC ELECTRODE MATERIALS FOR O_2 AND H_2O_2 SENSING

4.1 Chapter Overview

Carbon composite electrodes often suffer from poor electrocatalytic activity and require complex, expensive, or time-consuming modifications to effectively detect certain analytes such as O_2 and H_2O_2. Thermoplastic electrodes (TPEs) are a new class of composite electrodes that exhibit superior electrochemical properties to typical carbon composite electrodes. This work investigates the properties of TPEs using two different binders – polycaprolactone (PCL) and polystyrene (PS) – with sanded and heat-pressed surface treatment using XPS and SEM. These techniques suggested that sanded TPEs have a higher density of graphitic edge planes and improved electrochemistry as a result. Electrochemical detection of O_2 and H_2O_2 was demonstrated on sanded PS-based TPEs. Additionally, this work introduces a new 3D-printed TPE sensor module that is reversibly sealed with magnets. A proof-of-concept sensor for detecting H_2O_2 in flow with the sensor module is presented. All data included in this chapter were collected and processed by myself. The 3D-printed sensor module was designed by Amanda Cherwin and the leakless reference electrode used in the device was adapted from a similar system fabricated by Jason Boes.

4.2 Introduction

Carbon composite electrodes have become popular for many biosensing applications due to their biocompatibility, wide potential windows, and low cost.[1-5] However, carbon composite electrodes often suffer from poor moldability and slow electron transfer kinetics.[6, 7] Recently, thermoplastic electrodes (TPEs) have been introduced as easily moldable carbon composites with

excellent conductivity and electron transfer kinetics.[7-14] A variety of thermoplastic binders have been used for TPEs including polymethyl methacrylate (PMMA),[7, 11] polycaprolactone (PCL),[8, 11, 15] cyclic olefin copolymer (COC),[9-11] polystyrene (PS),[13, 14] and Ecoflex®.[16] While all of the binders used have resulted in successful sensors, carbon composite binder choice must be carefully considered for all applications as it contributes greatly to mechanical and electrochemical properties.[17, 18]

PCL and PS are of particular interest to this work as they can be pressed into templates without use of inorganic solvent.[8, 11, 13-15] PCL has a low melting point and is FDA approved for medical applications because of its biocompatibility.[19-21] Prior to use as a TPE binder, PCL was not commonly used in electrochemical sensors. PS has also been used in many biomedical applications and, alternatively to PCL, has been reported more in electrochemical sensors.[22, 23] PS electrodes have been applied to biological[22, 24-32] and environmental[27, 33-36] applications. In addition, PS-based TPEs have been shown to have enhanced electrode kinetics compared to other reported techniques using PS.[13] Additionally, the PS-based TPEs were also shown to have more resolved voltametric peaks than those of PCL-based TPEs, likely due to the aromatic side chain groups in PS that could allow for π-π interactions with the graphite.[14]

While carbon composite electrodes have many advantageous properties, they are unable to detect many important biomolecules, such as O_2 and H_2O_2, without complex modification procedures. Monitoring dissolved O_2 is important in various biochemical and physiological processes.[37] Because O_2 is hard to detect electrochemically, precious metals or expensive and hard to fabricate carbon allotropes, such as boron doped diamond or glassy carbon, are typically used.[37-40] While there are reports of oxygen sensors from carbon composite electrodes, these require oxygen sensitive mediators,[37] precious metal nanoparticles,[41, 42] novel nano-carbon structures,[42, 43]

electrocatalysts,[44] and/or other complex additives or modifications. H_2O_2 also plays an important role as a signaling molecule in regulating diverse biological processes such as immune cell activation and is also a product from oxidase enzymes such as glucose oxidase (GOx), lactate oxidase (LOx), and cholesterol oxidase (ChoOx).[45] Similarly, detection of H_2O_2 requires expensive, complex, or time-consuming modifiers such as metal hexacyanoferrates, heme proteins, CNTs and graphene, metals and metal oxides, and metallophthalocyanines.[45-47] In this work, PS-based TPEs are used to successfully detect O_2 and H_2O_2 without electrode modifications for the first time.

Fluidic and microfluidic devices have been used for a wide variety of electrochemical applications to improve signal and monitor analyte concentration changes in real-time.[48-51] Traditionally, integration of carbon composite electrodes into fluidic devices can be challenging due to flow interruption from raised features[52-54] or complex electrode or channel fabrication techniques. Furthermore, electrode modification is difficult in systems where carbon composite electrodes can be incorporated.[55-57] Often analysis is done off-chip or in the waste area of the fluidic device to avoid integration, but this reduces signal and/or prevents time resolved measurements.[58] TPEs have been incorporated into a variety of fluidic devices including paper-based devices,[9, 11, 59, 60] droplet microfluidics,[8] and microfluidic flow cells.[15] While these examples overcome many obstacles for electrode integration in fluidic devices, there are still many challenges for sensor integration, particularly for reusable devices. For devices with integrated sensors, if the sensor fails, both the device and the sensor require replacement.[61] Sensor modules are separate devices with integrated sensors that can be coupled to an existing fluidic system and allow for real-time measurement to be collected in flow without causing disruption to the system if the sensor needs to be replaced.[61]

A plug-and-play sensor module for use in fluidic systems was previously demonstrated.[62] That sensor module used 3D-printed components to incorporate swappable PCL-based TPE sensors housed in commercial PEEK fingertight fittings.[62, 63] Unfortunately, this design was not easily translatable for PS-based TPEs. The increased temperature required for TPE fabrication with PS melted and deformed the fingertight fittings. This work introduces a new 3D-printed sensor module to accommodate PS-based TPEs. Prior to the TPE integration into the sensor module, the properties of the PCL- and PS-based TPEs were further investigated through XPS, SEM, and redox probes. The PS-based TPEs could detect both O_2 and H_2O_2 without any modification. A proof-of-concept for H_2O_2 detection in flow was demonstrated in the sensor module.

4.3 Experimental Section

Reagents

Solutions were prepared using 18.2 M Ω · cm water purified using a Milli-Q system (MilliporeSigma, USA). Graphite (MG-1599, size ~15 μm) was purchased from Great Lakes Graphite, Inc. (Toronto, Canada). Polycaprolactone (PCL) was purchased from ThermoMorph® (Toledo, OH) and polystyrene m.w. 45,000 (45K PS) was purchased from Sigma Aldrich (Saint Louis, MO). ACS grade dichloromethane, potassium nitrate, and 30% hydrogen peroxide were purchased from Sigma-Aldrich (Saint Louis, MO). Dopamine hydrochloride (99%) was purchased from Alfa Aesar (Haverhill, MA). Ferrocenylmethyl trimethylammonium ($FcTMA^+$) synthesized in house with the help of Andrea Westlie using a method previously reported.[64]

Electrode Fabrication

Polycaprolactone (PCL) or polystyrene (PS) was first dissolved in dichloromethane (DCM). The polymer and graphite (MG-1599) were weighed to make a 1:2 polymer:carbon ratio by mass. The dissolved polymer and graphite were mixed using a wooden applicator and poured onto a Si wafer to continue mixing and drying. Once the electrode material is completely dry (typically less than 10 min), it can be stored in vials at ambient conditions for later use or incorporated into electrode templates. For electrode characterization experiments, polymethyl methacrylate templates were designed to make simple disk electrodes that were 2.5 mm diameter/3 mm thick using CorelDRAW (Corel, Ontario, Canada) and cut using a CO_2 laser cutter (Zing 10000, Epilog Laser). The electrode material was then pressed into the templates using a hydraulic heat press at 60°C for PCL electrodes and 85°C for PS electrodes with pressure of 1500-2000 psi. Excess material was then polished away with 600 grit sandpaper, and electrical connections were attached with silver paint. Further polishing to achieve more uniform or regenerate surface was done with finer 1200 grit sandpaper. The TPEs referred to as "sanded" were treated as described above. Those referred to as "pressed" were heat-pressed again for approximately 20 s after the final fabrication step. Electric connections were added with Ag paint and copper wire.

Surface Analysis (XPS and SEM)

X-ray photoelectron spectroscopy (XPS) was used to analyze the composition of electrode surfaces (PHI Physical Electronics PE-5800 X-ray Photoelectron Spectrometer). Data were collected using a 1 mm diameter circular aperture. Surface images also were taken of the electrode material using scanning electron microscope (JEOL JSM-6500F). XPS spectra were analyzed and peaks were fit using CasaXPS (Casa Software Ltd., Teignmouth, United Kingdom). Peaks were normalized by calibrating the C-C peak to 285.00 eV, as commonly reported.[65]

Characterization Electrochemical Measurements

Electrochemical measurements for characterization were recorded using a CHI660b potentiostat (CH Instruments, Inc., Austin, TX). All experiments were performed with a three-electrode system using the TPEs as the working electrode, a saturated calomel electrode (SCE) as a reference electrode, and larger surface area TPE as the counter electrode. All solutions were prepared and diluted in 0.1 KNO_3 or 0.05 M phosphate buffer (pH 7.4) prior to measurements (denoted in figure captions). Cyclic voltammetry (CV) was performed to characterize $FcTMA^+$ detection by scanning from 0.0 V to +0.8 V at a scan rate of 100 mV/s. CVs to characterize dopamine detection were scanned from -0.2 V to +0.8 V at a scan rate of 100 mV/s. CVs to characterize O_2 detection were scanned from -0.9 V to +0.9 V at a scan rate of 100 mV/s. CVs to characterize H_2O_2 detection were scanned from -0.4 V to +0.8 V at a scan rate of 100 mV/s. Replicate measurements for all CVs were recorded in the same solutions with different TPEs.

Device Design and Fabrication

The sensor module device was designed in SolidWorks CAD software (Dassault Systems, Waltham, MA) and the top and bottom layers were 3D-printed with a Form 3 SLA printer (Formlabs, Somerville, MA) using Clear V4 resin. After printing, the devices were soaked in isopropyl alcohol for 20 min to remove uncured resin and subsequently post-cured according to Formlabs recommendations. N42 Neodymium bar magnets from K&J Magnets Inc. (Pipersville, PA) were glued in slots on the inner surface of each 3D-printed layers using cyanoacrylate glue (Krazy Glue, High Point, NC), providing 11.5 lbf of total clamping force. The middle layer consists of a 20A durometer silicone gasket (McMaster-Carr, Elmhurst, IL) cut with an Epilog Zing laser cutter to define the microfluidic channel.

Leakless Bipolar Ag|AgCl Reference Electrode Fabrication

A leakless bipolar Ag|AgCl reference was fabricated using a similar method to previously reported.[66] Annealed platinum wire (Alfa Aesar, Haverhill, MA) with a diameter of 0.5 mm and a length of 2 cm was inserted into the opening of a 200 uL polypropylene pipette tip (Neptune Scientific, San Diego, CA). The wire was sealed into the tip with two-part epoxy (3M, Saint Paul, MN), with exposed portions both inside and protruding from the pipette tip. Annealed silver wire (Thermo Fischer, Waltham, MA) with a diameter of 0.5mm and a length of 3 cm was similarly sealed with epoxy into a 10 μL pipette tip. Chloride was electrodeposited onto the exposed portion of silver wire protruding from the tip by holding the Ag wire at a +1.0 V potential vs. SCE reference in 1 M KCl for 3 min. The 200 μL tip portion of the reference electrode was incorporated into the flow device using epoxy, and the platinum wire was trimmed to avoid clogging the channel. Before use, the 200 μL tip with wire was filled with 1M KCl and capped with the 10 μL pipette tip. Parafilm was used to seal the two pipette tips together, taking care to ensure that the wires were only electrically connected through the KCl solution, creating a self-contained bipolar reference electrode.

Sensor Module Flow Experiment Set Up and Electrochemical Measurements

The sensor module was tested amperometrically in flow with 1 mM H_2O_2. Two syringe pumps (New Era Pump Systems, Inc. and Harvard Apparatus) were connected to a T-junction manual valve which was then connected to the inlet for the sensor module. One syringe contained 0.05 M phosphate buffer (pH 7.4) and the other contained 1 mM H_2O_2 in 0.05 M phosphate buffer (pH 7.4). Flow rate for both pumps was set to 1.0 mL/min. The valve was switched back and forth from one pump to the other (stopping flow for the pump for which the valve was closed). Potential was held at +0.6 V vs. an Ag|AgCl reference for amperometry experiments with H_2O_2.

4.4 Results and Discussion

XPS Analysis of PCL- and PS-based TPEs

Prior to integration into the flow sensor module, the electrode material was characterized. As previously noted, PCL and PS were chosen here because they both could be pressed into templates without use of solvent. The most notable difference in the structures of PCL and PS (shown in **Figure 4.2**) is that PCL has O-containing groups and PS has an aromatic side group. TPEs were fabricated with both polymers and to better understand the interactions between the polymers and graphite, some TPEs were sanded (denoted as PCLS and PSS) as typically done and others were heat-pressed (denoted as PCLP and PSP) as described in **4.3**.

Due to the complexity of the graphite used, carbon composite electrodes tend to have many functional groups on the surface and therefore have very complex surface chemistry. When edges of graphene sheets are cleaved during fabrication or polishing, they react with oxygen and water forming various oxygen functional groups to complete the valences, which can include carbonyls, hydroxyls, carboxyls, ethers, and lactones.[3, 67] X-ray Photoelectron Spectroscopy (XPS) was performed on PCL and PS TPEs that were sanded and heat-pressed (as well as the corresponding isolated polymers) to better understand the surface chemistry that contributes to the electrode material properties.[68] **Figure 4.3** shows XPS survey scan spectra of all materials. Overall, all TPEs and polymers look relatively similar, and there are no significant peaks other than oxygen and carbon. The steps seen in the baselines are a result of electrons ejected that are below the top 10 nm of the sample surface, which is typical of XPS spectra.[69] Based on the survey spectra and knowledge of the samples, C1s and O1s were further investigated with high resolution scans.

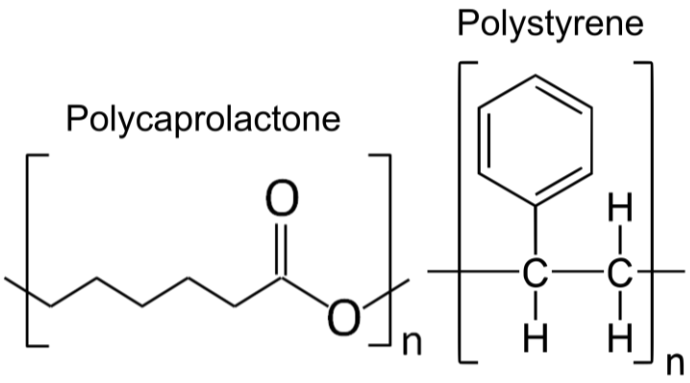

Figure 4.2 Chemical structure of PCL and PS.

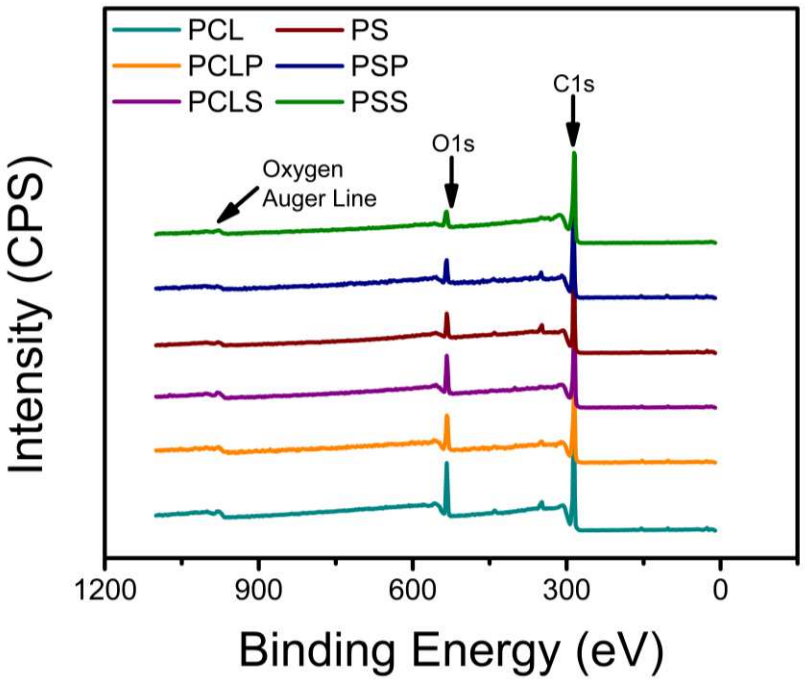

Figure 4.3 XPS survey scan spectra of the PCL, TPEs made with PCL that are heat-pressed and sanded after fabrication (PCLP, PCLS), PS, and TPEs made with PS that are heat-pressed and sanded after fabrication (PSP, PSS).

High resolution scan spectra for PCL and PCL-based TPEs are shown in **Figure 4.4** with relative quantities for different functional groups based on the peak fitting summarized in **Table 4.1**. High resolution scan spectra for PS and PS-based TPEs are shown in **Figure 4.5** with relative quantities based on the peak fitting summarized in **Table 4.2**. O1s peaks are often not fit because

it is difficult to get an accurate fitting due to the overlapping of binding energies of the oxygen functionalities.[70] O1s spectra are displayed in **Figure 4.4 & 4.5**, however, the discussion for the materials will be based on the C1s peaks and quantities. The C1s peaks were assigned based binding energy values previously reported for similar materials.[65] It is important to note that all the TPEs (including the heat-pressed TPEs) initially needed to be sanded in fabrication; therefore, these data are not mutually exclusive.

The data for the PCL polymer shows a high quantity of C-C bonds (75.29%) on the surface, and there was no C=C peak which is expected since the functionality is not present in PCL. When graphite is added to the PCL and heat-pressed (PCLP), a C=C peak appears with a low relative quantity (2.19%). This contribution is likely from the graphitic planes in which the majority of the carbon is sp^2 hybridized. The C-O peak also increases from 11.85% to 26.62% with the addition of graphite. The initial contribution of C-O bonds from the PCL remains with the added contributions of the surface oxides that are present in graphite. The C-C quantity also dropped to 63.35% with the increases from the other types of C bonds. When the PCL-based TPE was sanded (PCLS), C-O decreased to 18.57% and C-C decreased to 54.00%. The C=C bonds increase greatly to 19.68%, implying that after sanding more graphite is exposed on the surface. The C=O peaks for the three PCL-based samples remained relatively unchanged between samples.

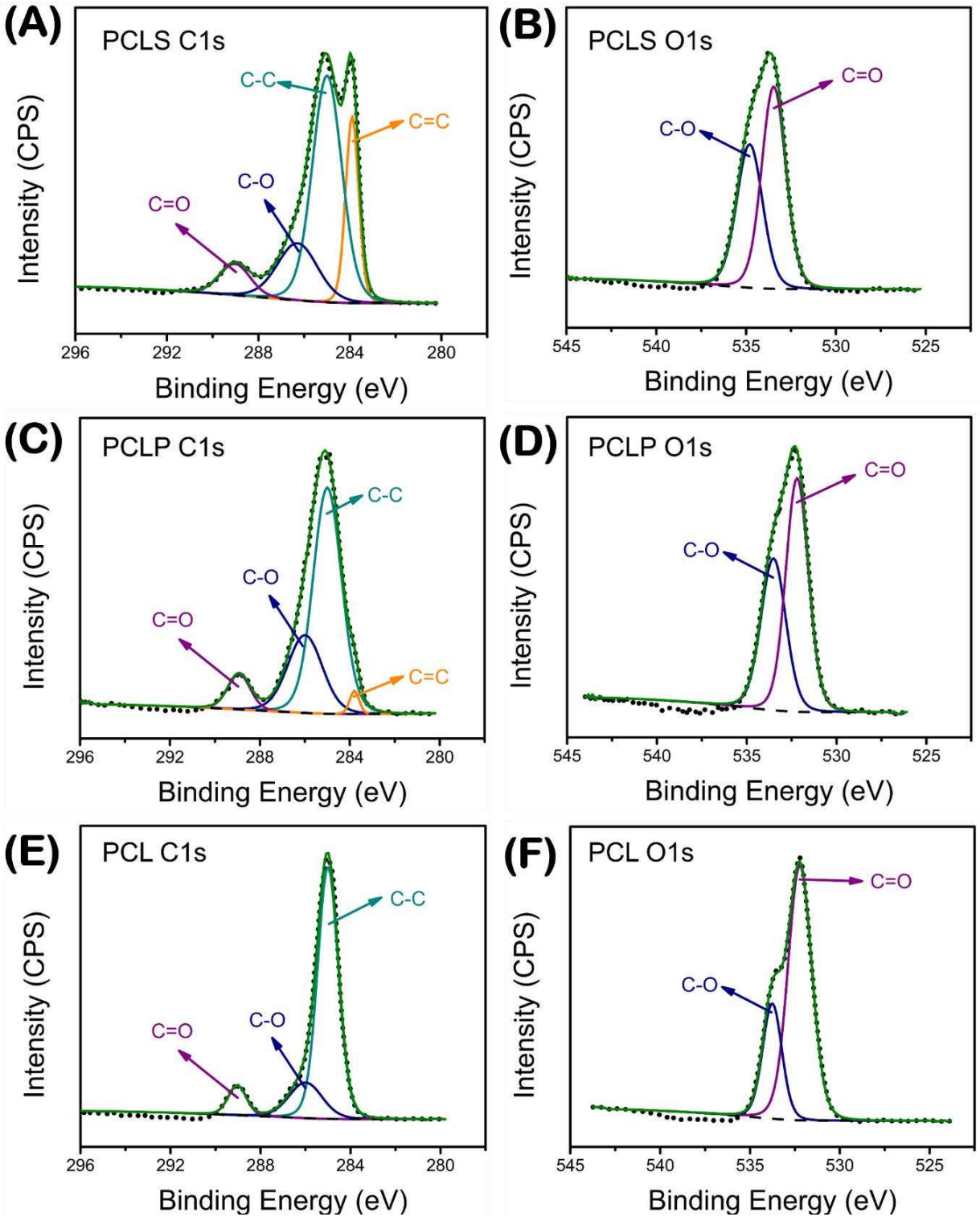

Figure 4.4 High resolution XPS spectra of the C1s (left) and O1s (right) regions for PCL-based TPEs that are **(A** & **B)** sanded and **(C** & **D)** heat-pressed after fabrication and the PCL polymer without any graphite added **(E** & **F)**. All spectra were normalized by calibrating the C-C peak to 285.00 eV.

Table 4.2 Binding energies and relative quantities (%) for PCL and PCL-based TPEs (heat-pressed and sanded) from the curve-fit analyses of C1s XPS spectra.

PCL

C1s Region			O1s Region		
	Position (eV)	**Concentration Percentage (%)**		**Position (eV)**	**Concentration Percentage (%)**
C-C	285.00	75.29	**C-O**	533.76	26.81
C=C	-	-	**C=O**	532.22	73.19
C-O	285.99	16.99			
C=O	289.03	7.72			

PCLP

C1s Region			O1s Region		
	Position (eV)	**Concentration Percentage (%)**		**Position (eV)**	**Concentration Percentage (%)**
C-C	285.00	63.35	**C-O**	533.51	41.79
C=C	283.80	2.19	**C=O**	532.19	58.21
C-O	285.99	26.62			
C=O	288.93	7.84			

PCLS

C1s Region			O1s Region		
	Position (eV)	**Concentration Percentage (%)**		**Position (eV)**	**Concentration Percentage (%)**
C-C	285.00	54.00	**C-O**	533.51	41.79
C=C	283.90	19.68	**C=O**	532.19	58.21
C-O	286.29	18.57			
C=O	289.03	7.75			

The PS polymer contains significantly less C-O (1.35%) and C=O (2.27%) bonds than PCL (11.85% and 7.90%, respectively). These quantities reconfirm the structure differences seen in **Figure 4.2** in which PS contains no oxygen in its pure form. C-C contributes 21.29% and C=C contributes 75.09% to the peaks, which is consistent with structure of PS including the bonds in the aromatic side chain. Surprisingly, when graphite is added to the material and it is heat-pressed (PSP), the C-C bonds increase from 21.29% to 86.31% and the C=C decrease from 75.09% to 9.64%. C-O and C=O quantities (0.61% and 3.44%, respectively) remain similar, which is consistent with the theory that the pressed PS-based TPEs contain mostly basal plane graphite. When the TPE is sanded (PSS), the C-C decreases significantly to 13.14% and the C=C increases to 27.49%. Most notably, the oxygen-containing groups on the surface in PSS increase over ten-fold (42.18% C-O and 17.20% C=O). This dramatic increase implies that the PSS facilitates the exposure of a large amount of edge plane graphite. Overall, the relative quantities of bond components in this work are comparable to other carbon composite materials reported.[71] Additionally, the quantities in the sanded PS-based TPEs reflect similar to values reported for more novel carbon materials like graphene oxide.[72, 73]

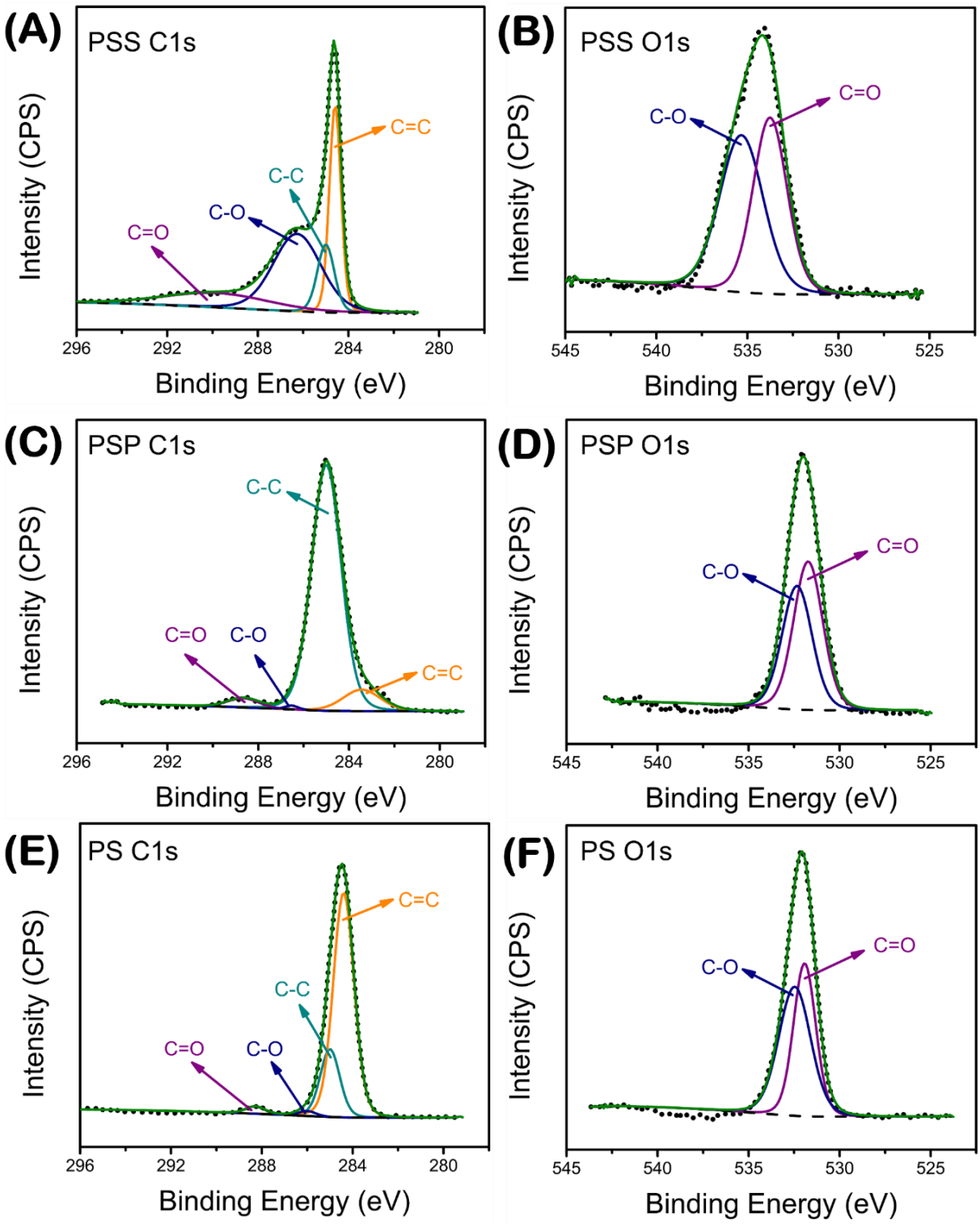

Figure 4.5 High resolution XPS spectra of the C1s (left) and O1s (right) regions for PS-based TPEs that are **(A** & **B)** sanded and **(C** & **D)** heat-pressed after fabrication and the PS polymer without any graphite added **(E** & **F)**. All spectra were normalized by calibrating the C-C peak to 285.00 eV.

Table 4.2 Table 4.1 Binding energies and relative quantities (%) for PS and PS-based TPEs (heat-pressed and sanded) from the curve-fit analyses of C1s XPS spectra.

PS

C1s Region			O1s Region		
	Position (eV)	**Concentration Percentage (%)**		**Position (eV)**	**Concentration Percentage (%)**
C-C	285.00	21.29	**C-O**	532.47	54.83
C=C	284.40	75.09	**C=O**	531.92	45.17
C-O	285.99	1.35			
C=O	288.29	2.27			

PSP

C1s Region			O1s Region		
	Position (eV)	**Concentration Percentage (%)**		**Position (eV)**	**Concentration Percentage (%)**
C-C	285.00	86.31	**C-O**	531.73	53.82
C=C	283.44	9.64	**C=O**	532.34	46.18
C-O	286.53	0.61			
C=O	288.66	3.44			

PSS

C1s Region			O1s Region		
	Position (eV)	**Concentration Percentage (%)**		**Position (eV)**	**Concentration Percentage (%)**
C-C	285.00	13.14	**C-O**	535.32	53.44
C=C	284.59	27.49	**C=O**	533.76	46.56
C-O	286.27	42.18			
C=O	289.82	17.20			

SEM Images of PCL- and PS-based TPEs

Scanning electron microscopy (SEM) images were taken of PCL-based TPEs and are shown in **Figure 4.6**. Over all magnifications, sanded PCL-based TPE material shows greater visible surface roughness than in the heat-pressed PCL-based TPE material. In all images, the surface has irregular topography with conductive regions (attributed to the graphite) and regions with more charging (attributed to the PCL polymer). The PCLS, however, has significantly more graphitic edge planes than the PCLP (most notably seen in 5000x and 50000x magnification). The PSS image at 50000x magnification also shows almost transparent features which are thin layers graphite or potentially even graphene sheets in some places. The PCLP shows more connected layers as opposed to edges which is consistent with graphitic basal plane. The lower electrocatalytic activity for heat-pressed TPEs was previously hypothesized to be a result of either the polymer coating graphitic particles or having more basal plane than edge plane graphite.[13] Because there is not a significant difference in conductivity seen between these images, it is more likely that the latter theory is correct since a polymer coating on the surface would be insulating and result in significant charging.

SEM images were also taken of PS-based TPEs and are shown in **Figure 4.7**. The PS-based TPEs follow the same trends as the PCL-based TPEs. Irregular surfaces with more graphitic edge planes in the PSS compared to the PSP. In the 500x magnification image of PSS, distinct grooves can be seen that are the result of sanding. A reason similar grooves are not seen in the PCLS could be due to PS being a much harder plastic than PCL.[74] The 5000x magnification image of PSP shows a conductive, mostly smooth surface containing major cracks and crevasses. This results from material crumbling away due to the PS-based TPEs being more brittle than the PCL-based TPEs, which should be considered when choosing a binder for specific applications. The formation

of large gaps in PSP but not PCLP could also be a result of difference in how each polymer flows when heat-pressed. Because PCL has a significantly lower melting point to PS and the temperatures applied is relatively much closer to the melting point of PCL than that of PS, it is possible that the PCL binder may flow more freely when heat-pressed carrying graphite and polymer to fill these gaps. Once again, the smooth regions on the PSP could be comparable to materials with large amounts of basal plane graphite. Overall, the PSS have a much higher density of graphitic edge planes than the PCLS which typically results in improved electrochemical activity. Edge planes also contain a greater amount of oxgen groups to complete the valences after the graphitic sheets are broken, which is consistent with the XPS data presented above. This phenomenon could be due to π-π stacking between the graphite and the PS π bonds helping orient the graphitic particles to expose more edge planes. Similar conclusions comparing PCL- and PS-based TPEs were reported previously.[13]

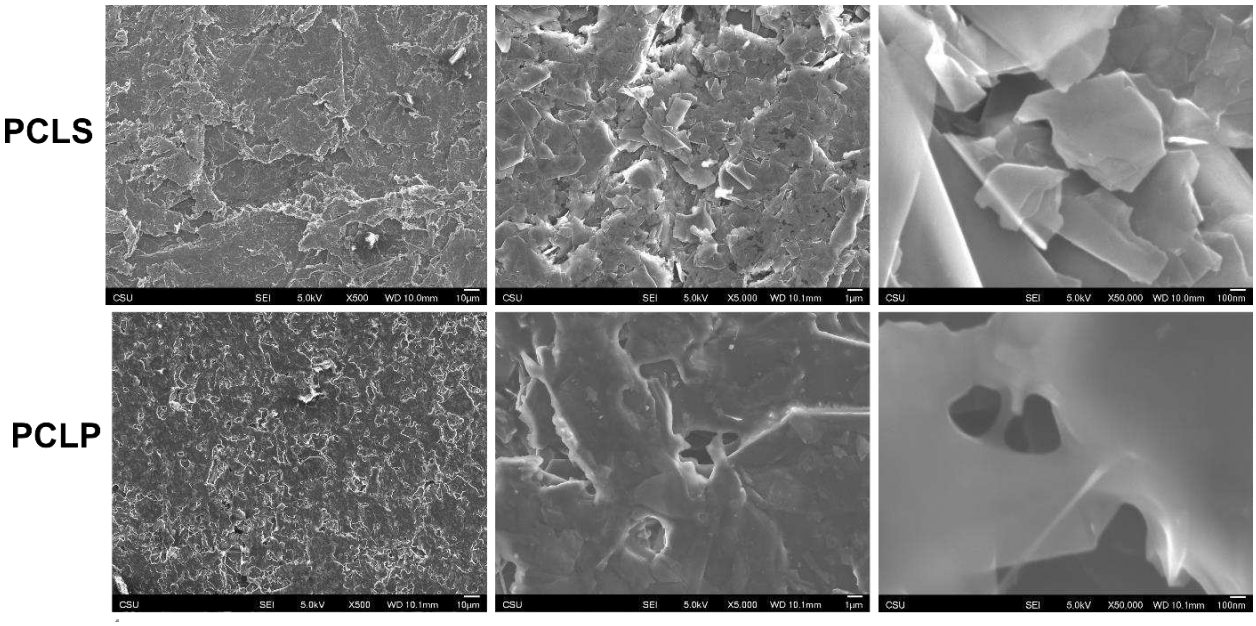

Figure 4.6 SEM images at (left to right) 500x, 5000x, and 50000x magnification of PCL-based TPE material that was (top) sanded and (bottom) heat-pressed.

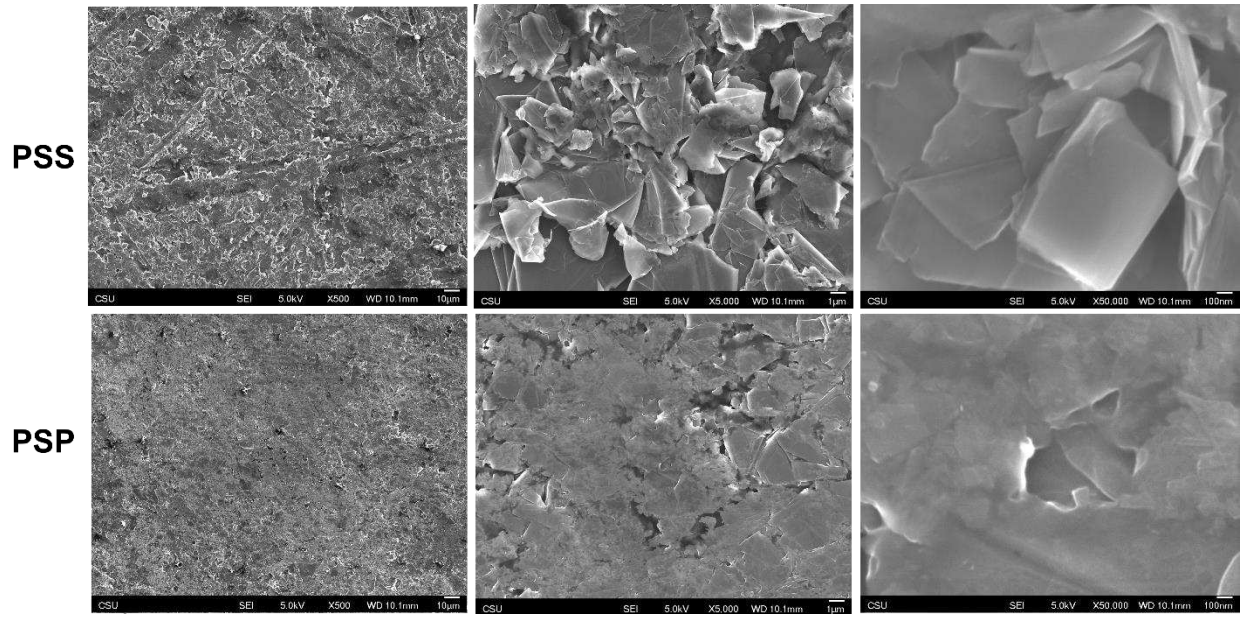

Figure 4.7 SEM images at (left to right) 500x, 5000x, and 50000x magnification of PS-based TPE material that was (top) sanded and (bottom) heat-pressed.

Electrochemical Characterization of PCL- and PS-based TPEs with Redox Probes

There are many well-known redox molecules that can be used to characterize an electrode material. Due to the significant differences in the surfaces shown in the SEM and XPS data, it was important to choose redox probes that interact with the electrode surface differently to gain the most information; therefore, an inner sphere and outer sphere probe were chosen. Inner sphere electron transfer requires the redox molecule to have a ligand that can break and form bonds with the electrode surface. As a result inner sphere redox molecules are very sensitive to changes in surface groups and morphology.[75] Outer sphere redox molecules do not need to form a bond for electron transfer, making the electron transfer only rely on density of electronic states as opposed to surface groups.[76] Typically, outer sphere electron transfer is much faster than inner sphere.[75]

$FcTMA^+$ was chosen as the outer sphere redox probe and cyclic voltammetry (CVs) of sanded and heat-pressed PCL- and PS-based TPEs are shown in **Figure 4.8(A)**. All the TPEs show

reversible electrochemistry, including the heat-pressed variations with significantly less edge planes. While outer sphere redox probes are less sensitive to surface defects, there are still significant differences in voltammetry for the different TPEs. The first difference is in the current magnitude. The sanded TPEs, as expected, had the highest current responses, with the anodic peak for PSS at 0.45 ± 0.04 mA cm^{-2} and the PCLS slightly lower at 0.35 ± 0.02 mA cm^{-2} (n=3). The sanded TPEs also have similar peak separation; however, the PCLS CV has much more capacitance, which can lead to higher background signal and higher detection limits. The increased capacitance is most likely a result of increased macroscopic surface roughness in PCL-based TPEs compared to PS-based TPEs previously reported, even though the microscopic topography has the opposite trend.[13] Additionally, the PSS CV contains an additional oxidative peak for PSS. The peak could be an oxygen peak from solution or surface functional groups. An alternative theory is it could result from very small amount of contaminant such as iron that was not detectable in the XPS survey scans. The heat-pressed TPEs have similar peak current with PSP at 0.17 ± 0.09 mA cm^{-2} and PCLP at 0.21 ± 0.01 mA cm^{-2}. The PSP CV interestingly is still very reversible with seemingly proportional capacitance to that of PSS. The unique shape of the PCLP CV appears sigmoidal, which is typically seen when steady-state current is obtained in flow.[77] However, assemblies of microelectrodes can also exhibit steady-state current, and O'Hare et al. demonstrated that carbon composite electrodes can behave similarly to microelectrodes given the proper composite ratios and conditions.[78] The PCLP could have pockets of conductive carbon and insulating PCL that could result in microelectrode behavior.

Dopamine was chosen as the inner sphere redox probe and CVs of sanded and heat-pressed PCL- and PS-based TPEs are shown in **Figure 4.8(B)**. Both heat-pressed PCL- and PS-based TPEs do not show reversible electrochemistry for dopamine. Slight current increases can be seen in the

PSP CV; however, these changes are minimal compared to the sanded TPEs. While basal planes are still conductive, electron transfer is generally considered much slower at the basal planes of graphite,[79] so this result continues to reaffirm the data from XPS and SEM of the PSP. The sanded TPEs, shown in the SEM (**Figure 4.6** & **4.7**) to have edge-plane rich surfaces, were more successful in electrochemically turning over dopamine.

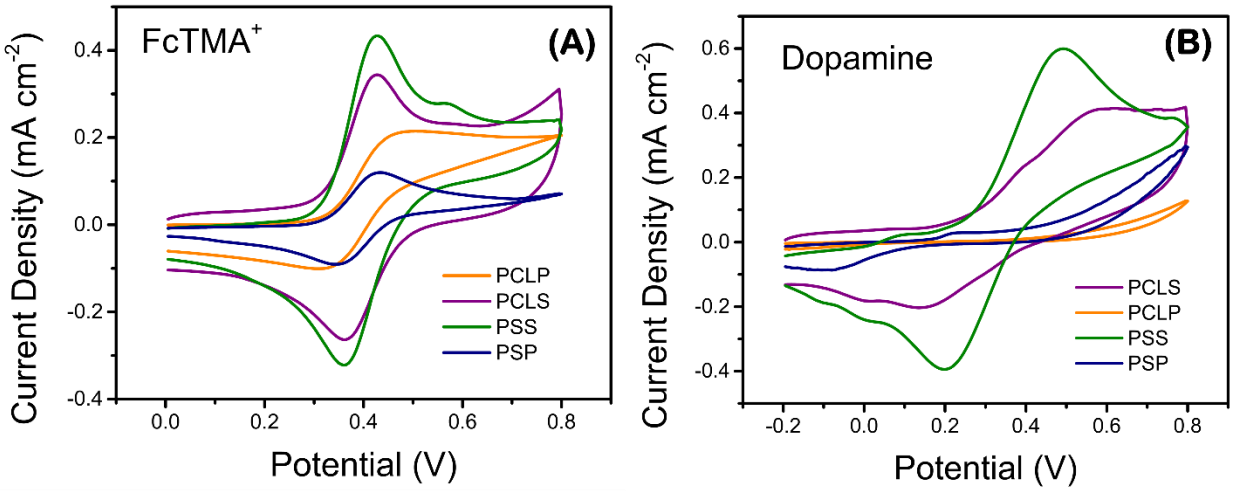

Figure 4.8 Representative CVs (n=3) of PCL- and PS-based TPEs that are sanded and heat-pressed in **(A)** 1 mM $FcTMA^+$ and **(B)** 1 mM dopamine in 0.1 M KNO_3. Potential was scanned vs. a SCE reference at a scan rate of 100 mV/s for both **(A)** and **(B)**.

PCLS is significantly more capacitive than PSS (like in the $FcTMA^+$ CVs) and has greater peak separation. In addition, PSS has higher peak current than PCLS (0.58 ± 0.06 versus 0.413 ± 0.006 mA cm^{-2} (n=3), respectively). The reversible electrochemistry exhibits excellent electrocatalytic activity on the unmodified TPEs, as carbon composite electrodes typically require modifications that can be expensive or time-consuming to achieve this type of electrochemistry with dopamine.[80] The PSS CVs are comparable to electrodes with glassy carbon, multiwalled carbon nanotubes, and graphene oxide.[2, 81-84]

Electrochemical Detection of O_2 and H_2O_2 of PS-based TPEs

Next, the ability of PS-based TPEs to detect O_2 was investigated. CVs of oxygen rich and oxygen deficient buffer were performed with sanded (**Figure 4.9(A)**) and heat-pressed (**Figure 4.9(B)**) PS-based electrodes. For PSS TPEs, reversible electrochemistry with an increase in both anodic and cathodic current is seen in phosphate buffer, likely from the oxidation and reduction of both the surface oxides and dissolved O_2. The cathodic current peak increases 13. ± 2. mA cm^{-2} (n=3) in the oxygen rich buffer. There is a slight change in the cathodic current for PSP but it does not contain peaks and the current is comparatively almost an order of magnitude lower than PSS.

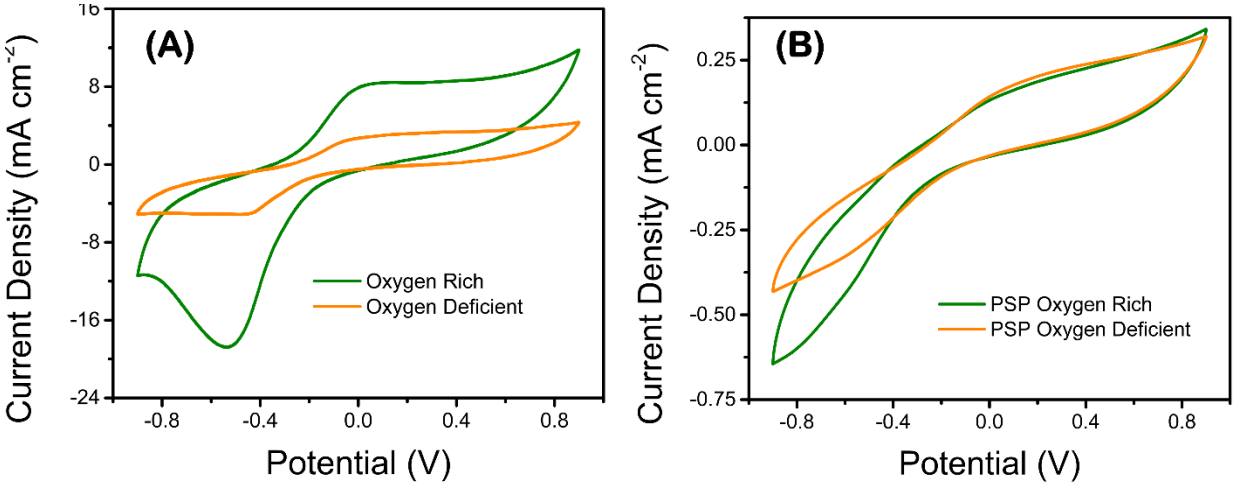

Figure 4.9 Representative CVs (n=3) of **(A)** sanded and **(B)** heat-pressed PS TPE in 0.05 M phosphate buffer (pH 7.4) with oxygen rich and oxygen deficient conditions. Oxygen rich conditions simply used the phosphate buffer as prepared. Oxygen deficient conditions were produced by sparging with N_2 for 30 min. Potential was scanned vs. a SCE reference at a scan rate of 100 mV/s for both A and B.

Figure 4.10 (A) shows CVs of increasing concentration of O_2 using sanded PS-based TPEs, and **Figure 4.10(B)** shows the correlation between cathodic peak height and sparging time. As the buffer is sparged with N_2, the dissolved O_2 concentration should decrease. The current decreases as expected with sparging time until 15 min where the O_2 appears to be fully depleted. These results are consistent with other carbon electrodes that involve more complex modification

for O_2 detection.[37, 41-44] Going forward, these data will need to be validated using a commercial O_2 sensor or other technique, but the results show great potential for ability to quantitatively detect O_2.

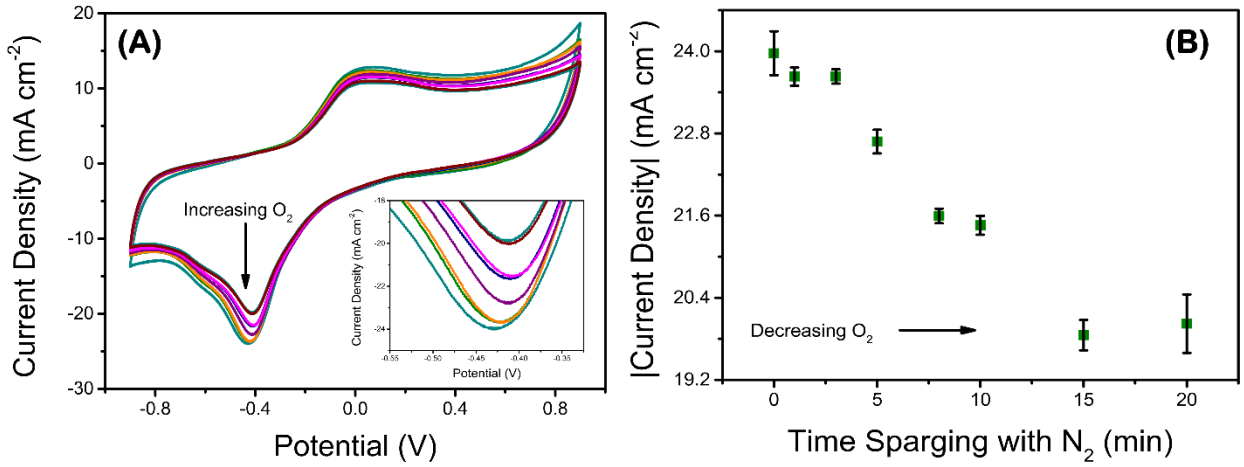

Figure 4.10 (A) Representative CVs (n=3) of sanded heat-pressed PS TPE in 0.05 M phosphate buffer (pH 7.4) with at varying time points of sparging N_2 from 0 to 20 min. Potential was scanned vs. a SCE reference at a scan rate of 100 mV/s. (Inset) Zoomed in plot of the cathodic peaks of the representative CVs. **(B)** Corresponding plot of the absolute value of the cathodic peak from the CVs vs. the time sparged. Symbols and error bars represent average and standard deviation of the cathodic peak current of different electrodes in the same sparged solution (n=3).

Similarly to O_2, an electrocatalyst or advanced electrochemical techniques (as fast scan cyclic voltammetry) is typically required to detect H_2O_2 on carbon composite electrodes.[44, 85] Because the sanded PS-based electrodes have consistently shown superior electrochemistry to the other TPEs, only the PSS TPEs were used to investigate H_2O_2 detection. The CVs shown in **Figure 4.11** show a significant current increase in both anodic and cathodic current in the presence of H_2O_2 and the blank signal from the electrolyte is an order of magnitude lower. The electrocatalytic activity towards molecules that are difficult to electrochemically detect, like H_2O_2 and O_2, demonstrates the fast electron transfer kinetics associated with the exposed edge planes that have also been confirmed with XPS and SEM.

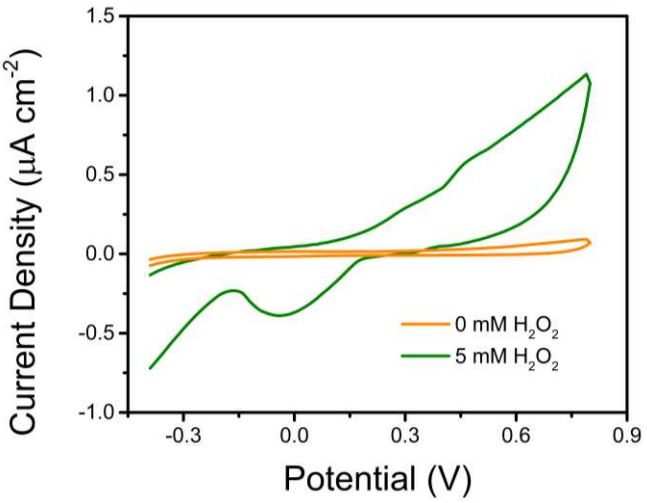

Figure 4.11 (A) Representative CVs (n=3) of sanded PS TPE in in 0.1 M KNO_3 with and without H_2O_2 (5mM). Potential was scanned vs. a SCE reference at a scan rate of 100 mV/s.

Sensor Module Design and Fabrication

After electrode material characterization, the PS-based TPEs were incorporated into a sensor module. TPEs have been previously reported as singular disk electrodes,[12-14] three electrode systems,[8, 11] and more complex electrochemical arrays.[9] All of these reports with the exception of those incorporated into fingertight fittings,[62, 63] used laser cutting or etching into plastics to produce the templates. This method is effective for most applications; however, complexity of electrode design is limited by the laser used and the electrode would need to undergo additional steps for integration into a fluidic device. This work presents the first use of a 3D-printed template for TPEs. 3D printing is an attractive method for device fabrication is because it allows all features of the electrode system template and fluidic channels to be fabricated at once and also enables rapid prototyping of different designs in one step.[86, 87] **Figure 4.1(A)** shows the quick, simple TPE fabrication technique to create the working and counter electrode in a 3D-printed template that serves as the top half of the sensor module. Briefly, the thermoplastic was solvated and combined with graphite. This mixture was mixed until it dried (typically under 10 minutes) and then heat-

pressed into the 3D-printed electrode template. Finally, excess material was sanded away. After the TPEs are integrated, the 3D-printed part a leakless Ag|AgCl reference electrode, previously reported.[66] Many reference electrodes require storage in a chloride solution when not in use, which would be inconvenient and potentially alter the surface of the other electrodes in the sensor module. The leakless reference used here does need storage solution and the solution needed for the electrode to function (described above in **4.3**) does not come into contact with the flow channels or other electrodes. A TPE carbon pseudo-reference electrode could also be used but Ag|AgCl is more stable.[88]

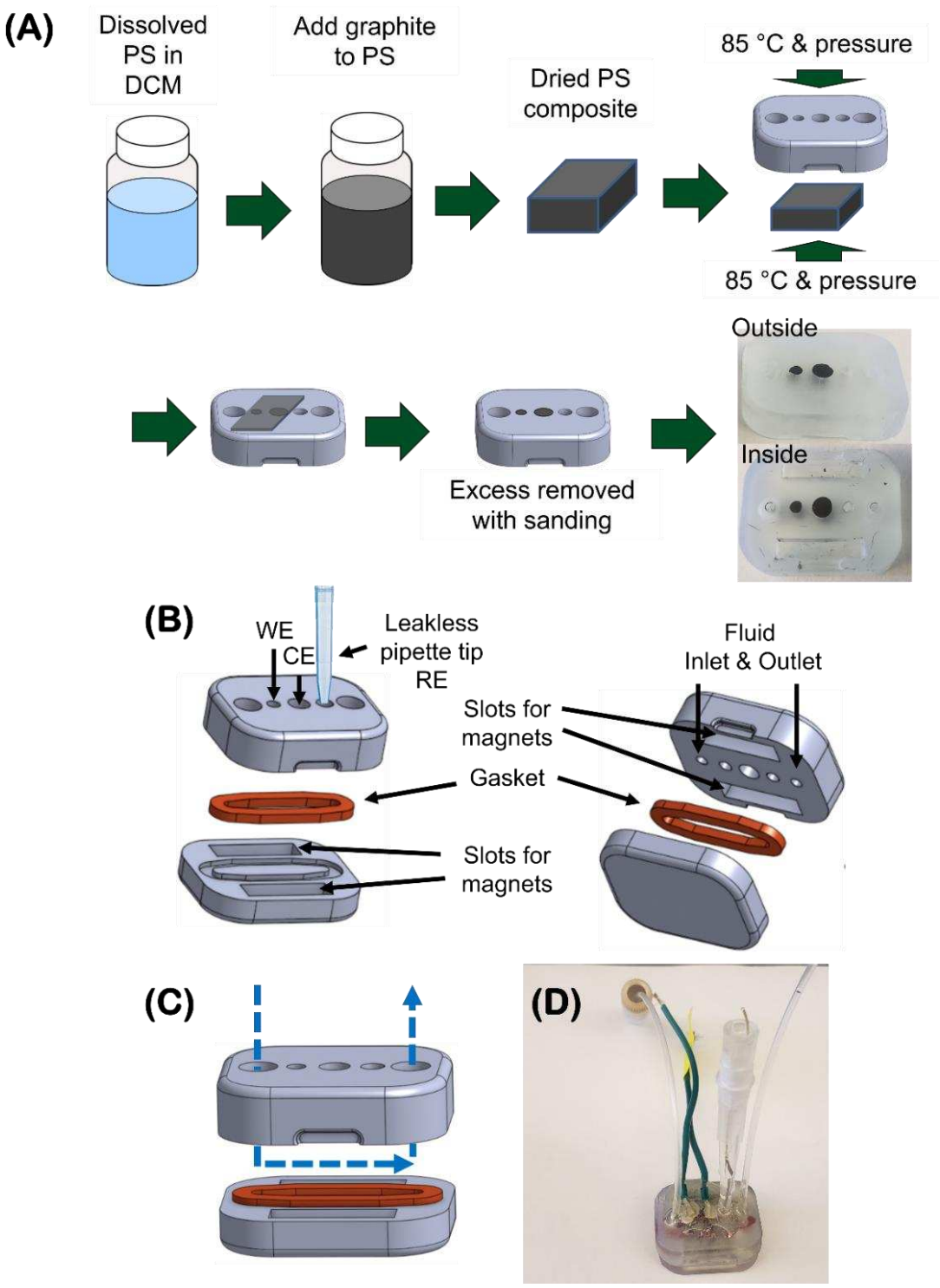

Figure 4.1 **(A)** Simple fabrication of PS TPEs, using a 3D- printed template for incorporation into a sensor module. **(B)** Exploded views of the sensor module showing 3D-printed parts, gasket, and locations for electrode integration. **(C)** Rendering of sensor module showing flow path. **(D)** Photograph of fully assembled TPE sensor module. 3D-printed device was designed by Amanda Cherwin. Leakless reference electrode was fabricated by Jason Boes.

Reversibly sealed fluidic devices are desirable because they can be disassembled, sterilized, and reused.[89] Different methods have been used to reversibly seal microfluidic devices, such as adhesive bonds,[90, 91] vacuum suction,[92, 93] and mechanical clamps fastened with screws[94, 95] or magnets.[96-98] The reported sensor module (a labeled exploded view shown in **Figure 4.1(B)**) uses magnets to allow for a simple, reversible seal. For the TPE sensor module, the reversible seal also allows for the TPE surface to be sanded and renewed or the entire sensor part can be swapped for a different set of electrodes that are optimized for different analytes. A gasket forms the fluidic channel (**Figure 4.1(C)**) between the electrode system and another 3D-printed part, using the magnets as the clamping force to seal the device. Once the gasket is placed, the sensor module self-aligns due to the arrangement of the magnets. Because the magnets dictate the alignment, the sensor module can be assembled correctly in under 5 s while maintaining high quality seals, even by untrained users. **Figure 4.1(D)** shows a picture of the fully assembled sensor module.

Proof-of-Concept H_2O_2 Detection in Flow with PS-based TPE Sensor Module

For a simple proof-of-concept, the reported sensor module with PS-based TPEs was used to detect H_2O_2 in flow. **Figure 4.12** shows a representative amperogram for long injections of H_2O_2 at a 1.0 mL/min flow rate. The relatively high flow rate and length of measurement (over 40 min) without leaks demonstrates the effectiveness reversible seal from the magnets. The peaks in the amperogram appear to stabilize and become more consistent after the first few injections. This plateau could be the result of the electrode's charging current still dissipating. It is very common for electrochemical sensors to require a significant "warm-up" period to reduce charging current in measurements.[99] **Figure 4.12** also shows the relative stability of the PS-based TPEs over a continuous 40+ min measurement. Even near the end of the measurement, the current still returns to the approximate baseline. The inconsistencies in peaks, baseline, and current response could be

a result of manual valve and pump changing. This proof-of-concept indicates the potential for this system to be used for enzymatic sensing in flow.

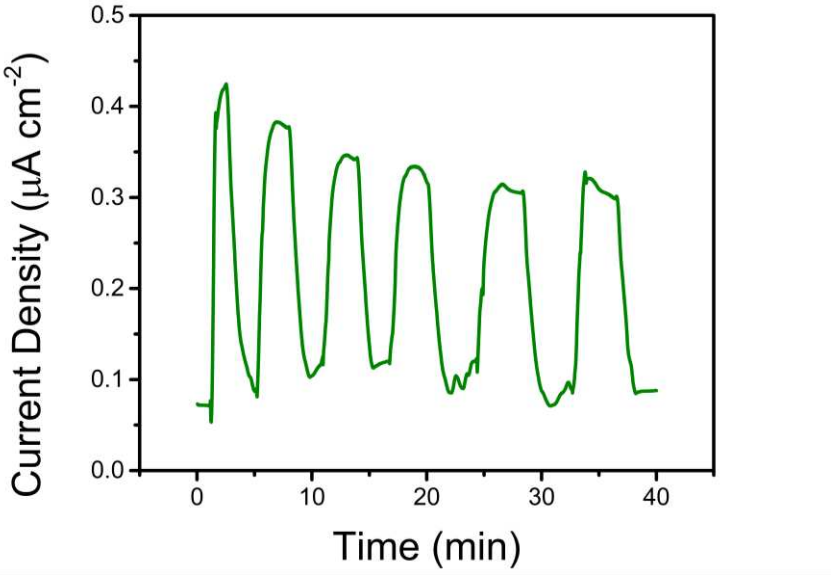

Figure 4.12 Amperogram showing changes in current measured the sensor module with sanded PS-based TPEs. Six additions of 1 mM H_2O_2 were measured across 40 min. Potential was held at +0.6 V vs. Ag|AgCl reference. Flow rate was 1.0 mL/min.

4.5 Conclusion

In summary, this work explores the electrochemical properties of TPEs with two different binders (PCL and PS). XPS and SEM analysis suggested that sanded TPEs had a high density of edge plane graphite on the surface and heat-pressed TPEs have more basal plane orientations. PS-based TPEs showed a particularly high density of edge planes likely due with π-π interactions between the aromatic groups in PS and the graphite. As a result, the sanded PS-based TPEs demonstrated increased electroactivity. The PS-based TPEs were used to detect H_2O_2 and O_2 without any electrode modification. The PS-based TPEs were also integrated into a reversibly sealed fluidic sensor module device in which detection of H_2O_2 demonstrated in flow. The design of the sensor module allows for simple electrode integration and assembly that can be coupled with a variety of

fluidic systems. The proof-of-concept detecting H_2O_2 with the sensor module will work towards a system for simple enzymatic detection of various biomolecules such as lactate and glucose in complex biological environments by incorporating an additional flow path with an oxidase enzyme.

REFERENCES

1. Adams, R. N., Carbon paste electrodes. *Analytical chemistry* **1958,** *30* (9), 1576-1576.

2. Aguilar, R.; Davila, M.; Elizalde, M.; Mattusch, J.; Wennrich, R., Capability of a carbon–polyvinylchloride composite electrode for the detection of dopamine, ascorbic acid and uric acid. *Electrochimica acta* **2004,** *49* (6), 851-859.

3. McCreery, R. L., Advanced carbon electrode materials for molecular electrochemistry. *Chem. Rev.* **2008,** *108* (7), 2646-2687.

4. Tallman, D. E.; Petersen, S. L., COMPOSITE ELECTRODES FOR ELECTROANALYSIS - PRINCIPLES AND APPLICATIONS. *Electroanalysis* **1990,** *2* (7), 499-510.

5. O'Hare, D.; Macpherson, J. V.; Willows, A., On the microelectrode behaviour of graphite-epoxy composite electrodes. *Electrochemistry Communications* **2002,** *4* (3), 245-250.

6. Wang, S. C.; Chang, K. S.; Yuan, C. J., Enhancement of electrochemical properties of screen-printed carbon electrodes by oxygen plasma treatment. *Electrochimica Acta* **2009,** *54* (21), 4937-4943.

7. Klunder, K. J.; Nilsson, Z.; Sambur, J. B.; Henry, C. S., Patternable Solvent-Processed Thermoplastic Graphite Electrodes. *J. Am. Chem. Soc.* **2017,** *139* (36), 12623-12631.

8. Klunder, K. J.; Clark, K. M.; McCord, C.; Berg, K. E.; Minteer, S. D.; Henry, C. S., Polycaprolactone-enabled sealing and carbon composite electrode integration into electrochemical microfluidics. *Lab on a Chip* **2019,** *19* (15), 2589-2597.

9. Noviana, E.; Klunder, K. J.; Channon, R. B.; Henry, C. S., Thermoplastic Electrode Arrays in Electrochemical Paper-Based Analytical Devices. *Analytical Chemistry* **2019,** *91* (3), 2431-2438.

10. Berg, K. E.; Leroux, Y. R.; Hapiot, P.; Henry, C. S., Increasing Applications of Graphite Thermoplastic Electrodes with Aryl Diazonium Grafting. *ChemElectroChem* **2019,** *6* (18), 4811-4816.

11. Pradela-Filho, L. A.; Noviana, E.; Araujo, D.; Takeuchi, R.; Santos, A.; Henry, C. S., Rapid Analysis in Continuous Flow Electrochemical Paper-Based Analytical Devices. *ACS sensors* **2020**.

12. Clark, K. M.; Henry, C. S., Thermoplastic Electrode (TPE)-based Enzymatic Glucose Sensor Using Polycaprolactone-graphite Composites. *Electroanalysis* **2021**.

13. McCord, C. P.; Summers, B.; Henry, C. S., Redox behavior and surface morphology of polystyrene thermoplastic electrodes. *Electrochimica Acta* **2021,** *393*, 139069.

14. McCord, C. P.; Summers, B.; Henry, C., Simultaneous Analysis of Ascorbic Acid, Uric Acid, and Dopamine at Bare Polystyrene Thermoplastic Electrodes. *ChemElectroChem* **2022**.

15. Berg, K. E.; Clark, K. M.; Li, X.; Carter, E. M.; Volckens, J.; Henry, C. S., High-throughput, semi-automated dithiothreitol (DTT) assays for oxidative potential of fine particulate matter. *Atmospheric Environment* **2020,** *222*, 117132.

16. de Lima, L. F.; de Freitas, A. d. S.; Ferreira, A. L.; Maciel, C. C.; Ferreira, M.; de Araujo, W. R., Enzymeless glucose sensor based on disposable Ecoflex®/graphite thermoplastic composite substrate modified with Au@ GQDs. *Sensors and Actuators Reports* **2022**, 100102.

17. Lee, Y. K., The effect of active material, conductive additives, and binder in a cathode composite electrode on battery performance. *Energies* **2019,** *12* (4), 658.

18. Wang, Y.; Dang, D.; Li, D.; Hu, J.; Zhan, X.; Cheng, Y.-T., Effects of polymeric binders on the cracking behavior of silicon composite electrodes during electrochemical cycling. *Journal of Power Sources* **2019,** *438*, 226938.

19. Labet, M.; Thielemans, W., Synthesis of polycaprolactone: a review. *Chemical Society Reviews* **2009,** *38* (12), 3484-3504.

20. Malikmammadov, E.; Tanir, T. E.; Kiziltay, A.; Hasirci, V.; Hasirci, N., PCL and PCL-based materials in biomedical applications. *Journal of Biomaterials Science, Polymer Edition* **2018,** *29* (7-9), 863-893.

21. Woodruff, M. A.; Hutmacher, D. W., The return of a forgotten polymer—Polycaprolactone in the 21st century. *Progress in Polymer Science* **2010,** *35* (10), 1217-1256.

22. Salminen, K.; Grönroos, P.; Eskola, J.; Nieminen, E.; Härmä, H.; Kulmala, S., Immunoassay of C-reactive protein by hot electron-induced electrochemiluminescence at polystyrene-carbon black composite electrodes. *Electrochimica Acta* **2018,** *282*, 147-154.

23. Jose, D. A.; Prakash, P.; Baby Chakrapani, P., Containers Based on Polymers in Biomedical Devices/Medical Applications. In *Micro-and Nano-containers for Smart Applications*, Springer: 2022; pp 179-195.

24. Salminen, K.; Grönroos, P.; Tuomi, S.; Kulmala, S., Cathodic electrogenerated chemiluminescence of aromatic Tb (III) chelates at polystyrene-graphite composite electrodes. *Anal. Chim. Acta* **2017,** *985*, 54-60.

25. Fernandez-Sanchez, C.; Pellicer, E.; Orozco, J.; Jimenez-Jorquera, C.; Lechuga, L. M.; Mendoza, E., Plasma-activated multi-walled carbon nanotube-polystyrene composite substrates for biosensing. *Nanotechnology* **2009,** *20* (33).

26. Quan, H.; Park, S.-U.; Park, J., Electrochemical oxidation of glucose on silver nanoparticle-modified composite electrodes. *Electrochimica Acta* **2010,** *55* (7), 2232-2237.

27. Orozco, J.; Fernandez-Sanchez, C.; Mendoza, E.; Baeza, M.; Cespedes, F.; Jimenez-Jorquera, C., Composite planar electrode for sensing electrochemical oxygen demand. *Anal. Chim. Acta* **2008,** *607* (2), 176-182.

28. Saghatforoush, L.; Hasanzadeh, M.; Shadjou, N., Polystyrene-graphene oxide modified glassy carbon electrode as a new class of polymeric nanosensors for electrochemical determination of histamine. *Chinese Chemical Letters* **2014,** *25* (4), 655-658.

29. Liu, W.; Xiao, J.; Wang, C.; Yin, H.; Xie, H.; Cheng, R., Synthesis of polystyrene-grafted-graphene hybrid and its application in electrochemical sensor of dopamine. *Materials Letters* **2013,** *100*, 70-73.

30. Khaskheli, A. R.; Fischer, J.; Barek, J.; Vyskocil, V.; Sirajuddin; Bhanger, M. I., Differential pulse voltammetric determination of paracetamol in tablet and urine samples at a micro-crystalline natural graphite-polystyrene composite film modified electrode. *Electrochimica Acta* **2013,** *101*, 238-242.

31. Lu, Y.; Wang, X.; Chen, D. F.; Chen, G., Polystyrene/graphene composite electrode fabricated by in situ polymerization for capillary electrophoretic determination of bioactive constituents in Herba Houttuyniae. *Electrophoresis* **2011,** *32* (14), 1906-1912.

32. Surkov, A. M.; Queiroz, R. G.; Rinco, R. S.; Rios, A. G.; Gutz, I. G.; Baccaro, A. L.; Angnes, L., Graphite-polystyrene composite with enhanced electrochemical and electroanalytical performance. *Talanta* **2021,** *223*, 121780.

33. Rymansaib, Z.; Iravani, P.; Emslie, E.; Medvidović-Kosanović, M.; Sak-Bosnar, M.; Verdejo, R.; Marken, F., All-Polystyrene 3D-Printed Electrochemical Device with Embedded Carbon Nanofiber-Graphite-Polystyrene Composite Conductor. *Electroanalysis* **2016,** *28* (7), 1517-1523.

34. Promphet, N.; Rattanarat, P.; Rangkupan, R.; Chailapakul, O.; Rodthongkum, N., An electrochemical sensor based on graphene/polyaniline/polystyrene nanoporous fibers modified electrode for simultaneous determination of lead and cadmium. *Sens. Actuator B-Chem.* **2015,** *207*, 526-534.

35. Gutiérrez-Capitán, M.; Baldi, A.; Gómez, R.; García, V.; Jiménez-Jorquera, C.; Fernández-Sánchez, C. s., Electrochemical nanocomposite-derived sensor for the analysis of chemical oxygen demand in urban wastewaters. *Analytical chemistry* **2015,** *87* (4), 2152-2160.

36. Xu, J.; Zhang, H.; Chen, G., Carbon nanotube/polystyrene composite electrode for microchip electrophoretic determination of rutin and quercetin in Flos Sophorae Immaturus. *Talanta* **2007,** *73* (5), 932-937.

37. Wei, Y.; Jiao, Y.; An, D.; Li, D.; Li, W.; Wei, Q., Review of dissolved oxygen detection technology: From laboratory analysis to online intelligent detection. *Sensors* **2019,** *19* (18), 3995.

38. Rivas, L.; Dulay, S.; Miserere, S.; Pla, L.; Marin, S. B.; Parra, J.; Eixarch, E.; Gratacós, E.; Illa, M.; Mir, M., Micro-needle implantable electrochemical oxygen sensor: ex-vivo and in-vivo studies. *Biosensors and Bioelectronics* **2020,** *153*, 112028.

39. Triana, Y.; Ogata, G.; Tomisaki, M.; Irkham; Einaga, Y., Blood Oxygen Sensor Using a Boron-Doped Diamond Electrode. *Analytical Chemistry* **2022,** *94* (9), 3948-3955.

40. Preidel, W.; Rao, J.; Mund, K.; Schunck, O.; David, E., A new principle for an electrochemical oxygen sensor. *Sensors and Actuators B: Chemical* **1995,** *28* (1), 71-74.

41. Cui, H.-F.; Ye, J.-S.; Zhang, W.-D.; Wang, J.; Sheu, F.-S., Electrocatalytic reduction of oxygen by a platinum nanoparticle/carbon nanotube composite electrode. *Journal of Electroanalytical Chemistry* **2005,** *577* (2), 295-302.

42. López-Gándara, C.; Ramos, F. M.; Cirera, A., YSZ-based oxygen sensors and the use of nanomaterials: a review from classical models to current trends. *Journal of Sensors* **2009,** *2009*.

43. Jose, S.; Rajeev, R.; Thadathil, D. A.; Varghese, A.; Hegde, G., A road map on nanostructured surface tuning strategies of carbon fiber paper electrode: Enhanced electrocatalytic applications. *Journal of Science: Advanced Materials and Devices* **2022**, 100460.

44. Liu, L.; Guo, L.-p.; Bo, X.-j.; Bai, J.; Cui, X.-j., Electrochemical sensors based on binuclear cobalt phthalocyanine/surfactant/ordered mesoporous carbon composite electrode. *Analytica chimica acta* **2010,** *673* (1), 88-94.

45. Chen, W.; Cai, S.; Ren, Q.-Q.; Wen, W.; Zhao, Y.-D., Recent advances in electrochemical sensing for hydrogen peroxide: a review. *Analyst* **2012,** *137* (1), 49-58.

46. Hosu, I. S.; Wang, Q.; Vasilescu, A.; Peteu, S. F.; Raditoiu, V.; Railian, S.; Zaitsev, V.; Turcheniuk, K.; Wang, Q.; Li, M., Cobalt phthalocyanine tetracarboxylic acid modified reduced graphene oxide: a sensitive matrix for the electrocatalytic detection of peroxynitrite and hydrogen peroxide. *RSC advances* **2015,** *5* (2), 1474-1484.

47. Wang, H.; Bu, Y.; Dai, W.; Li, K.; Wang, H.; Zuo, X., Well-dispersed cobalt phthalocyanine nanorods on graphene for the electrochemical detection of hydrogen peroxide and glucose sensing. *Sensors and Actuators B: Chemical* **2015,** *216*, 298-306.

48. Liu, C.; Qu, Y.; Luo, Y.; Fang, N., Recent advances in single-molecule detection on micro- and nano-fluidic devices. *ELECTROPHORESIS* **2011,** *32* (23), 3308-3318.

49. Ng, A. H. C.; Uddayasankar, U.; Wheeler, A. R., Immunoassays in microfluidic systems. *Analytical and Bioanalytical Chemistry* **2010,** *397* (3), 991-1007.

50. Ozer, T.; McMahon, C.; Henry, C. S., Advances in Paper-Based Analytical Devices. *Annual Review of Analytical Chemistry* **2020,** *13* (1), 85-109.

51. Bhatia, S. N.; Ingber, D. E., Microfluidic organs-on-chips. *Nature Biotechnology* **2014,** *32* (8), 760-772.

52. Hamedi, M. M.; Unal, B.; Kerr, E.; Glavan, A. C.; Fernandez-Abedul, M. T.; Whitesides, G. M., Coated and uncoated cellophane as materials for microplates and open-channel microfluidics devices. *Lab on a Chip* **2016,** *16* (20), 3885-3897.

53. Pereira, S. V.; Bertolino, F. A.; Fernandez-Baldo, M. A.; Messina, G. A.; Salinas, E.; Sanz, M. I.; Raba, J., A microfluidic device based on a screen-printed carbon electrode with electrodeposited gold nanoparticles for the detection of IgG anti-Trypanosoma cruziantibodies. *Analyst* **2011,** *136* (22), 4745-4751.

54. Kovarik, M. L.; Torrence, N. J.; Spence, D. M.; Martin, R. S., Fabrication of carbon microelectrodes with a micromolding technique and their use in microchip-based flow analyses. *Analyst* **2004,** *129* (5), 400-405.

55. Moore, C. M.; Minteer, S. D.; Martin, R. S., Microchip-based ethanol/oxygen biofuel cell. *Lab on a Chip* **2005,** *5* (2), 218-225.

56. Chen, C.-H.; Lin, Y.-T.; Lin, M.-S., Fabrication of a totally renewable off-channel amperometric platform for microchip electrophoresis. *Analytica Chimica Acta* **2015,** *874*, 33-39.

57. Erkal, J. L.; Selimovic, A.; Gross, B. C.; Lockwood, S. Y.; Walton, E. L.; McNamara, S.; Martin, R. S.; Spence, D. M., 3D Printed Microfluidic Devices with Integrated Versatile and Reusable Electrodes. *Lab on a chip* **2014,** *14* (12), 2023-2032.

58. Wang, J.; Pumera, M.; Chatrathi, M. P.; Escarpa, A.; Konrad, R.; Griebel, A.; Dörner, W.; Löwe, H., Towards disposable lab-on-a-chip: Poly(methylmethacrylate) microchip electrophoresis device with electrochemical detection. *ELECTROPHORESIS* **2002,** *23* (4), 596-601.

59. Pradela-Filho, L. A.; Araújo, D. A.; Takeuchi, R. M.; Santos, A. L.; Henry, C. S., Thermoplastic electrodes as a new electrochemical platform coupled to microfluidic devices for tryptamine determination. *Analytica Chimica Acta* **2021,** *1147*, 116-123.

60. Pradela-Filho, L. A.; Noviana, E.; Araujo, D. A.; Takeuchi, R. M.; Santos, A. L.; Henry, C. S., Rapid analysis in continuous-flow electrochemical paper-based analytical devices. *ACS sensors* **2020,** *5* (1), 274-281.

61. Zhang, Y. S.; Aleman, J.; Shin, S. R.; Kilic, T.; Kim, D.; Mousavi Shaegh, S. A.; Massa, S.; Riahi, R.; Chae, S.; Hu, N.; Avci, H.; Zhang, W.; Silvestri, A.; Sanati Nezhad, A.; Manbohi, A.; De Ferrari, F.; Polini, A.; Calzone, G.; Shaikh, N.; Alerasool, P.; Budina, E.; Kang, J.; Bhise, N.; Ribas, J.; Pourmand, A.; Skardal, A.; Shupe, T.; Bishop, C. E.; Dokmeci, M. R.; Atala, A.; Khademhosseini, A., Multisensor-integrated organs-on-chips platform for automated and continual in situ monitoring of organoid behaviors. *Proc Natl Acad Sci U S A* **2017,** *114* (12), E2293-E2302.

62. Roley, A.; Clark, K.; Richardson, A.; Martinez, B.; Tobet, S.; Henry, C., User-friendly, magnetically sealed plug-and-play sensor module for online electrochemical sensing for fluidic devices. **2021**.

63. Ozer, T.; McCord, C.; Geiss, B.; Dandy, D.; Henry, C. S., Thermoplastic Electrodes for Detection of Escherichia coli. *Journal of the Electrochemical Society* **2021,** *168* (4).

64. Lemay, S. G.; van den Broek, D. M.; Storm, A. J.; Krapf, D.; Smeets, R. M.; Heering, H. A.; Dekker, C., Lithographically fabricated nanopore-based electrodes for electrochemistry. *Analytical chemistry* **2005,** *77* (6), 1911-1915.

65. Chen, X.; Wang, X.; Fang, D., A review on C1s XPS-spectra for some kinds of carbon materials. *Fullerenes, Nanotubes and Carbon Nanostructures* **2020,** *28* (12), 1048-1058.

66. Walker, N. L.; Dick, J. E., Leakless, Bipolar Reference Electrodes: Fabrication, Performance, and Miniaturization. *Analytical chemistry* **2021,** *93* (29), 10065-10074.

67. Eng, A. Y. S.; Chua, C. K.; Pumera, M., Refinements to the structure of graphite oxide: absolute quantification of functional groups via selective labelling. *Nanoscale* **2015,** *7* (47), 20256-20266.

68. Mazzotta, E.; Rella, S.; Turco, A.; Malitesta, C., XPS in development of chemical sensors. *RSC advances* **2015,** *5* (101), 83164-83186.

69. Gengenbach, T. R.; Major, G. H.; Linford, M. R.; Easton, C. D., Practical guides for x-ray photoelectron spectroscopy (XPS): Interpreting the carbon 1s spectrum. *Journal of Vacuum Science & Technology A: Vacuum, Surfaces, and Films* **2021,** *39* (1), 013204.

70. Morgan, D. J., Comments on the XPS analysis of carbon materials. *C* **2021,** *7* (3), 51.

71. Richter, E. M.; Rocha, D. P.; Cardoso, R. M.; Keefe, E. M.; Foster, C. W.; Munoz, R. A.; Banks, C. E., Complete additively manufactured (3D-printed) electrochemical sensing platform. *Analytical chemistry* **2019,** *91* (20), 12844-12851.

72. Al-Gaashani, R.; Najjar, A.; Zakaria, Y.; Mansour, S.; Atieh, M., XPS and structural studies of high quality graphene oxide and reduced graphene oxide prepared by different chemical oxidation methods. *Ceramics International* **2019,** *45* (11), 14439-14448.

73. Sheshmani, S.; Fashapoyeh, M. A., Suitable chemical methods for preparation of graphene oxide, graphene and surface functionalized graphene nanosheets. *Acta Chimica Slovenica* **2014,** *60* (4), 813-825.

74. Deanin, R. D., Compatibility and practical properties of polymer blends. In *Applications of Polymers*, Springer: 1988; pp 53-63.

75. Bard, A. J.; Faulkner, L. R., Electrochemical Methods: Fundamentals and Applications. *Surface Technology* **1983,** *20* (1), 91-92.

76. Velický, M. j.; Toth, P. S.; Woods, C. R.; Novoselov, K. S.; Dryfe, R. A., Electrochemistry of the basal plane versus edge plane of graphite revisited. *The Journal of Physical Chemistry C* **2019,** *123* (18), 11677-11685.

77. Adesokan, B. J.; Quan, X.; Evgrafov, A.; Heiskanen, A.; Boisen, A.; Sørensen, M. P., Experimentation and numerical modeling of cyclic voltammetry for electrochemical micro-sized sensors under the influence of electrolyte flow. *Journal of Electroanalytical Chemistry* **2016,** *763*, 141-148.

78. O'Hare, D.; Macpherson, J. V.; Willows, A., On the microelectrode behaviour of graphite–epoxy composite electrodes. *Electrochemistry Communications* **2002,** *4* (3), 245-250.

79. Banks, C. E.; Compton, R. G., New electrodes for old: from carbon nanotubes to edge plane pyrolytic graphite. *Analyst* **2006,** *131* (1), 15-21.

80. Sajid, M.; Baig, N.; Alhooshani, K., Chemically modified electrodes for electrochemical detection of dopamine: Challenges and opportunities. *TrAC Trends in Analytical Chemistry* **2019,** *118*, 368-385.

81. Chen, P.-Y.; Vittal, R.; Nien, P.-C.; Ho, K.-C., Enhancing dopamine detection using a glassy carbon electrode modified with MWCNTs, quercetin, and Nafion®. *Biosensors and Bioelectronics* **2009,** *24* (12), 3504-3509.

82. Cheemalapati, S.; Palanisamy, S.; Mani, V.; Chen, S.-M., Simultaneous electrochemical determination of dopamine and paracetamol on multiwalled carbon nanotubes/graphene oxide nanocomposite-modified glassy carbon electrode. *Talanta* **2013,** *117*, 297-304.

83. Khan, M., Graphene oxide modified electrodes for dopamine sensing. *Journal of Nanomaterials* **2017,** *2017*.

84. Kumar, M.; Swamy, B. K.; Reddy, S.; Zhao, W.; Chetana, S.; Kumar, V. G., ZnO/functionalized MWCNT and Ag/functionalized MWCNT modified carbon paste electrodes for the determination of dopamine, paracetamol and folic acid. *Journal of Electroanalytical Chemistry* **2019,** *835*, 96-105.

85. Puthongkham, P.; Venton, B. J., Recent advances in fast-scan cyclic voltammetry. *Analyst* **2020,** *145* (4), 1087-1102.

86. Samper, I. C.; Gowers, S. A. N.; Rogers, M. L.; Murray, D. R. K.; Jewell, S. L.; Pahl, C.; Strong, A. J.; Boutelle, M. G., 3D printed microfluidic device for online detection of neurochemical changes with high temporal resolution in human brain microdialysate. *Lab Chip* **2019,** *19* (11), 2038-2048.

87. Waldbaur, A.; Rapp, H.; Länge, K.; Rapp, B. E., Let there be chip—towards rapid prototyping of microfluidic devices: one-step manufacturing processes. *Analytical Methods* **2011,** *3* (12).

88. Ruch, P. W.; Cericola, D.; Hahn, M.; Kötz, R.; Wokaun, A., On the use of activated carbon as a quasi-reference electrode in non-aqueous electrolyte solutions. *Journal of Electroanalytical Chemistry* **2009,** *636* (1-2), 128-131.

89. Temiz, Y.; Lovchik, R. D.; Kaigala, G. V.; Delamarche, E., Lab-on-a-chip devices: How to close and plug the lab? *Microelectronic Engineering* **2015,** *132*, 156-175.

90. Thompson, C. S.; Abate, A. R., Adhesive-based bonding technique for PDMS microfluidic devices. *Lab Chip* **2013,** *13* (4), 632-5.

91. Gong, X.; Yi, X.; Xiao, K.; Li, S.; Kodzius, R.; Qin, J.; Wen, W., Wax-bonding 3D microfluidic chips. *Lab Chip* **2010,** *10* (19), 2622-7.

92. Chung, B. G.; Park, J. W.; Hu, J. S.; Huang, C.; Monuki, E. S.; Jeon, N. L., A hybrid microfluidic-vacuum device for direct interfacing with conventional cell culture methods. *BMC Biotechnol* **2007,** *7*, 60.

93. Schaff, U. Y.; Xing, M. M.; Lin, K. K.; Pan, N.; Jeon, N. L.; Simon, S. I., Vascular mimetics based on microfluidics for imaging the leukocyte--endothelial inflammatory response. *Lab Chip* **2007,** *7* (4), 448-56.

94. Lamberti, A.; Sacco, A.; Bianco, S.; Giuri, E.; Quaglio, M.; Chiodoni, A.; Tresso, E., Microfluidic sealing and housing system for innovative dye-sensitized solar cell architecture. *Microelectronic Engineering* **2011,** *88* (8), 2308-2310.

95. Konda, A.; Taylor, J. M.; Stoller, M. A.; Morin, S. A., Reconfigurable microfluidic systems with reversible seals compatible with 2D and 3D surfaces of arbitrary chemical composition. *Lab Chip* **2015,** *15* (9), 2009-17.

96. Abhyankar, V. V.; Wu, M.; Koh, C. Y.; Hatch, A. V., A Reversibly Sealed, Easy Access, Modular (SEAM) Microfluidic Architecture to Establish In Vitro Tissue Interfaces. *PLoS One* **2016,** *11* (5), e0156341.

97. Tkachenko, E.; Gutierrez, E.; Ginsberg, M. H.; Groisman, A., An easy to assemble microfluidic perfusion device with a magnetic clamp. *Lab Chip* **2009,** *9* (8), 1085-95.

98. Rafat, M.; Raad, D. R.; Rowat, A. C.; Auguste, D. T., Fabrication of reversibly adhesive fluidic devices using magnetism. *Lab Chip* **2009,** *9* (20), 3016-9.

99. Mujeeb-U-Rahman, M.; Nazari, M. H.; Sencan, M., A novel semiconductor based wireless electrochemical sensing platform for chronic disease management. *Biosensors and Bioelectronics* **2019,** *124*, 66-74.

CHAPTER 5: ELECTROCHEMICAL CAPILLARY DRIVEN IMMUNOASSAY FOR DETECTION OF SARS-COV-2

5.1 Chapter Overview

The COVID-19 pandemic focused attention on a pressing need for fast, accurate, and low-cost diagnostic tests. This work presents an electrochemical capillary driven immunoassay (eCaDI) developed to detect SARS-CoV-2 nucleocapsid (N) protein. The low-cost flow device is made of polyethylene terephthalate (PET) and adhesive films. Upon addition of a sample, reagents and washes are sequentially delivered to an integrated screen-printed carbon electrode for detection, thus automating a full sandwich immunoassay with a single end-user step. The modified electrodes are sensitive and selective for COVID-19 N protein and stable for over seven weeks. The eCaDI was tested with influenza A and Sindbis virus and proved to be selective. The eCaDI was also successfully applied to detect nine different SARS-CoV-2 variants, including Omicron (NR-56486). The work in this chapter is submitted to *ACS Measurement Science Au* entitled "Electrochemical Capillary Driven Immunoassay for Detection Of SARS-CoV-2." This was a multi-author work built on the contributions of many. Illhoon Jang, Wisarut Khamcharoen, and Isabelle Samper performed preliminary work not included in this dissertation, but without their contributions the work presented here would not exist. Loran Anderson inactivated and titered the virus solutions used in this work. Melissa Schenkel and Trey Pittman assisted with experimental preparation in this work. Additionally, Melissa Schenkel collected some of the data presented in this chapter, further denoted in the figure captions. If not denoted in the figure caption, the data included in this chapter was collected and processed by myself.

5.2 Introduction

The outbreak of COVID-19, caused by the infectious severe acute respiratory syndrome coronavirus-2 (SARS-CoV-2), demonstrated a critical need for developments in point-of-care diagnostics.[1] There are many COVID-19 tests on the market,[2] yet reverse transcriptase polymerase chain reaction (rt-PCR) is still often the recommended and/or required testing option. Rt-PCR tests detect the viral RNA and remain the gold standard for testing due to low LODs and high specificity.[3] Unfortunately, the rt-PCR assay requires specialized laboratories and takes hours to complete, and the demand created by the COVID-19 pandemic overwhelmed the facilities that run these assays. Consequently, it often takes several days from test to result.[4] Enzyme linked immunosorbent assays (ELISAs) are another diagnostic tool that can be used to detect COVID-19-associated antigens or antibodies.[4] Unfortunately, traditional ELISAs also need to be performed in a laboratory setting, require many tedious steps or complicated robotics, and can take several hours to complete.[5]

Alternatively, lateral flow assays (LFAs) detect antigens or antibodies and greatly reduce the time to result.[6] Generally, the addition of a sample induces capillary flow through a nitrocellulose strip, and dried reagents are delivered sequentially to produce a colorimetric signal of two lines for a positive sample and one line for a negative sample. Unfortunately, these devices are significantly less sensitive with higher limits of detection than more sophisticated techniques like ELISA.[7, 8] There is not an ideal test with the optimal accuracy, accessibility, affordability, and timeliness of results. Therefore, carefully balancing the benefits and drawbacks of these factors is important for controlling the COVID-19 pandemic as well as endemic diseases in the future.[9] Many COVID-19 tests reported in academic literature are attempting to fill the gaps in currently available tests.[10-12]

Microfluidic and other flow devices have been developed to perform traditional lab-based techniques like rt-PCR, rt-LAMP, nested PCR, nucleic acid hybridization, ELISA, and fluorescence based assays.[13] These relatively low cost devices reduce the sample volumes needed and provide platforms to control reactions, separations, delivery of reagents, and quick detection with high sensitivity.[14] There have been many attempts to automate multi-step assays such as ELISA in inexpensive flow devices.[15] Flow of reagent delivery has been controlled by chemical barriers,[16, 17] physical barriers,[18, 19] hydrophobic barriers, [20] and complex geometric fluid paths in the paper-based devices.[21, 22] Many still require more than one user step.[20] In 2013, Apilux et al. introduced an automated sandwich ELISA with one sample addition step in a paper device.[21] This device was a promising step forward; however, paper devices have been known to suffer from slow and non-uniform flow and difficulties in particle and reagent transport..[23, 24]

Capillary-driven fluidic devices have become popular due to their lack of need for external pumps and other laboratory equipment.[25] A new class of hollow channel capillary-driven devices using polyethylene terephthalate (PET) and double-sided adhesive (DSA) was recently introduced by our group. These devices have been used to demonstrate advanced mixing and flow control[26, 27] and applied for viscosity measurements[28] and SARS-CoV-2 serology tests.[29, 30] While other examples of using PET for capillary-driven devices has been shown,[31] they lack the complexity necessary for sequential delivery and precise flow control.

Colorimetry is the most common detection mechanism for capillary-driven and paper-based flow devices, but it often suffers from low sensitivity and small linear ranges.[32] Electrochemical detection is an attractive alternative because it allows for rapid, inexpensive, sensitive, and quantitative results.[33] Additionally, the double line readout of a traditional LFA relies on user interpretation and does not provide quantitative results to the end-user. By using

electrochemical instead of colorimetric detection, LFA sensitivity can be improved.[34] Electrodes have also been incorporated into various other flow devices to improve detection.[35, 36] Additionally, electrodes have previously been used for e-ELISA, using electrochemistry as an alternate detection for traditional ELISA.[37-39]

Previous work presented a device for the detection of IgG antibodies against SARS-CoV-2 N proteins in whole blood;[30] however, this device required two distinct steps for the end user making it difficult for untrained users to operate. While monitoring antibodies is useful to study immune response in an individual and the overall population, it cannot be used to detect active infection. This work describes an electrochemical capillary driven immunoassay (eCaDI) device made from polyethylene terephthalate (PET) and adhesive films with an incorporated screen-printed carbon electrode system. The eCaDI is modified to detect active infections of SARS-CoV-2 through quantification of the N protein. Upon a one-step addition of a sample, the flow device sequentially delivers all the reagents necessary to perform an automated ELISA, producing quantitative detection of SARS-CoV-2.

5.3 Experimental Section

Reagents & Materials

Solutions were prepared using 18.2 MΩ · cm water purified using a Milli-Q system (MilliporeSigma, USA). Phosphate buffer saline (PBS) tablets, 3,3',5,5'-tetramethylbenzidine (TMB), ethylenediaminetetraacetic acid, ferrous sulfate heptahydrate, sodium hydroxide, D-(+)-trehalose dihydrate, and sodium tetraborate were purchased from Sigma-Aldrich (Saint Louis, MO). Tween80, boric acid, casein, 10X Stable Peroxide Buffer, bovine serum albumin, and sucrose were purchased from Thermo Fisher Scientific (Waltham, MA). Commercial SARS-CoV-

2 anti-N antibodies (MM08) and SARS-CoV-2 detection-HRP (MM05-H) antibodies were purchased from Sino Biological (Beijing, China). Igepal was purchased from MP Biomedicals (Irvine, CA). Unmodified glass fiber with PVA binder was purchased from MilliporeSigma (Burlington, MA). Zeba 40K Micro Spin Desalting Columns were purchased from Thermo Scientific (Rockford, IL). Polyethylene terephthalate sheets (2500 and 9984) and double-sided adhesive (467) were purchased from 3M (Saint Paul, MN). Carbon ink (CI-2057) was purchased from Engineered Materials Solutions, Inc. (Attleboro, MA). BQ-947 dielectric ink was purchased from Dupont (Wilmington, DE).

Solutions

10 mM phosphate buffer solution (PBS) with 140 mM sodium chloride and 2.7 mM potassium chloride, pH 7.4 was prepared by dissolving a tablet in DI water according to package instructions. 10 mM phosphate buffer solution with Tween20 (PBST) was made by adding 0.05% Tween20 to PBS. Antibody immobilization buffer was prepared by adding 0.0005% Tween 20 to PBS. 1x stable peroxide buffer (SPB) was prepared by diluting commercial 10x stable peroxide buffer 1:10 and adding 0.1% Igepal and 0.1% Tween 80. 1 M borate buffer, pH 8.5, was prepared by dissolving boric acid in water and adding sodium hydroxide. The buffer was then diluted to 50 mM in water and used to dilute the aged casein blocker. A bulk solution of 6% aged casein was prepared as previously reported.[40] Briefly, 6 g of casein was dissolved in 80 mL of 50 mM sodium hydroxide overnight. Then 0.26 g boric acid and 0.45 g sodium tetraborate were added and the solution was pH adjusted to 8.5. The solution was diluted to 100 mL with Millipore distilled water and heated at 37°C for 7 days. The aged casein was aliquoted and stored at –20°C. Drying buffer was prepared as previously reported.[41] First, a 1M solution of EDTA was prepared in PBS. Ferrous

sulfate was added to a concentration of 0.01 M. Then 4% trehalose and 0.1% BSA was added, and the solution was stored at 4°C for up to 3 months.

Inactivated Virus Samples

SARS-CoV-2 (USA-WA1/2020 = NR-52281, UK00 = NR-54000, UK11 = NR-54011, SA08 = NR-54008, SA09 = NR-54009, WA = NR-52281 (wildtype), Delta = NR-55486, Gamma = NR-54982, Kappa = NR-55486, Omicron = NR-56486) were obtained from BEI Resources and grown/quantified to produce viral stocks in BSL-3 containment in Vero E6 cells (ATCC (CRL-1586) in DMEM media containing 2% fetal bovine serum at 50mM HEPES (pH 7.5). Stocks were stored at -80°C in single-use aliquots. Viral stocks were quantified for infectivity via plaque assay (plaque-forming units (PFU)/ml) following procedures outlined in previous work.[42] Sindbis virus TE3'2J was quantified as described by Steel *et al.*[43], and Influenza A (H1N1) A/Swine/1976/31 (ATCC VR-1682) virus was quantified on MDCK cells (ATCC CCL-34) essentially as previously described.[44] To inactivate all virus, viral stocks were thawed and 0.1% Igepal was added to a final concentration of 0.1% for 30 minutes on ice, followed by storage at -20°C. All inactivated virus samples were verified for lack of infectivity prior to removal from BSL-2/BSL-3 containment via plaque assay. After the viruses were inactivated, all steps and experiments using inactivated virus were performed in a BSL-2 cabinet. Dilutions of inactivated viral stocks were made in stable peroxide buffer (SPB) immediately prior to addition to devices.

Desalting and Quantification of Antibodies

MM08 and MM05-H antibodies were de-salted using Zeba Spin Desalting Columns according to directions. Briefly, the columns were dried, then rinsed 3 times with PBS by spinning at 4700 rpm for 60 s. Then 7 µL of commercial antibody solution was added and spun for 2 min.

MM08 was diluted 1:100 in antibody immobilization buffer and used immediately for electrode modification. MM05-H was diluted to 80 µL in PBS, quantified using variable pathlength UV/Vis Solo-VPE (C Technologies, Inc., Bridgewater, NJ), then diluted to 1 µg/mL in SPB for static experiments and diluted to 20 µg/mL in drying buffer for fluidic experiments. More information on the quantification can be found in SI (**Figure SI1** and **Table SI1**).

The SoloVPE calculates the antibody concentration using Beer-Lambert Law:

$$A = \alpha \cdot l \cdot c$$

where "A" is the measured absorbance, "α" is the wavelength dependent molar absorption coefficient, "l" is the pathlength, and "c" is the sample concentration. This can be rearranged to show the relationship between absorbance and pathlength.

$$\frac{A}{l} = \alpha \cdot c = slope\ of\ regression\ line$$

The SoloVPE measures and plots absorbance vs. the varying pathlength (example shown in **Figure 5.1**). The slope of the regression lines are then used to calculate concentration if a molar molar adsorption coefficient is set in the instrument. There was no information on the molar adsorption coefficient for the specific antibodies in this work available. The majority of monoclonal antibodies have a molar adsorption coefficient between 1.4 and 1.6 mg/(mL·cm),[45] so 1.5 mg/(mL·cm) was used for the duration of the project. Representative plot details and calculated values can be seen in **Table 5.1**.

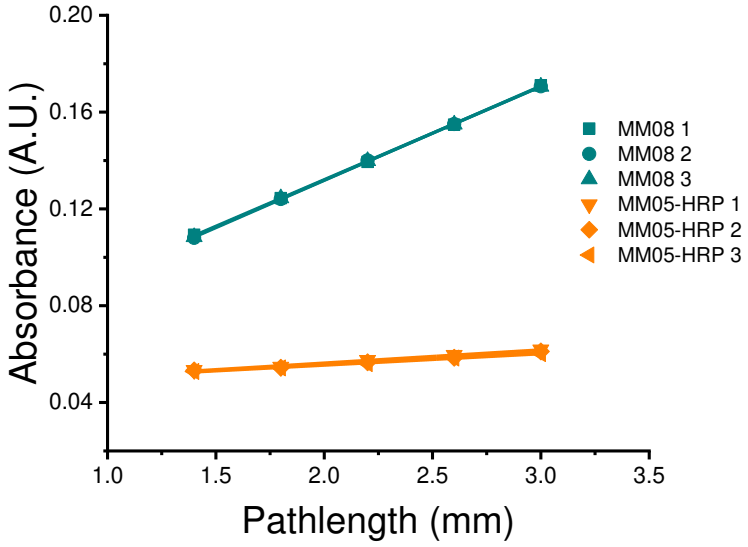

Figure 5.1 Plot of representative absorbance data for varying pathlengths collected with SoloVPE to quantify antibody concentration after spun through a desalting column.

Table 5.1: Table of representative plot details for data collected by the SoloVPE used for the software to calculate the concentrations.

Antibody Name	Linear Fit Equation	R^2	Calculated Concentration (mg/mL)	Average ± Standard Deviation (mg/mL)
MM08 1	y = (0.0385 ± 0.0004)x + (0.0552 ± 0.0008)	0.9997	0.26085	
MM08 2	y = (0.0391 ± 0.0003)x + (0.0536 ± 0.0006)	0.9998	0.26041	0.260 ± 0.002
MM08 3	y = (0.0387 ± 0.0002)x + (0.0545 ± 0.0005)	0.9999	0.25783	
MM05-H 1	y = (0.0055 ± 0.0003)x + (0.0455 ± 0.0007)	0.9879	0.03647	
MM05-H 2	y = (0.0050 ± 0.0004)x + (0.0459 ± 0.0008)	0.9803	0.03739	0.035 ± 0.003
MM05-H 3	y = (0.0047 ± 0.0002)x + (0.0460 ± 0.0005)	0.9922	0.03144	

Electrode Fabrication

A 3-electrode system was screen printed on 3M 2500 PET film using carbon ink and a 305 count mesh screen. After printing, the ink was dried for 30 min at 60°C. Dielectric ink wells were then screen-printed around the working electrode and UV cured until dry. Reference electrode was painted over with a thin layer of Ag|AgCl paste (Sigma-Aldrich Saint Louis, MO) and dried for 30 min at 60°C. The electrode coversheets (PET sheets on which electrodes were screen printed) were then cut using a CO_2 laser cutter according to the device layout and serve as top layer of the device.

Electrode Modification with Drying Method

The electrodes were functionalized by dropcasting 10 µL of 10 µg/mL capture antibody (MM08) in antibody immobilization buffer on to the working electrode, inside the dielectric ink well. The electrodes were dried in a petri dish at 37 °C for about 45 min. Once dry, 5 µL of 0.3% aged casein in 50 mM borate buffer was dropped into the dielectric well and allowed to dry at room temperature.

Device fabrication

The fluidic devices were designed using CorelDRAW (Corel, Ontario, Canada) and cut using a CO_2 laser cutter (Zing 10000, Epilog Laser) to pattern layers of PET films (9984) and 3M 467 DSA and sandwich the layers together. Glass fiber conjugate release pads were cut to fit in a medium size petri dish. A solution of 10 mM PBS was prepared with 0.1% thimersol and 0.5% Tween 20. Sucrose was added to a final concentration of 3% w/v. The glass fiber pad was fully submerged and soaked in this solution for 15 min at room temperature, then removed from the solution and dried in a 37°C incubator overnight until completely dry. After pretreatment, pads

were cut to 3 mm × 5 mm. TMB reagent pads were made by pipetting 5 µL of TMB solution onto pretreated glass fiber pads and incubated at 37°C for 15 min. This process was repeated 2 additional times resulting in 15 µL of TMB for each reagent pad. Next, 5 µL of 80X diluted Great Value™ blue food dye in Milli-Q distilled water was added and incubated at 37°C for 1 h. The reason for adding food dye is to create a visual aid within the eCaDI that allows the operator to evaluate the flow through the device and determine the correct time to start the chronoamperometry measurement. HRP-antibody conjugate release pads were made by pipetting 5 µl of 20 µg/mL HRP conjugated secondary antibody solution onto glass fiber pads and incubated at 37 °C for 15 min. This process was repeated once, resulting in 10 µL of 20 µg/mL HRP-antibody solution for each reagent pad. Finally, 5 µL of 80x diluted Great Value™ yellow food dye in Milli-Q distilled water was added and incubated at 37°C for 1 h. After preparation of both conjugate release pads, the pads were placed within the channels of the device, and the cover-layer containing the functionalized electrode was placed on top and sealed to the exposed DSA. Devices were kept out of the light until used for experiments. Before use, a 17 mm diameter (shape shown in **Figure 5.2**) Whatman 1 waste pad was inserted to the opening at the bottom of the device.

Static Electrochemical Detection Method

For static assay experiments, wells made with 3M 467 double sided adhesive (DSA) mimicking the size of the fluidic channel were placed over the working, counter, and reference electrodes to confine the solutions. To complete the assay, 20 µL of the selected inactivated virus concentration, diluted in SPB, was dropped in the well and incubated for 30 min. After washing with PBST followed by PBS, 20 µL of 1 µg/mL labeled antibody (MM05-H) solution in SPB was dropped into the well and incubated for 25 min. The electrodes were washed a final time, and 20 µL of 10 mM PBS (pH 7.4) was dropped until measurements could be taken. Just before the

measurement, the 20 µL of PBS was removed with a pipette. 50 µl of TMB was then added to the electrode surface, confined by the adhesive well, and incubated for 2 min. Immediately following the TMB incubation, a 2-min chronoamperometry measurement was started using a potentiostat (PalmSens4). A 0.0 V potential was applied to the working electrode (vs. the Ag|AgCl reference electrode), while the current was recorded.

Fluidic assay

The modified electrode coversheets and reagent pads were prepared as described above. 95 µL of sample was added to the inlet of the device to initiate flow and sequential delivery of reagents and the device was connected to PalmSens4. Once the blue dye visibly reached the detection channel, a 0.0 V potential was applied and current was measured until the peak was complete.

Electrochemical Data Processing

For the data collected using the static detection method, the current from the chronoamperograms was averaged over 10 s centered at 60 s for three or six measurements. For fluidic experiments, the highest point of the current peak from the amperogram was averaged for each device for three devices.

5.4 Results and Discussion

Electrochemical Capillary Driven Immunoassay Device and Mechanism

SARS-CoV-2 virus contains multiple structural proteins that can be used as the target for diagnostic assays including the envelope spike glycoprotein (S protein), envelope protein (E protein), membrane protein (M protein), helicase (Hel), and nucleocapsid protein (N protein).[46]

Early in the SARS-CoV-2 diagnostic development literature (and still now), S protein was a popular target choice.[47-52] S protein detection received considerable attention because it is responsible for the coronavirus iconic structure, plays a vital role in invasion of host cells, and induces an immune response.[53] The N protein and the S protein in SARS-CoV-2 both produce specific antibody responses,[54] and these are both now commercially available for purchase. For this work, N protein was chosen as the analyte. In SARS-CoV-2, the quantity of N:S proteins is approximately 1000:100 per virus particle, respectively,[55] which could lead to better sensitivity with more detectable analyte per virus. Other antibody-based assays that have been made for both SARS-CoV-2 S and N proteins have shown a lower LOD for that of N protein vs S protein.[56]

This work introduces a device that automates the steps of a sandwich ELISA with an electrochemical detection and only requires one final user step. The presented electrochemical capillary driven immunoassay (eCaDI) device consists of alternating layers of polyethylene terephthalate (PET) and double-sided adhesive (DSA) (shown in **Figure 5.2(A)**). The flow channels are cut and assembled entirely in a CO_2 laser cutter which eliminates some of the difficulty of aligning layers that has been previously reported for similar device.[27, 29, 30] The assembly in the laser cutter was achieved by optimizing laser parameters to only cut through intended layers at a time in different steps so that the different channels could be created without outside assembly even with varying channel heights. The middle three layers (DSA/PET/DSA) define a channel height of 200 μm for all the channels except the channel that flows over the electrode which has a channel height of 50 μm. The reagent pads contain dried HRP-labelled antibody (yellow pad) and the TMB substrate (blue pad). The sample inlet has a half moon (shown in **Figure 5.2(A)** on the third and fourth layer from the top) with the 50 μm height which forces the sample to flow through the detection channel first before filling other channels.

Figure 5.2(B) illustrates the function of the device for sample and reagent delivery demonstrated with dyes, and **Figure 5.2(C)** summarizes the sensing mechanism of the eCaDI. A video of the device running can also be found in SI. Briefly, the electrode is modified by drying the anti-N protein capture antibody and aged casein blocker, binding through passive adsorption. After the device is fully assembled, the sample is added to the inlet and the sample flows over the modified electrode (**Figure 5.2(B)(i)**). If present in the sample, the N protein is captured by the antibody on the electrode surface. Simultaneously, the remaining channels fill and rehydrate the reagent storage pads. Due to the difference in channel lengths the HRP-labelled anti-N protein antibody is hydrated and delivered first and, if the N protein is present, will bind to it (**Figure 5.2(B)(ii)**). Finally, the TMB is delivered to the electrode and the measurement is recorded (**Figure 5.2(B)(iii)**).

Reagent delivery was estimated using dyes added to reagent pads in addition to the reagents in all devices used for this study. The HRP-labelled antibody was delivered to the electrode on average at 4:17 ± 0:50 MM:SS following sample addition, and the TMB was delivered at 14:45 ± 1:26 MM:SS (n=46) (**Table 5.2**). The total measurement (started as the TMB is delivered) reported in this work can take 6-12 min; however, since the peak height is used to determine the presence of virus, in its final application the measurement would be able to stop as soon as the current begins decreasing. Overall, compared to traditional ELISAs, eCaDI greatly reduces the time required for a full sandwich immunoassay.

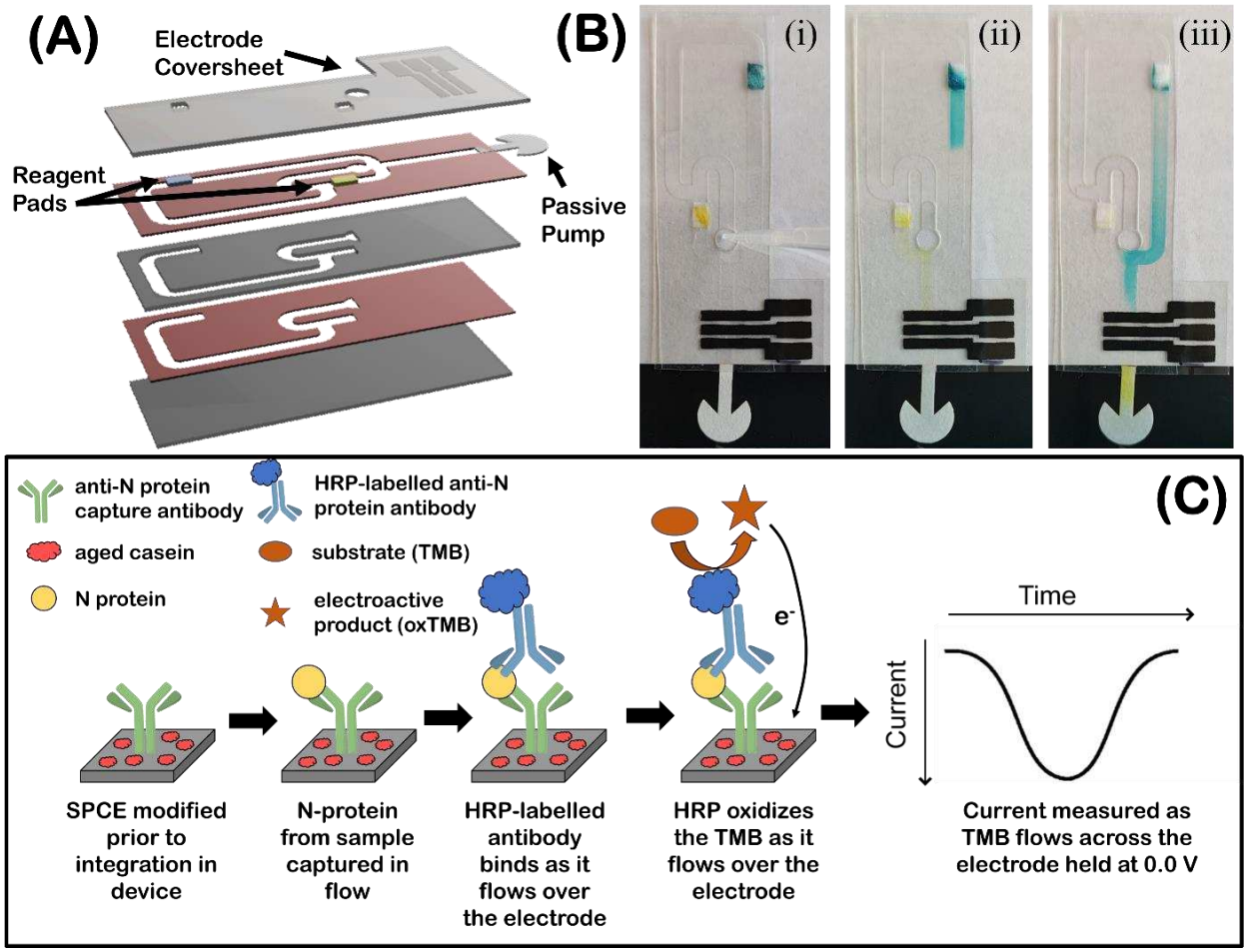

Figure 5.2 (A) Exploded view of eCaDI showing alternating PET (gray) and adhesive (red) layers. The second layer from the top shows the two reagent pads (blue = TMB, yellow= HRP ab) and the passive pump on the far right. **(B)** Flow of eCaDI (i) Addition of sample and sequential delivery of (ii) HRP-Antibodies (with yellow dye) and (iii) TMB (with blue dye) to the SPCE. **(C)** Electrochemical immunoassay and detection mechanism, showing modified electrode, target capture, secondary antibody binding, turnover of substrate, and electrochemical detection.

Table 5.2: Reagent delivery times estimated by adding dyes to the reagent pads while eCaDI devices ran.

Device #	HRP Delivery Time (MM:SS)	TMB Delivery Time (MM:SS)	Device #	HRP Delivery Time (MM:SS)	TMB Delivery Time (MM:SS)
1	4:45	12:15	24	5:40	15:00
2	2:40	13:00	25	4:00	14:40
3	4:30	14:30	26	4:00	15:15
4	4:00	15:50	27	4:50	14:30
5	6:20	14:15	28	2:15	15:20
6	3:00	12:50	29	5:30	17:20
7	4:00	10:45	30	3:40	13:50
8	4:50	16:10	31	3:55	13:45
9	3:30	15:00	32	4:55	16:45
10	5:30	16:50	33	5:15	15:05
11	3:45	14:30	34	4:00	13:30
12	2:50	13:00	35	4:30	14:00
13	3:00	14:00	36	3:40	13:05
14	4:45	15:00	37	4:15	15:50
15	3:30	15:25	38	4:30	14:15
16	3:45	17:05	39	5:10	14:50
17	3:55	13:55	40	4:20	15:00
18	4:15	15:00	41	3:50	15:00
19	4:00	13:05	42	4:25	15:45
20	4:00	16:55	43	4:50	16:45
21	5:00	12:30	44	4:30	14:45
22	5:50	16:30	45	4:55	15:25
23	4:30	13:45	46	4:30	17:00
HRP Delivery Average & Standard Deviation (MM:SS):		**4:17 ± 0:50**	**TMB Delivery Average & Standard Deviation (MM:SS):**		**14:45 ± 1:26**

Evaluation of Electrode Modification for SARS-CoV-2 Detection

Before integrating the electrodes into the eCaDI, the electrode modification was studied independently. Our group previously reported a method in which the capture antibody and aged casein was incubated for an hour each and required manual washing steps between incubations.[57] Initially, the same incubation and washing steps were used to modify the electrode before incorporation into the device. While there were significant signal differences between the blank and SARS-CoV-2 (representative amperograms shown in **Figure 5.3**), these steps were not practical for the long-term goals of the device. The previous modification required 1.75 h. Here, the capture antibody is dried completely in a 37°C incubator, which typically takes 30-40 min. The aged casein is then dried on the working electrode in ambient conditions, typically dried in under 15 min, bringing the total modification time to under 1 h. The aged casein blocks the surface of the electrode where there is no capture antibody to prevent non-specific adsorption of interferents and the HRP-labelled antibodies. In addition to greatly reducing the time required to under an hour for both modification steps, this method eliminates the need for manual washing steps and significantly less antibody and reagents are needed, making this method more cost-effective for manufacturing. The washing steps also negatively altered the hydrophilicity of the PET films used for the devices which impeded flow.

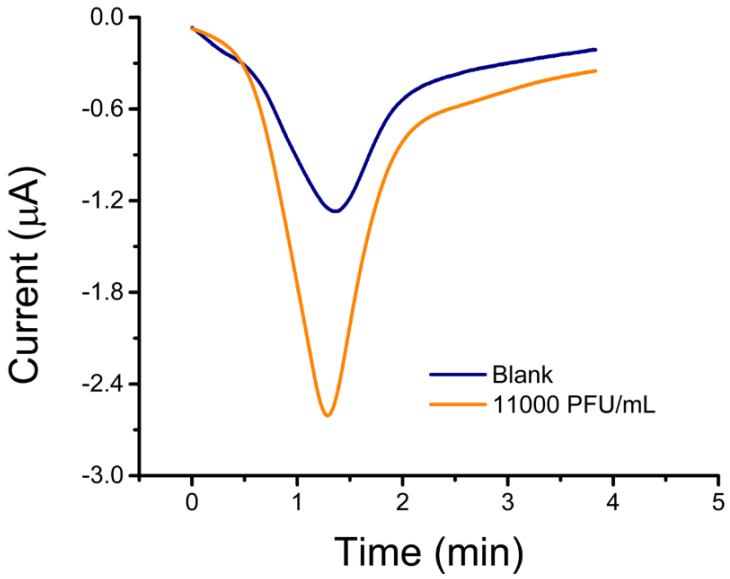

Figure 5.3 Detection of SARS-CoV-2 N protein from viral samples with eCaDI. Amperometry data recorded from eCaDI without (black) and with inactivated SARS-CoV-2. Potential was held at 0.0 V vs. Ag|AgCl reference for the duration of the runs. Data was time-aligned with TMB delivery to the electrode (t=0). Mean and error from 3 different devices.

Figure 5.4(A) shows the current responses for varying concentrations of SARS-CoV-2 inactivated virus. Although the assay is specifically detecting N protein, concentrations are reported in equivalent plaque forming units (PFU)/mL which only quantifies viral particles capable of infection. This unit was chosen because the end goal of this device is to detect active infection and the limited quantification techniques capable of being performed in a BSL-3 cabinet. Stock virus solutions were titered to get these values and more information can be found in Methods. A clear difference can be seen in the current response for each concentration and the resulting calibration curve (**Figure 5.4(B)**) demonstrates the concentration dependent signal for concentrations ranging from 340-11,000 equivalent PFU/mL. The data are fit to a dose response logistic fit and presents a sigmoidal shape, which is expected for immunoassays.[58, 59] Equations for the fitting of the calibration curve are shown here:

$$y = A1 + \frac{(A2 - A1)}{(1 + 10^{(\log x_0 - x)(p)})}$$

$$y = -0.1241 + \frac{(1.430 + 0.1241)}{(1 + 10^{(3207 - x)(2.693E-4)})}$$

The LOD for this assay was calculated to be 68 equivalent PFU/mL using the theoretical blank plus 3 times the standard deviation of the blank. This calculated LOD is comparable or lower than the measured LOD of most commercially available rapid antigen tests, which are typically between 80 and 500 equivalent PFU/mL.[60, 61] Many of these LODs, however, were measured not calculated LODs. The lowest concentration tested by the modified SARS-CoV-2 electrodes reported here was 340 equivalent PFU/mL. Long term future work should determine the LOD by serial dilution measurements to have a more realistic understanding of the sensors' capabilities at low concentrations. While the drying process as opposed to incubation may have resulted in a slight loss of signal compared to the method our group reported before,[57] this method is much more practical heading towards manufacturing and it's working range and LOD are still sufficient for most COVID-19 cases, which have an extremely wide range of concentration from 5-10^6 equivalent PFU/mL.[62] Higher infectivity has also been shown to be correlated with higher equivalent PFU/mL values.[63]

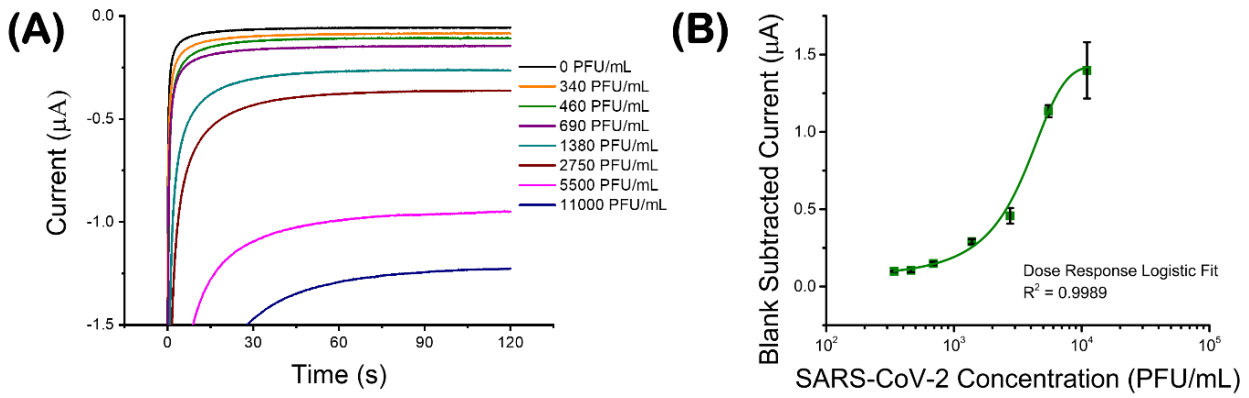

Figure 5.4 (A) Representative chronoamperograms for varying concentrations of inactivated SARS-CoV-2 virus in SPB taken on modified electrodes outside of the eCaDI using the static electrochemical detection method. Potential held at 0.0 V vs. Ag|AgCl reference for 2 min. **(B)** Corresponding calibration curve plotted on a log scale showing blank subtracted current. Symbols and error bars represent average and standard deviation over a 10 s interval centered on 60 s (n=3). Data is fit with a dose response logistic fit. The data for these plots were collected by Melissa Schenkel.

Stability of Electrode Modification

To determine the ideal storage conditions for the electrodes after modification, four conditions were tested: with and without desiccant, at 5°C and room temperature. These conditions were chosen because they would be easily implemented in a commercial setting. The plot showing the stability over 24 days for each condition can be found in **Figure 5.5(A)**. The electrode signal was most stable at room temperature with desiccant. Many other sensors with immobilized antibodies have been found to store better in dry conditions, due to faster protein degradation in humid environments.[64-66] It is interesting that ambient temperature resulted in better signal because the majority of literature reports for various storage temperatures have shown that 4-5°C is optimal storage for antibody based sensors.[64, 67] Several theories to explain this could be increased humidity in the fridge even in a desiccator or perhaps the electrochemical signal of the SPCE (as opposed

to the modification itself) is impacted by the lower temperature. The exact mechanism still remains unclear and was outside the scope of the current investigation.

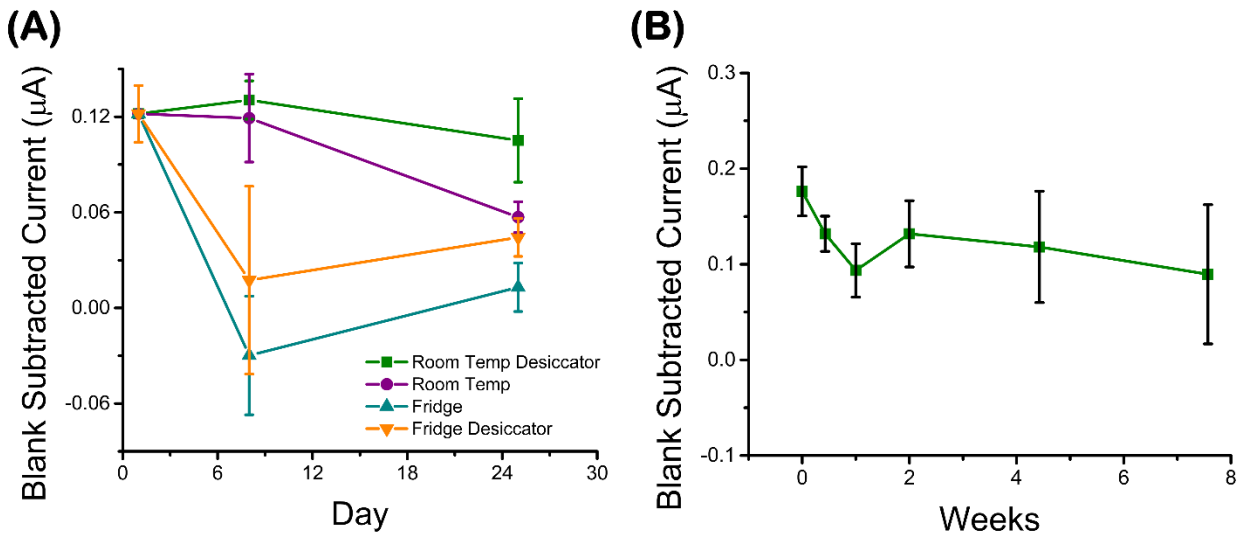

Figure 5.5 (A) Plot showing stability of blank subtracted current for modified electrodes in different storage conditions. Data is from chronoamperometry recorded using the static electrochemical detection method for 1380 equivalent PFU/mL inactivated SARS-CoV-2 minus the blank current. Mean and error is from 3 electrodes ran for each day and for each condition. **(B)** Plot showing stability of blank subtracted current for modified electrodes stored in a desiccator at room temperature. Data is from chronoamperometry recorded static electrochemical detection method for equivalent 1380 equivalent PFU/mL inactivated SARS-CoV-2 in SPB minus the blank current with SPB. Symbols and error bars represent average and standard deviation over a 10 s interval centered on 60 s (n=8). The data for these plots were collected by Melissa Schenkel.

After the storage conditions with desiccant at room temperature were chosen, a long-term stability study was performed, and the results are shown in **Figure 5.5(B)**. After an initial decrease in the first several days, the electrode response remained stable between 0.09-0.13 μA for 1380 PFU/mL inactivated SARS-CoV-2 and all within error of the other points for over seven weeks. This stability is comparable to or better than most other reports.[67] Additionally, more controlled fabrication and storage environments would likely increase the stability and reduce the variability of the electrodes. Error in this study can stem from variability in fresh solutions made for each

time point, differences in electrode fabrication and modification, as well as effects of modification stability. The long-term stability of the electrodes is promising for further real-world applications that require stability for manufacturing, shipping, and use.

Detection of Varying SARS-CoV-2 Concentrations with eCaDI Device

The full eCaDI device was used for in-flow detection of five SARS-CoV-2 concentrations. Each sample was diluted in SPB, which contains surfactant that will lyse the virus to release the N protein into the solution, and H_2O_2 that is necessary for the enzymatic reaction between the HRP and TMB substrate. **Figure 5.6(A)** shows representative (n=3) amperograms of each concentration tested in the eCaDI. An increase in the cathodic current that forms a peak can be seen as the TMB flows over the electrode. With increasing viral concentration, the resulting peak current increases, demonstrating that the eCaDI produces concentration dependent signal. Plots of the average peak currents for each concentration are shown in **Figure 5.6(B)**. Additionally, this confirms that the reagents are being delivered in the appropriate sequence to perform a sandwich immunoassay and aligns with the dye delivery shown in **Figure 5.2(B)**. It is important to note that the blank measurement without virus present also has a current peak. The peak is likely a result of autooxidation of the TMB combined with non-specific adsorption of the HRP-antibody to the fluidic channels and electrode. Because of the non-zero blank signal, data moving forward are blank-subtracted. Long-term, a positive diagnosis would be based on a current exceeding a target threshold. There are also noticeable differences in the shape of each amperogram, particularly later in the measurement, which can be attributed to slight differences in flow. Ideally, these differences are expected to decrease if the devices are no longer made, modified, and assembled by hand.

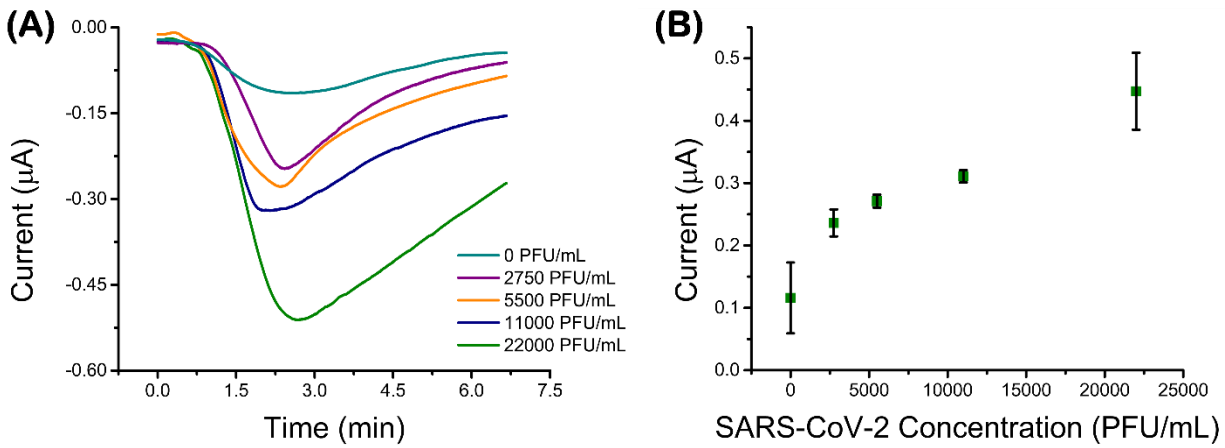

Figure 5.6 (A) Representative amperograms from full eCaDI device for varying concentration of SARS-CoV-2 in SPB (n=3). Potential was held at 0.0 V for the duration of the runs. Data was time-aligned with TMB delivery to the electrode. **(B)** Corresponding plot of various concentrations of inactivated SARS-CoV-2 virus in SPB. Symbols and error bars represent average and standard deviation of peak current from amperograms (n=3 for each blank and concentration).

Investigation of Potential Interferents and Ability to Detect SARS-CoV-2 Variants

To be effective, a diagnostic tool must be able to differentiate between the target, in this case SARS-CoV-2, and other viruses. To verify selectivity, the eCaDI was tested with influenza A and Sindbis virus. This is especially important for influenza A, as it presents symptoms that can easily be mistaken for COVID-19 and is a common respiratory pathogen.[68] Both interferents tested approximately at or below the signal of the average blank signal (SPB). Representative amperograms are shown in **Figure 5.7(A)** and a bar graph comparing the interferent signals to that of SARS-CoV-2 in **Figure 5.7(B)**. The negative blank-subtracted current might be due to proteins in the interferent samples blocking access of the HRP-antibodies to the electrode surface, decreasing the electron turnover by TMB. The selectivity of the eCaDI for SARS-CoV-2 demonstrates feasibility for application as a COVID-19 diagnostic.

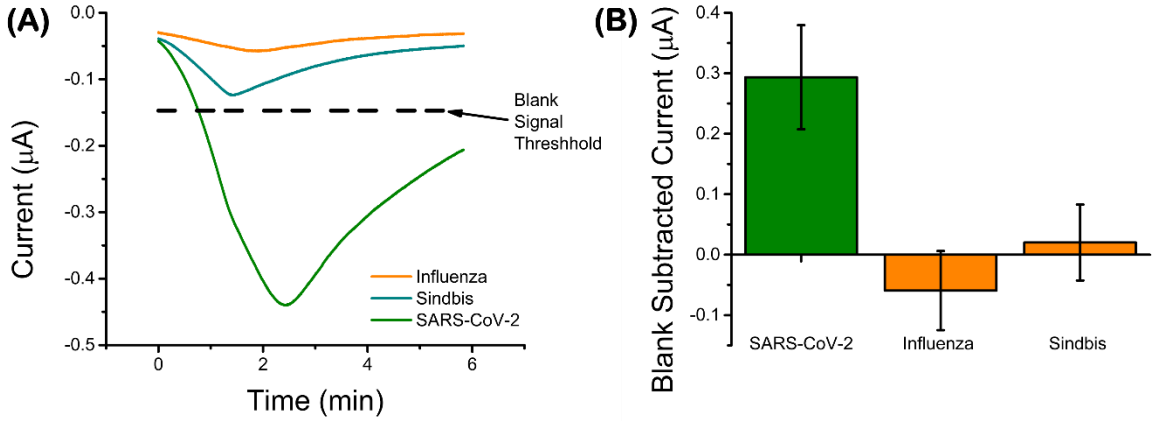

Figure 5.7 (A) Representative amperograms from full eCaDI device of potential interferents all at equivalent 11,000 PFU/mL (Influenza A and Sindbis) (n=3). The black dashed line represents the average peak current of blank SPB without virus (n=3). Potential was held at 0.0 V vs. Ag|AgCl reference for the duration of the runs. Data was time-aligned with TMB delivery to the electrode. **(B)** Bar graph showing the blank subtracted current responses of the full eCaDI for interferents (orange) compared to the signal of SARS-CoV-2 virus (green) in SPB. Columns and error bars represent average and standard deviation of peak current from amperograms held at 0.0 V (n=3 for each blank and interferent).

Nine SARS-CoV-2 variants with different gene mutations were tested with the eCaDI, including UK (UK00, UK11), South African (SA08, SA09), Washington (WA), Delta, Kappa, Gamma, and Omicron. All nine variants produced positive signal above the average blank threshold (**Figure 5.8(A)**). The positive results for the Omicron variant were especially encouraging since it has significant mutations to both S and N proteins and has presented a challenge to rapid diagnostics on the market.[69] While all the variants were diluted to the same equivalent PFU/mL concentration before tested, the signal responses varied significantly for each, which can be seen more clearly in **Figure 5.8(B)**. The variation is likely due to genomic differences in each that result in different N protein expression or number of N protein per virus particle.[70] Additionally, equivalent PFU/mL, as previously mentioned, only quantifies infective virus particles not free N protein or inactive virus particles which can lead to greater variability when testing different samples as these would still be quantified in this assay.

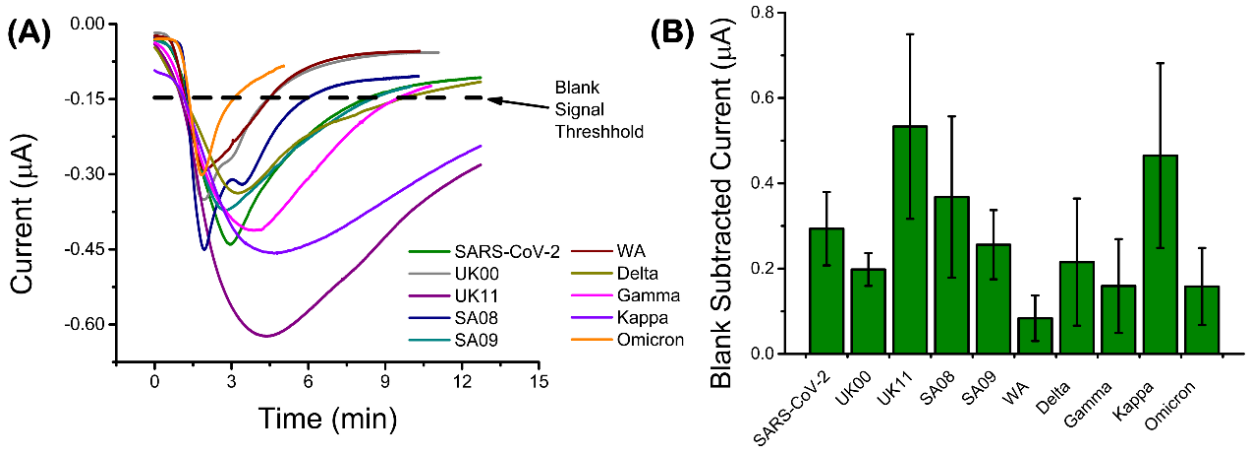

Figure 5.8 (A) Representative amperograms (n=3) from full eCaDI device of variants of SARS-CoV-2 virus. The black dashed line represents the average peak current of blank SPB without virus (n=3). Potential was held at 0.0 V vs. Ag|AgCl reference for the duration of the runs. Data was time-aligned with TMB delivery to the electrode. **(B)** Bar graph showing the blank subtracted current responses of the full eCaDI for variants of SARS-CoV-2 virus in SPB. Columns and error bars represent average and standard deviation of peak current from amperograms held at 0.0 V (n=3 for each blank and variant).

5.5 Conclusions

This work presents an electrochemical capillary driven immunoassay (eCaDI) device, that automates the steps of a sandwich ELISA using electrochemical detection. A drying modification technique is reported that achieves a limit of detection of 68 equivalent PFU/mL. The new device greatly reduces the time required for traditional ELISA and eliminates all steps that would require trained personnel. The electrochemical detection method offers the potential for more sensitive and quantitative detection of SARS-CoV-2. The modification and device assembly methods are also promising steps toward manufacturing of similar devices. While a reasonably low limit of detection was achieved in this study, the device could be improved by further optimization of the attachment chemistry of the capture antibody to the electrode surface, the pre-treatment method for the reagent pads, and extraction buffer composition in the device. Future work will focus on detection of COVID-19 N-protein in physiological samples, improving stability of the entire

device, decreasing time to readout, and testing compatibility with near field communication (NFC) readout. Overall, this work presents an important step to enable large scale manufacturing and commercialization of point-of-care devices for various biological analytes that have been traditionally detected using ELISA.

REFERENCES

1. Ji, T.; Liu, Z.; Wang, G.; Guo, X.; Lai, C.; Chen, H.; Huang, S.; Xia, S.; Chen, B.; Jia, H., Detection of COVID-19: A review of the current literature and future perspectives. *Biosensors and Bioelectronics* **2020,** *166*, 112455.

2. Administration, U. S. F. D. COVID-19 Test Basics. https://www.fda.gov/consumers/consumer-updates/covid-19-test-basics

3. van Kasteren, P. B.; van Der Veer, B.; van den Brink, S.; Wijsman, L.; de Jonge, J.; van den Brandt, A.; Molenkamp, R.; Reusken, C. B.; Meijer, A., Comparison of seven commercial RT-PCR diagnostic kits for COVID-19. *Journal of Clinical Virology* **2020,** *128*, 104412.

4. Weissleder, R.; Lee, H.; Ko, J.; Pittet, M. J., COVID-19 diagnostics in context. *Science translational medicine* **2020,** *12* (546), eabc1931.

5. Carter, L. J.; Garner, L. V.; Smoot, J. W.; Li, Y.; Zhou, Q.; Saveson, C. J.; Sasso, J. M.; Gregg, A. C.; Soares, D. J.; Beskid, T. R., Assay techniques and test development for COVID-19 diagnosis. ACS Publications: 2020.

6. Chau, C. H.; Strope, J. D.; Figg, W. D., COVID-19 clinical diagnostics and testing technology. *Pharmacotherapy: The Journal of Human Pharmacology and Drug Therapy* **2020,** *40* (8), 857-868.

7. Mahmoudinobar, F.; Britton, D.; Montclare, J. K., Protein-based lateral flow assays for COVID-19 detection. *Protein Engineering, Design and Selection* **2021,** *34*.

8. Ong, D. S.; De Man, S.; Lindeboom, F. A.; Koeleman, J. G., Comparison of diagnostic accuracies of rapid serological tests and ELISA to molecular diagnostics in patients with suspected coronavirus disease 2019 presenting to the hospital. *Clinical Microbiology and Infection* **2020,** *26* (8), 1094. e7-1094. e10.

9. Peeling, R. W.; Olliaro, P. L.; Boeras, D. I.; Fongwen, N., Scaling up COVID-19 rapid antigen tests: promises and challenges. *The Lancet infectious diseases* **2021,** *21* (9), e290-e295.

10. Giri, B.; Pandey, S.; Shrestha, R.; Pokharel, K.; Ligler, F. S.; Neupane, B. B., Review of analytical performance of COVID-19 detection methods. *Analytical and bioanalytical chemistry* **2021,** *413* (1), 35-48.

11. Rai, P.; Kumar, B. K.; Deekshit, V. K.; Karunasagar, I.; Karunasagar, I., Detection technologies and recent developments in the diagnosis of COVID-19 infection. *Applied microbiology and biotechnology* **2021,** *105* (2), 441-455.

12. Song, Q.; Sun, X.; Dai, Z.; Gao, Y.; Gong, X.; Zhou, B.; Wu, J.; Wen, W., Point-of-care testing detection methods for COVID-19. *Lab on a Chip* **2021,** *21* (9), 1634-1660.

13. Basiri, A.; Heidari, A.; Nadi, M. F.; Fallahy, M. T. P.; Nezamabadi, S. S.; Sedighi, M.; Saghazadeh, A.; Rezaei, N., Microfluidic devices for detection of RNA viruses. *Reviews in medical virology* **2021,** *31* (1), 1-11.

14. Yeo, L. Y.; Chang, H. C.; Chan, P. P.; Friend, J. R., Microfluidic devices for bioapplications. *small* **2011,** *7* (1), 12-48.

15. Jeong, S.-G.; Kim, J.; Jin, S. H.; Park, K.-S.; Lee, C.-S., Flow control in paper-based microfluidic device for automatic multistep assays: A focused minireview. *Korean Journal of Chemical Engineering* **2016,** *33* (10), 2761-2770.

16. Lutz, B.; Liang, T.; Fu, E.; Ramachandran, S.; Kauffman, P.; Yager, P., Dissolvable fluidic time delays for programming multi-step assays in instrument-free paper diagnostics. *Lab on a Chip* **2013,** *13* (14), 2840-2847.

17. Chen, H.; Cogswell, J.; Anagnostopoulos, C.; Faghri, M., A fluidic diode, valves, and a sequential-loading circuit fabricated on layered paper. *Lab on a Chip* **2012,** *12* (16), 2909-2913.

18. Giokas, D. L.; Tsogas, G. Z.; Vlessidis, A. G., Programming fluid transport in paper-based microfluidic devices using razor-crafted open channels. *Analytical chemistry* **2014,** *86* (13), 6202-6207.

19. He, P.; Katis, I.; Eason, R.; Sones, C., Engineering fluidic delays in paper-based devices using laser direct-writing. *Lab on a Chip* **2015,** *15* (20), 4054-4061.

20. Lai, Y.-T.; Tsai, J.-S.; Hsu, J.-C.; Lu, Y.-W. In *Automated paper-based devices by microfluidic timing-valve for competitive ELISA*, 2017 IEEE 30th International Conference on Micro Electro Mechanical Systems (MEMS), IEEE: 2017; pp 1321-1324.

21. Apilux, A.; Ukita, Y.; Chikae, M.; Chailapakul, O.; Takamura, Y., Development of automated paper-based devices for sequential multistep sandwich enzyme-linked immunosorbent assays using inkjet printing. *Lab on a Chip* **2013,** *13* (1), 126-135.

22. Fu, E.; Lutz, B.; Kauffman, P.; Yager, P., Controlled reagent transport in disposable 2D paper networks. *Lab on a Chip* **2010,** *10* (7), 918-920.

23. Gong, M. M.; Sinton, D., Turning the page: advancing paper-based microfluidics for broad diagnostic application. *Chemical reviews* **2017,** *117* (12), 8447-8480.

24. Nguyen, M. P.; Meredith, N. A.; Kelly, S. P.; Henry, C. S., Design considerations for reducing sample loss in microfluidic paper-based analytical devices. *Analytica chimica acta* **2018,** *1017*, 20-25.

25. Yetisen, A. K.; Akram, M. S.; Lowe, C. R., Paper-based microfluidic point-of-care diagnostic devices. *Lab on a Chip* **2013,** *13* (12), 2210-2251.

26. Jang, I.; Carrão, D. B.; Menger, R. F.; Moraes de Oliveira, A. R.; Henry, C. S., Pump-free microfluidic rapid mixer combined with a paper-based channel. *ACS sensors* **2020,** *5* (7), 2230-2238.

27. Jang, I.; Kang, H.; Song, S.; Dandy, D. S.; Geiss, B. J.; Henry, C. S., Flow control in a laminate capillary-driven microfluidic device. *Analyst* **2021,** *146* (6), 1932-1939.

28. Jang, I.; Berg, K. E.; Henry, C. S., Viscosity measurements utilizing a fast-flow microfluidic paper-based device. *Sensors and Actuators B: Chemical* **2020,** *319*, 128240.

29. Carrell, C.; Link, J.; Jang, I.; Terry, J.; Scherman, M.; Call, Z.; Panraksa, Y.; Dandy, D. S.; Geiss, B. J.; Henry, C., Point-of-Need Disposable ELISA System for COVID-19 Serology Testing. **2020**.

30. Samper, I. C.; Sánchez-Cano, A.; Khamcharoen, W.; Jang, I.; Siangproh, W.; Baldrich, E.; Geiss, B. J.; Dandy, D. S.; Henry, C. S., Electrochemical Capillary-Flow Immunoassay for Detecting Anti-SARS-CoV-2 Nucleocapsid Protein Antibodies at the Point of Care. *ACS sensors* **2021,** *6* (11), 4067-4075.

31. Moreira, N. S.; Chagas, C. L.; Oliveira, K. A.; Duarte-Junior, G. F.; de Souza, F. R.; Santhiago, M.; Garcia, C. D.; Kubota, L. T.; Coltro, W. K., Fabrication of microwell plates and microfluidic devices in polyester films using a cutting printer. *Analytica Chimica Acta* **2020,** *1119*, 1-10.

32. Morbioli, G. G.; Mazzu-Nascimento, T.; Stockton, A. M.; Carrilho, E., Technical aspects and challenges of colorimetric detection with microfluidic paper-based analytical devices (μPADs)-A review. *Analytica chimica acta* **2017,** *970*, 1-22.

33. Kaya, H. O.; Cetin, A. E.; Azimzadeh, M.; Topkaya, S. N., Pathogen detection with electrochemical biosensors: Advantages, challenges and future perspectives. *Journal of Electroanalytical Chemistry* **2021,** *882*, 114989.

34. Mak, W. C.; Beni, V.; Turner, A. P., Lateral-flow technology: From visual to instrumental. *TrAC Trends in Analytical Chemistry* **2016,** *79*, 297-305.

35. Trojanowicz, M., Recent developments in electrochemical flow detections—a review: part I. Flow analysis and capillary electrophoresis. *Analytica chimica acta* **2009,** *653* (1), 36-58.

36. Noviana, E.; McCord, C. P.; Clark, K. M.; Jang, I.; Henry, C. S., Electrochemical paper-based devices: Sensing approaches and progress toward practical applications. *Lab on a Chip* **2020,** *20* (1), 9-34.

37. Singh, B.; Flampouri, E.; Dempsey, E., Electrochemical enzyme-linked immunosorbent assay (e-ELISA) for parasitic nematode Ostertagia ostertagi (brown stomach worm) infections in dairy cattle. *Analyst* **2019,** *144* (19), 5748-5754.

38. Rossier, J. S.; Girault, H. H., Enzyme linked immunosorbent assay on a microchip with electrochemical detection. *Lab on a Chip* **2001,** *1* (2), 153-157.

39. Bhimji, A.; Zaragoza, A. A.; Live, L. S.; Kelley, S. O., Electrochemical enzyme-linked immunosorbent assay featuring proximal reagent generation: detection of human immunodeficiency virus antibodies in clinical samples. *Analytical chemistry* **2013,** *85* (14), 6813-6819.

40. Grant, B. D.; Anderson, C. E.; Williford, J. R.; Alonzo, L. F.; Glukhova, V. A.; Boyle, D. S.; Weigl, B. H.; Nichols, K. P., SARS-CoV-2 coronavirus nucleocapsid antigen-detecting half-strip lateral flow assay toward the development of point of care tests using commercially available reagents. *Analytical chemistry* **2020,** *92* (16), 11305-11309.

41. Ramachandran, S.; Fu, E.; Lutz, B.; Yager, P., Long-term dry storage of an enzyme-based reagent system for ELISA in point-of-care devices. *Analyst* **2014,** *139* (6), 1456-1462.

42. Case, J. B.; Bailey, A. L.; Kim, A. S.; Chen, R. E.; Diamond, M. S., Growth, detection, quantification, and inactivation of SARS-CoV-2. *Virology* **2020,** *548*, 39-48.

43. Steel, J. J.; Henderson, B. R.; Lama, S. B.; Olson, K. E.; Geiss, B. J., Infectious alphavirus production from a simple plasmid transfection. *Virology journal* **2011,** *8* (1), 1-8.

44. Huprikar, J.; Rabinowitz, S., A simplified plaque assay for influenza viruses in Madin-Darby kidney (MDCK) cells. *Journal of virological methods* **1980,** *1* (2), 117-120.

45. Zhang, Y.; Qi, P., Determination of free sulfhydryl contents for proteins including monoclonal antibodies by use of SoloVPE. *Journal of Pharmaceutical and Biomedical Analysis* **2021,** *201*, 114092.

46. Kudr, J.; Michalek, P.; Ilieva, L.; Adam, V.; Zitka, O., COVID-19: A challenge for electrochemical biosensors. *TrAC Trends in Analytical Chemistry* **2021,** *136*, 116192.

47. Pinals, R. L.; Ledesma, F.; Yang, D.; Navarro, N.; Jeong, S.; Pak, J. E.; Kuo, L.; Chuang, Y.-C.; Cheng, Y.-W.; Sun, H.-Y., Rapid SARS-CoV-2 spike protein detection by carbon nanotube-based near-infrared nanosensors. *Nano Letters* **2021,** *21* (5), 2272-2280.

48. Mavrikou, S.; Moschopoulou, G.; Tsekouras, V.; Kintzios, S., Development of a portable, ultra-rapid and ultra-sensitive cell-based biosensor for the direct detection of the SARS-CoV-2 S1 spike protein antigen. *Sensors* **2020,** *20* (11), 3121.

49. Mavrikou, S.; Tsekouras, V.; Hatziagapiou, K.; Paradeisi, F.; Bakakos, P.; Michos, A.; Koutsoukou, A.; Konstantellou, E.; Lambrou, G. I.; Koniari, E., Clinical Application of the Novel Cell-Based Biosensor for the Ultra-Rapid Detection of the SARS-CoV-2 S1 Spike Protein Antigen: A Practical Approach. *Biosensors* **2021,** *11* (7), 224.

50. Perkmann, T.; Perkmann-Nagele, N.; Koller, T.; Mucher, P.; Radakovics, A.; Marculescu, R.; Wolzt, M.; Wagner, O. F.; Binder, C. J.; Haslacher, H., Anti-spike protein assays to determine SARS-CoV-2 antibody levels: a head-to-head comparison of five quantitative assays. *Microbiology Spectrum* **2021,** *9* (1), e00247-21.

51. Idili, A.; Parolo, C.; Alvarez-Diduk, R.; Merkoçi, A., Rapid and efficient detection of the SARS-CoV-2 spike protein using an electrochemical aptamer-based sensor. *ACS sensors* **2021,** *6* (8), 3093-3101.

52. Ayankojo, A. G.; Boroznjak, R.; Reut, J.; Öpik, A.; Syritski, V., Molecularly imprinted polymer based electrochemical sensor for quantitative detection of SARS-CoV-2 spike protein. *Sensors and Actuators B: Chemical* **2022,** *353*, 131160.

53. Huang, Y.; Yang, C.; Xu, X.-f.; Xu, W.; Liu, S.-w., Structural and functional properties of SARS-CoV-2 spike protein: potential antivirus drug development for COVID-19. *Acta Pharmacologica Sinica* **2020,** *41* (9), 1141-1149.

54. Fenwick, C.; Croxatto, A.; Coste, A. T.; Pojer, F.; André, C.; Pellaton, C.; Farina, A.; Campos, J.; Hacker, D.; Lau, K., Changes in SARS-CoV-2 spike versus nucleoprotein antibody responses impact the estimates of infections in population-based seroprevalence studies. *Journal of virology* **2021,** *95* (3), e01828-20.

55. Bar-On, Y. M.; Flamholz, A.; Phillips, R.; Milo, R., Science Forum: SARS-CoV-2 (COVID-19) by the numbers. *elife* **2020,** *9*, e57309.

56. Fabiani, L.; Saroglia, M.; Galatà, G.; De Santis, R.; Fillo, S.; Luca, V.; Faggioni, G.; D'Amore, N.; Regalbuto, E.; Salvatori, P., Magnetic beads combined with carbon black-based screen-printed electrodes for COVID-19: A reliable and miniaturized electrochemical immunosensor for SARS-CoV-2 detection in saliva. *Biosensors and Bioelectronics* **2021,** *171*, 112686.

57. Samper, I. C.; McMahon, C. J.; Schenkel, M. S.; Clark, K. M.; Khamcharoen, W.; Anderson, L. B.; Terry, J. S.; Gallichotte, E. N.; Ebel, G. D.; Geiss, B. J., Electrochemical

Immunoassay for the Detection of SARS-CoV-2 Nucleocapsid Protein in Nasopharyngeal Samples. *Analytical Chemistry* **2022**.

58. Dudley, R.; Edwards, P.; Ekins, R.; Finney, D.; McKenzie, I.; Raab, G.; Rodbard, D.; Rodgers, R., Guidelines for immunoassay data processing. *Clinical chemistry* **1985,** *31* (8), 1264-1271.

59. Cox, K. L.; Devanarayan, V.; Kriauciunas, A.; Manetta, J.; Montrose, C.; Sittampalam, S., Immunoassay methods. *Assay Guidance Manual [Internet]* **2019**.

60. Cubas-Atienzar, A. I.; Kontogianni, K.; Edwards, T.; Wooding, D.; Buist, K.; Thompson, C. R.; Williams, C. T.; Patterson, E. I.; Hughes, G. L.; Baldwin, L., Limit of detection in different matrices of 19 commercially available rapid antigen tests for the detection of SARS-CoV-2. *Scientific reports* **2021,** *11* (1), 1-8.

61. Corman, V. M.; Haage, V. C.; Bleicker, T.; Schmidt, M. L.; Mühlemann, B.; Zuchowski, M.; Jo, W. K.; Tscheak, P.; Möncke-Buchner, E.; Müller, M. A., Comparison of seven commercial SARS-CoV-2 rapid point-of-care antigen tests: a single-centre laboratory evaluation study. *The Lancet Microbe* **2021,** *2* (7), e311-e319.

62. Lin, Y.-C.; Malott, R. J.; Ward, L.; Kiplagat, L.; Pabbaraju, K.; Gill, K.; Berenger, B. M.; Hu, J.; Fonseca, K.; Noyce, R. S., Detection and quantification of infectious severe acute respiratory coronavirus-2 in diverse clinical and environmental samples. *Scientific reports* **2022,** *12* (1), 1-19.

63. Karimzadeh, S.; Bhopal, R.; Tien, H. N., Review of infective dose, routes of transmission and outcome of COVID-19 caused by the SARS-COV-2: comparison with other respiratory viruses. *Epidemiology & Infection* **2021,** *149*.

64. Kaduskar, O.; Bhatt, V.; Prosperi, C.; Hayford, K.; Hasan, A. Z.; Deshpande, G. R.; Tilekar, B.; Vivian Thangaraj, J. W.; Kumar, M. S.; Gupta, N., Optimization and stability testing of four commercially available dried blood spot devices for estimating measles and rubella IgG antibodies. *Msphere* **2021,** *6* (4), e00490-21.

65. Flounders, A.; Brandon, D.; Bates, A., Patterning of immobilized antibody layers via photolithography and oxygen plasma exposure. *Biosensors and Bioelectronics* **1997,** *12* (6), 447-456.

66. Li, X.; Liu, X., A microfluidic paper-based origami nanobiosensor for label-free, ultrasensitive immunoassays. *Advanced healthcare materials* **2016,** *5* (11), 1326-1335.

67. Li, F.; You, M.; Li, S.; Hu, J.; Liu, C.; Gong, Y.; Yang, H.; Xu, F., Paper-based point-of-care immunoassays: Recent advances and emerging trends. *Biotechnology advances* **2020,** *39*, 107442.

68. Osman, M.; Klopfenstein, T.; Belfeki, N.; Gendrin, V.; Zayet, S., A comparative systematic review of COVID-19 and influenza. *Viruses* **2021,** *13* (3), 452.

69. Osterman, A.; Badell, I.; Basara, E.; Stern, M.; Kriesel, F.; Eletreby, M.; Öztan, G. N.; Huber, M.; Autenrieth, H.; Knabe, R., Impaired detection of omicron by SARS-CoV-2 rapid antigen tests. *Medical microbiology and immunology* **2022**, 1-13.

70. Almubaid, Z.; Al-Mubaid, H., Analysis and comparison of genetic variants and mutations of the novel coronavirus SARS-CoV-2. *Gene reports* **2021,** *23*, 101064.

CHAPTER 6: CONCLUSIONS AND FUTURE DIRECTIONS

Access to effective medical tests is crucial because early diagnosis and accurate monitoring can greatly improve health outcomes of many diseases.[1] Unfortunately, many diagnostic and monitoring tools rely on specialized laboratory techniques and trained personnel, making many of these inaccessible or unaffordable.[2-7] Additionally, some tests take hours or days from test to result where quick results are key, especially for diagnosing infectious diseases like COVID-19.[5, 8] Electrochemical biosensors are an attractive alternative for understanding and monitoring health due to their quick response time, sensitivity, and quantitative results.[9, 10] However, many electrochemical biosensors use expensive precious metal electrodes, like gold and platinum. Carbon composite electrodes are an attractive option for biosensing due to their low cost, easy fabrication, biocompatibility, and wide potential windows,[11] but they often suffer from slow electron transfer kinetics and poor electrochemical properties compared to metallic electrodes.[12] In addition to cost, another obstacle in the biosensing field is the low concentrations of many analytes. Electrochemical signals can be amplified by improving the mass transport to the electrode through flow.[13] Unfortunately, carbon composite electrodes are also very challenging to integrate into fluidic devices.[14-18] This dissertation aims to meet a critical need by improving carbon composite materials for biosensing applications and integration of electrochemical sensors into fluidic devices.

Chapter 2 introduced polycaprolactone (PCL) as a new thermoplastic electrode (TPE) binder material. The electrode material presented in this work is quickly fabricated and can be molded easily into templates by simple heat-pressing without the use of solvent. This overcomes a major challenge of carbon composite electrodes by allowing fabrication of intricate shapes without use of solvent. The new PCL composite electrodes have electrocatalytic activity that is

comparable or superior to other composite electrodes that require complicated syntheses or fabrication. Chapter 2 also demonstrated the simple integration of carbon composite electrodes into complex microfluidics using PCL, overcoming many of the challenges common to electrode integration. This work has significant impact for a wide range of applications requiring intricate, well-integrated electrodes within microfluidic devices.

PCL-based TPEs were then applied in Chapter 3 to produce robust, bulk-modified glucose sensors as a proof-of-concept for enzymatic sensors. The work introduces a simple bulk-modification technique for electrocatalysts, enzymes, and other additives. These sensors were able to be renewed via sanding and reused for months, as opposed to surface modification methods typically used that are easily damaged, lack stability, or often become unusable due to fouling. With the current scheme, the enzyme incorporated into the TPE can be substituted for 200+ types of enzymes to sense different biomolecules. This technique gives a platform for not only enzymatic sensors, but for many applications that currently rely on surface modification including other sensors,[19, 20] fuel cells,[21] and capacitors.[22]

Chapter 4 continued the characterization of TPEs started in Chapter 2 with a focus on sensing H_2O_2 and O_2. The work explored the physical, chemical, and electrochemical properties of TPEs with two different binders – PCL (as used in Chapter 2-3) and polystyrene (PS) – to gain a better understanding of the properties that make successful carbon composite electrodes and subsequently biosensors. XPS and SEM analysis suggested that sanded TPEs had a high density of edge plane graphite on the surface and heat-pressed TPEs have more basal plane orientations. PS-based TPEs showed a particularly high density of edge planes which resulted increased electroactivity which allowed them to detect H_2O_2 and O_2 without any electrode modification. In Chapter 4, the PS-based TPEs were also integrated into a reversibly sealed fluidic sensor module

device in which detection of H_2O_2 was demonstrated in flow. The design of the sensor module allows for simple TPE integration and assembly that can be coupled with a variety of fluidic systems.

The detection of H_2O_2 in flow demonstrated in this chapter is the first step towards a system for simple enzymatic detection of various biomolecules in complex biological environments. A two pump system will flow a sample to meet with an oxidase enzyme solution (lactate oxidase or glucose oxidase) at a Y-junction. In the channel where both solutions are combined, the enzyme will react with the lactate or glucose in the sample, producing H_2O_2 as a byproduct which can then be quantified using the sensor module. A simplified schematic is shown in **Figure 6.1**. Long-term, this will then be coupled to a gut-on-chip system, similar to previously reported;[23] however, it could potentially be integrated into a multitude of biological flow systems. The gut-on-chip system bridges the gap between current *in vitro* and *in vivo* studies to make a more representative model of the intestines, which is both physically and functionally complex.[24, 25] Common problems encountered in monitoring in gut-on-chip systems include sensor integration, fouling, and multiplexing.[26] The sensor module could address some of these concerns due to its easy integration and assembly and ability to renew the electrode surface. Additionally, the sensor module could be modified to contain multiple electrodes for multiplexing or another sensor module could be added into the flow system to detect a different analyte. The gut-on-chip system coupled with the sensor module could give better understanding of the intestines. This coupled model could be applied for more effective drug testing, where there is currently a 90% fail rate when drug test moves from *in vitro* studies to clinical trials.[24, 25] Additionally, this system could be used to better understand deadly medical complications, such as anastomotic leaks, to improve prevention and treatment.[27]

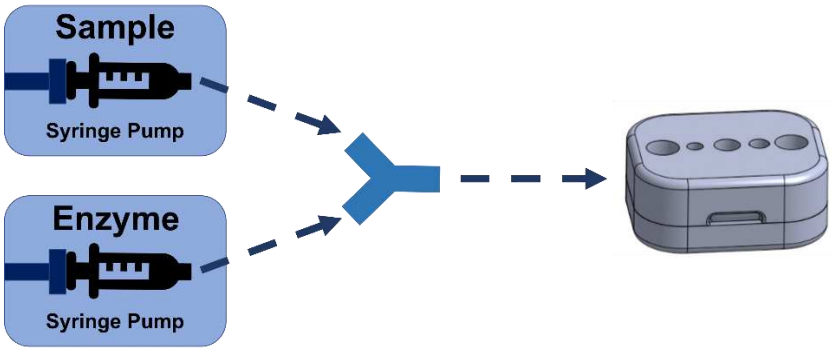

Figure 6.1 Simplified schematic of enzymatic detection system in flow with the TPE sensor module. The sensor module (used in Chapter 4) was designed by Amanda Cherwin.

Finally, Chapter 5 introduced an electrochemical capillary driven immunoassay (eCaDI) device, that automates the steps of a sandwich ELISA using electrochemical detection, offering the potential for more sensitive and quantitative detection of SARS-CoV-2. The device is made from inexpensive materials, greatly reduces the time required for traditional ELISA, and eliminates the need for trained personnel. All these factors make the eCaDI affordable and therefore in the long-term more accessible. The modification and device assembly methods presented in this work are also promising steps to enable large scale manufacturing and commercialization of point-of-care devices for various biological analytes that have been traditionally detected using ELISA. Therefore, the modification could be altered to detect a variety of antigens including other viral proteins, hormones, bacteria, and biomarkers.[28]

Future work will focus on detection of COVID-19 N-protein in physiological samples, improving stability of the entire device, decreasing time to readout, altering modification for different antigens, multiplex detection, and coupling the eCaDI with near field communication (NFC) potentiostats. Changes to the eCaDI device can be used to have two detection zones with separately modified electrodes for different analytes (**Figure 6.2**). The first multiplex system being worked towards is SARS-CoV-2 and influenza A, as they both present similar symptoms easily

mistaken for the other.[29]. NFC potentiostats can be used with any smartphone and are becoming popular for biosensing applications at the point-of-care for quick result readouts without the need for specialized equipment.[30-33] The technology is also summarized in **Figure 6.2**. Long term, this platform could fill a need at the point-of-care for automated, multiplex detection of various antigens for quicker, easier, more reliable diagnostics.

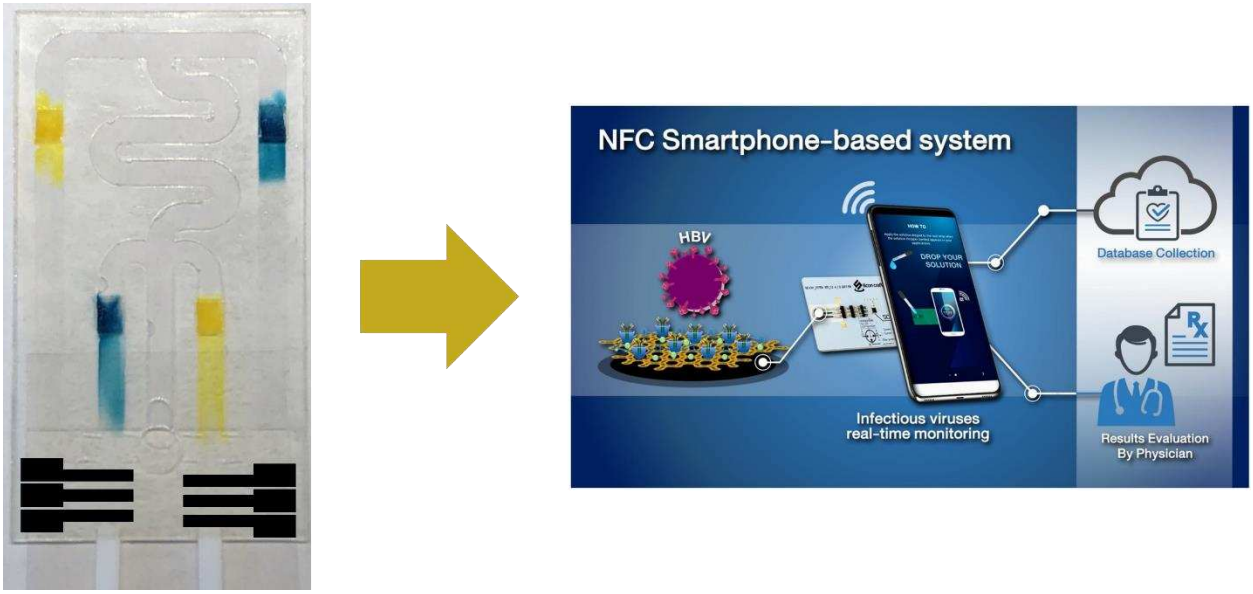

Figure 6.2 Schematic showing (left) image of multiplexed eCaDI device with electrode schematic showing the theoretical position of electrode integration working towards a smartphone-based system using NFC potentiostats. Device in picture before theoretical electrode were placed (left) was designed and fabricated by Jeremy Link. The photo was also taken by Jeremy Link. Infographic (right) is from Teengam *et al*.[30]

In summary, this dissertation presents work to improve carbon composite electrodes for applications as biosensors and beyond. The fabrication and modification techniques move towards more affordable biosensors for medical and other biological sensing. This work demonstrates uncomplicated electrode integration strategies in several types of fluidic devices for simpler and more sensitive detection of biologically relevant analytes. Moreover, the platforms established and presented in these works can be adapted for a wide variety of analytes and applications by making

small changes to the electrodes and devices. The work reported in this dissertation takes a step towards more affordable and accessible biosensors without sacrificing reliability and sensitivity.

REFERENCES

1. Bai, Y.; Xu, T.; Zhang, X., Graphene-based biosensors for detection of biomarkers. *Micromachines* **2020,** *11* (1), 60.

2. Campuzano, S.; Pedrero, M.; Yáñez-Sedeño, P.; Pingarrón, J. M., New challenges in point of care electrochemical detection of clinical biomarkers. *Sensors and Actuators B: Chemical* **2021,** *345*, 130349.

3. Bernabé-Ortiz, A.; Zafra-Tanaka, J. H.; Moscoso-Porras, M.; Sampath, R.; Vetter, B.; Miranda, J. J.; Beran, D., Diagnostics and monitoring tools for noncommunicable diseases: a missing component in the global response. *Globalization and health* **2021,** *17* (1), 1-5.

4. Dhara, K.; Debiprosad, R. M., Review on nanomaterials-enabled electrochemical sensors for ascorbic acid detection. *Analytical biochemistry* **2019,** *586*, 113415.

5. Weissleder, R.; Lee, H.; Ko, J.; Pittet, M. J., COVID-19 diagnostics in context. *Science translational medicine* **2020,** *12* (546), eabc1931.

6. Lakshmi, D.; Whitcombe, M. J.; Davis, F.; Sharma, P. S.; Prasad, B. B., Electrochemical detection of uric acid in mixed and clinical samples: a review. *Electroanalysis* **2011,** *23* (2), 305-320.

7. Liu, D.; Wang, J.; Wu, L.; Huang, Y.; Zhang, Y.; Zhu, M.; Wang, Y.; Zhu, Z.; Yang, C., Trends in miniaturized biosensors for point-of-care testing. *TrAC Trends in Analytical Chemistry* **2020,** *122*, 115701.

8. Carter, L. J.; Garner, L. V.; Smoot, J. W.; Li, Y.; Zhou, Q.; Saveson, C. J.; Sasso, J. M.; Gregg, A. C.; Soares, D. J.; Beskid, T. R., Assay techniques and test development for COVID-19 diagnosis. ACS Publications: 2020.

9. Ronkainen, N. J.; Halsall, H. B.; Heineman, W. R., Electrochemical biosensors. *Chemical Society Reviews* **2010,** *39* (5), 1747-1763.

10. Kaya, H. O.; Cetin, A. E.; Azimzadeh, M.; Topkaya, S. N., Pathogen detection with electrochemical biosensors: Advantages, challenges and future perspectives. *Journal of Electroanalytical Chemistry* **2021,** *882*, 114989.

11. O'Hare, D.; Macpherson, J. V.; Willows, A., On the microelectrode behaviour of graphite–epoxy composite electrodes. *Electrochemistry Communications* **2002,** *4* (3), 245-250.

12. McCreery, R. L., Advanced carbon electrode materials for molecular electrochemistry. *Chemical reviews* **2008,** *108* (7), 2646-2687.

13. Brownlee, B. J.; Marr, K. M.; Claussen, J. C.; Iverson, B. D., Improving sensitivity of electrochemical sensors with convective transport in free-standing, carbon nanotube structures. *Sensors and Actuators B: Chemical* **2017,** *246*, 20-28.

14. Hamedi, M. M.; Unal, B.; Kerr, E.; Glavan, A. C.; Fernandez-Abedul, M. T.; Whitesides, G. M., Coated and uncoated cellophane as materials for microplates and open-channel microfluidics devices. *Lab on a Chip* **2016,** *16* (20), 3885-3897.

15. Pereira, S. V.; Bertolino, F. A.; Fernandez-Baldo, M. A.; Messina, G. A.; Salinas, E.; Sanz, M. I.; Raba, J., A microfluidic device based on a screen-printed carbon electrode with electrodeposited gold nanoparticles for the detection of IgG anti-Trypanosoma cruziantibodies. *Analyst* **2011,** *136* (22), 4745-4751.

16. Kovarik, M. L.; Torrence, N. J.; Spence, D. M.; Martin, R. S., Fabrication of carbon microelectrodes with a micromolding technique and their use in microchip-based flow analyses. *Analyst* **2004,** *129* (5), 400-405.

17. Moore, C. M.; Minteer, S. D.; Martin, R. S., Microchip-based ethanol/oxygen biofuel cell. *Lab on a Chip* **2005,** *5* (2), 218-225.

18. Chen, C.-H.; Lin, Y.-T.; Lin, M.-S., Fabrication of a totally renewable off-channel amperometric platform for microchip electrophoresis. *Analytica Chimica Acta* **2015,** *874*, 33-39.

19. Antuña-Jiménez, D.; González-García, M. B.; Hernández-Santos, D.; Fanjul-Bolado, P., Screen-printed electrodes modified with metal nanoparticles for small molecule sensing. *Biosensors* **2020,** *10* (2), 9.

20. Economou, A., Screen-printed electrodes modified with "green" metals for electrochemical stripping analysis of toxic elements. *Sensors* **2018,** *18* (4), 1032.

21. Narayanasamy, S.; Jayaprakash, J., Application of carbon-polymer based composite electrodes for Microbial fuel cells. *Reviews in Environmental Science and Bio/Technology* **2020,** *19* (3), 595-620.

22. Tang, K.; Hong, T. Z. X.; You, L.; Zhou, K., Carbon–metal compound composite electrodes for capacitive deionization: synthesis, development and applications. *Journal of Materials Chemistry A* **2019,** *7* (47), 26693-26743.

23. Richardson, A.; Schwerdtfeger, L. A.; Eaton, D.; Mclean, I.; Henry, C. S.; Tobet, S. A., A microfluidic organotypic device for culture of mammalian intestines ex vivo. *Analytical Methods* **2020,** *12* (3), 297-303.

24. Shim, K.-Y.; Lee, D.; Han, J.; Nguyen, N.-T.; Park, S.; Sung, J. H., Microfluidic gut-on-a-chip with three-dimensional villi structure. *Biomedical microdevices* **2017,** *19* (2), 37.

25. Bein, A.; Shin, W.; Jalili-Firoozinezhad, S.; Park, M. H.; Sontheimer-Phelps, A.; Tovaglieri, A.; Chalkiadaki, A.; Kim, H. J.; Ingber, D. E., Microfluidic organ-on-a-chip models

of human intestine. *Cellular and molecular gastroenterology and hepatology* **2018,** *5* (4), 659-668.

26. Signore, M. A.; De Pascali, C.; Giampetruzzi, L.; Siciliano, P. A.; Francioso, L., Gut-on-Chip microphysiological systems: Latest advances in the integration of sensing strategies and adoption of mature detection mechanisms. *Sensing and Bio-Sensing Research* **2021,** *33*, 100443.

27. Gaines, S.; Shao, C.; Hyman, N.; Alverdy, J., Gut microbiome influences on anastomotic leak and recurrence rates following colorectal cancer surgery. *Journal of British Surgery* **2018,** *105* (2), e131-e141.

28. Gan, S. D.; Patel, K. R., Enzyme immunoassay and enzyme-linked immunosorbent assay. *J Invest Dermatol* **2013,** *133* (9), e12.

29. Osman, M.; Klopfenstein, T.; Belfeki, N.; Gendrin, V.; Zayet, S., A comparative systematic review of COVID-19 and influenza. *Viruses* **2021,** *13* (3), 452.

30. Teengam, P.; Siangproh, W.; Tontisirin, S.; Jiraseree-amornkun, A.; Chuaypen, N.; Tangkijvanich, P.; Henry, C. S.; Ngamrojanavanich, N.; Chailapakul, O., NFC-enabling smartphone-based portable amperometric immunosensor for hepatitis B virus detection. *Sensors and Actuators B: Chemical* **2021,** *326*, 128825.

31. Olenik, S.; Lee, H. S.; Güder, F., The future of near-field communication-based wireless sensing. *Nature Reviews Materials* **2021,** *6* (4), 286-288.

32. Kholafazad-Kordasht, H.; Hasanzadeh, M.; Seidi, F., Smartphone based immunosensors as next generation of healthcare tools: Technical and analytical overview towards improvement of personalized medicine. *TrAC Trends in Analytical Chemistry* **2021,** *145*, 116455.

33. Chandra Kishore, S.; Samikannu, K.; Atchudan, R.; Perumal, S.; Edison, T. N. J. I.; Alagan, M.; Sundramoorthy, A. K.; Lee, Y. R., Smartphone-Operated Wireless Chemical Sensors: A Review. *Chemosensors* **2022,** *10* (2), 55.